

REPORT DOCUMENTATION PAGE

Form Approved
OMB NO. 0704-0188

Public Reporting burden for this collection of information is estimated to average 1 hour per response, including the time for reviewing instructions, searching existing data sources, gathering and maintaining the data needed, and completing and reviewing the collection of information. Send comment regarding this burden estimates or any other aspect of this collection of information, including suggestions for reducing this burden, to Washington Headquarters Services, Directorate for information Operations and Reports, 1215 Jefferson Davis Highway, Suite 1204, Arlington, VA 22202-4302, and to the Office of Management and Budget, Paperwork Reduction Project (0704-0188,) Washington, DC 20503.

1. AGENCY USE ONLY (Leave Blank)		2. REPORT DATE 12 September 2003	3. REPORT TYPE AND DATES COVERED Final Report: May 1997 - May 2003 5 May 97 - 4 May 03	
4. TITLE AND SUBTITLE Spatial and Quasi-Optical Power Combining A Multidisciplinary University Research Initiative			5. FUNDING NUMBERS DAAG55-97-1-0132	
6. AUTHOR(S) L. Wilson Pearson				
7. PERFORMING ORGANIZATION NAME(S) AND ADDRESS(ES) Holcombe Department of Electrical and Computer Engineering Box 340915 Clemson, SC 29634-0915			8. PERFORMING ORGANIZATION REPORT NUMBER	
9. SPONSORING / MONITORING AGENCY NAME(S) AND ADDRESS(ES) U. S. Army Research Office P.O. Box 12211 Research Triangle Park, NC 27709-2211			10. SPONSORING / MONITORING AGENCY REPORT NUMBER 37253.46-EL-MUR	
11. SUPPLEMENTARY NOTES The views, opinions and/or findings contained in this report are those of the author(s) and should not be construed as an official Department of the Army position, policy or decision, unless so designated by other documentation.				
12 a. DISTRIBUTION / AVAILABILITY STATEMENT Approved for public release; distribution unlimited.			12 b. DISTRIBUTION CODE	
13. ABSTRACT (Maximum 200 words) This MURI program comprised an integrated effort for computer aided design (CAD) modeling of quasi optical structures and three related experimental efforts. The CAD activity involved the electromagnetic modeling of radiation from planar structures, state-variable modeling of microwave circuits, and thermal modeling of microwave circuits. The latter two have been combined into a unified CAD system that deals with microwave circuits, including electro-thermal effects. Electromagnetic structures can be coupled to this CAD system through a y-parameter interface. A closely related experimental effort has led to an electro-optical sampling system capable of measuring all three components of electric field and the temperature at distances quite close to planar radiating structures in an essentially non-perturbing fashion. The probe is a Pockel-effect crystal affixed to the end of an optical fiber. The fiber can be supported over substantial length so that the fiber and a dielectric support for the fiber are the only materials near the device under test. A tray-architecture for quasi-optical amplifiers has been extensively studied. State of the art amplifiers have been fabricated at X and Ka bands and have been thoroughly characterized. Schemes for coupled-oscillator phased-array realizations have been investigated. The parameter space in which coupled-oscillator arrays can be suitably operated has been defined, and issues relating to practical oscillator design for coupled-oscillator arrays have been identified so that a design practice suitable to MMIC fabrication is established.				
14. SUBJECT TERMS quasi-optics, microwaves, millimeter waves, thermal effects, electromagnetic field measurement microwave amplifiers, microwave oscillators, microwave CAD, planar antennas			15. NUMBER OF PAGES	
			16. PRICE CODE	
17. SECURITY CLASSIFICATION OR REPORT UNCLASSIFIED	18. SECURITY CLASSIFICATION ON THIS PAGE UNCLASSIFIED	19. SECURITY CLASSIFICATION OF ABSTRACT UNCLASSIFIED	20. LIMITATION OF ABSTRACT UL	

Final Report

Spatial and Quasi-Optical Power Combining

a

Multidisciplinary University Research Initiative

Contract Number

DAAG55-97-1-0132

Principal Investigator

L. Wilson Pearson

Holcombe Department of Electrical and Computer Engineering

Clemson University

Clemson, SC 29634-0915

Introduction

This document is the final report for the Multidisciplinary University Research Initiative, “Spatial and Quasi-Optical Power Combining.” The contract extended between May, 1997, and May 2003, spanning the five-year duration of a MURI program along with a one-year no-cost extension. The report is organized chronologically. The material immediately following deals with the period January, 2002 through May 2003. Reports of progress for previous years follow, in reverse chronological order.

Principal Investigators

The institutional Principal Investigators for the duration of the program are as follows:

L. Wilson Pearson, Lead Investigator, Clemson University

Andreas Cangelaris, University of Illinois

Christopher Snowden, University of Leeds

Linda P. B. Katehi, Amir Mortazawi, University of Michigan

Michael Steer, North Carolina State University

Zoya Popovic, University of Colorado (1997, only. She joined the Caltech MURI team in 1998)

Prof. Mortazawi joined Prof. Katehi as a second University of Michigan PI when he joined the Michigan faculty in 2002. In earlier years, he had been with the University of Central Florida, then the North Carolina State University.

Other Senior Workers

William Batty, Postdoctoral Research Associate, University of Leeds

John F. Whitaker, Research Scientist, University of Michigan

Dr. Vladimir Okhmatovski. Post-Doctoral Fellow

Student Graduates (2002-2003)

Jason Morsey. University of Illinois, Ph.D., 2003

(Dr. Morsey completed his M.S. at Clemson University funded by this MURI)

Chris Hicks, North Carolina State University, Ph.D., 2002

Satish Uppathil, North Carolina State University, M.S. 2002.

Sean Ortiz, North Carolina State University, Ph.D., 2002

Mete Ozkar, North Carolina State University, Ph.D., 2003

Ayman Al-Zayed, North Carolina State University, Ph.D., December, 2003 (anticipated)

Xin Jiang, North Carolina State University, M.S., 2002

Rizwan Bashirullah, North Carolina State University, M. S. 2002

Jinjin Shin, Clemson University, Ph.D., 2002

Xing Wang, Clemson University, Ph.D. 2003

Chris Tompkins, Clemson University, Ph.D., 2004 (anticipated)

Technical Progress—January 2002-May 2003

Electro-Optical Sampling

Optical excitation and bandgap modulation near the conduction band edge of gallium arsenide, along with electro-optic modulation via the Pockels effect, have resulted in the invention of electrothermal probes capable of simultaneously measuring electric and thermal fields. The previous update report from late 2002 detailed how the reduced-size electro-thermal probes were fabricated, how the system was assembled, and how initial measurements at X-band were demonstrated for an RF MEMS switch. The latter is particularly important, since heating in capacitive MEMS switches may be caused when RF power creates current densities that lead to dissipation when loss mechanisms are present. Due to material thermal expansion from this heating, changes in internal stresses could affect MEMS-device performance and/or reliability.

The effort during the final reporting period of the MURI has extended this effort to now include electric field and thermal characterizations performed at Ka-band, as well as a methodology to determine directly the temperature of a capacitive-switch membrane (as compared to the temperature experienced by the probe when it is positioned slightly above the membrane). This experimental campaign represents, to the best of our knowledge, the first direct measurement of temperature at the internal regions of an operating RF MEMS switch.

In order to determine the temperature rise of the switch membrane itself, a finite-element-method simulation is first performed to compute the correspondence between the thermal load of the probe and the temperature of the probe itself. This is done for probes situated above two different structures: a CPW line and an RF MEMS membrane switch. Then the FEM model is used to compute the correspondence between the temperature of the probe and the thermal load of either the membrane or the CPW. By measuring the thermal load of the probe and utilizing the FEM models, one can solve for the membrane temperature. The temperature extracted for our MEMS switch was found to be 6.5 °C above ambient when the Ka-band input from a TWT was 1 W. This temperature rise will be analyzed and scaled to determine if it will degrade device performance over different periods of time.

Line scans of the electric field were also conducted along the length of the CPW for the two switch states, “up” and “down.” These are shown in Fig. 1, where one may note that traveling waves with a finite SWR are observed on the CPW for the “up” state operation, while a standing wave that terminates at the switch appears for the “down” state. Relevant information regarding the experiment, such as the position of the switch, the operating frequency, and the fact that the on-wafer probes used to introduce the RF input and the termination were not de-embedded (leading to the standing wave behavior in the “up” state, for instance), is included within the figure itself.

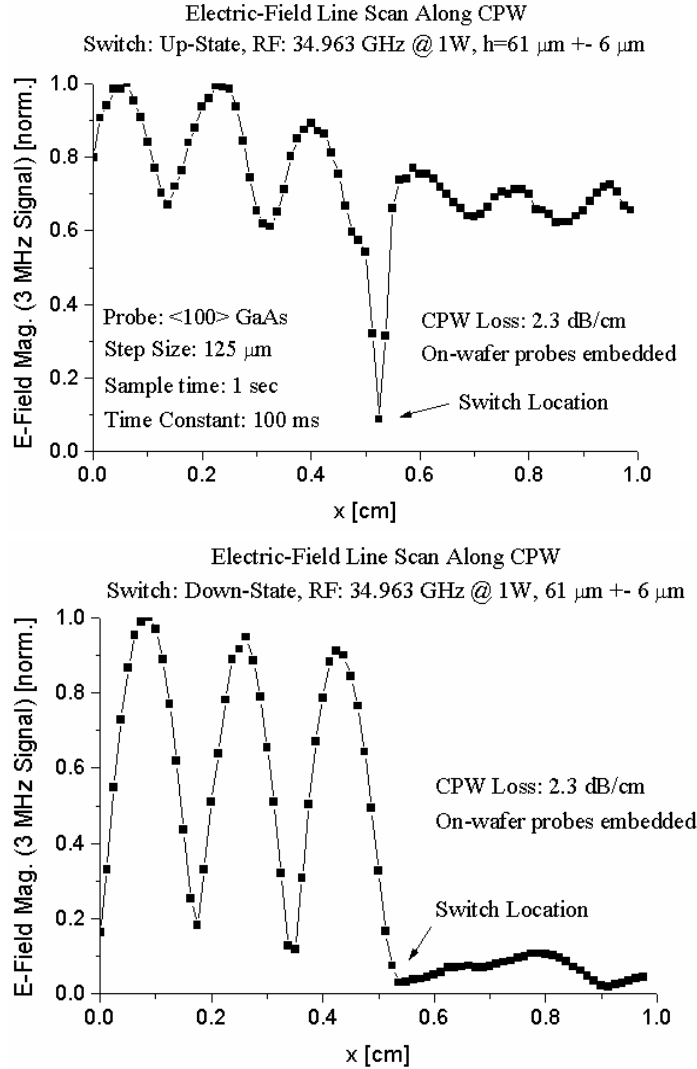


Figure 1. Electric-field line scans measured 60 μm above a Ka-band CPW with RF MEMS membrane capacitive switch in “up” state (top) and “down” state (bottom). The electric field is briefly blocked by the membrane “bridge” when the electro-optic probe passes this switch location.

Electro-Thermal CAD Modeling

Recent work on the Leeds thermal model has concentrated on demonstrating this (semi-) analytical solution in complicated volumes, with series acceleration and numerical Laplace inversion, as an efficient and general model order reduction technique, highly competitive with currently topical model order reduction methods such as Krylov subspace approaches.

Steps have been taken towards the analytical treatment of arbitrarily inhomogeneous subvolumes ‘in one go’, without expensive volume, surface or interface discretization. The same techniques treat arbitrarily position varying surface heat flux coefficients, and also allow domain decomposition without subvolume interface discretization. Such an approach is based on the view that the global basis function expansion method (analytical solution) will be superior to local basis function expansion approaches (conventional numerical methods) for very large

systems. In particular, the cost of the analytical solution depends only on finest resolved feature size, independent of complexity, in contrast with local basis function methods for which the order of the system matrix increases rapidly with system complexity. This generalization of the analytical method to arbitrarily inhomogeneous subvolumes gives rise to solutions in terms of the exponential matrix operator, for which rapid Krylov approximations have already been constructed.

Like the boundary element method (BEM), and in contrast with conventional discretized and meshed numerical methods, such as finite element (FE) and finite difference (FD) techniques, analytical solution gives rise to dense system matrices. Preliminary studies have been made of the dense matrix manipulation problem and reduction of storage and computational costs by a variety of techniques. Brief consideration has been given to techniques including: preconditioned Krylov subspace approaches for $O(N^2)$ solution, particularly with use of the explicit analytical solution of homogeneous problems as a diagonal preconditioner for arbitrarily inhomogeneous problems; wavelet techniques applied directly to the diagonally dominant, analytically constructed system matrix, and panel clustering methods adapted for use with global basis function expansion, both approaches solving in $O(N \log N)$; and fast multipole methods combined with the analytical approach for $O(N)$ solution.

Efforts have also been made to extend the output format of the compact thermal model from its present generalized network parameter representation to an explicit, lumped element RC-ladder approximation. Although the network parameter description allows immediate implementation in microwave circuit simulator fREEDA (NCSU), the lumped element description is required for less flexible, but highly popular, circuit simulators such as SPICE. This lumped element, time-constant or pole-zero form, also allows implementation of recursive convolution in $O(N)$ operations, in contrast to the asymptotically $O(N^2)$ cost of electro-thermal simulations by numerical Laplace inversion currently forming part of the fREEDA implementation. (Note, however, that despite the high asymptotic costs, the existing fREEDA implementation is still highly competitive for even moderately large systems, by virtue of the low absolute operations cost of the analytical thermal impedance matrix solution.)

Recently published work demonstrates that a compact RC-ladder representation is easily obtainable from existing time-domain, thermal step response by simple linear least squares fitting. This method avoids the stability problems of frequency-space fitting and Pade approximation, and can also be shown to give rise to passive reduced networks using the authors' approach of surface averaged power dissipations and temperature rises.

Finally, numerical series acceleration approaches have been studied to complement existing analytical methods. These are central to computationally efficient implementation of analytical solutions.

Tray-Architecture Arrays

In our previous work, based on a resonant multi-slot waveguide coupling structure, we have proposed power dividing/combining circuit designs that achieved high power combining efficiencies both at X band and Ka band. Due to the resonant nature of these designs, they have relatively narrow bandwidth (3-dB bandwidth is on the order of 5%).

In 2002, a broadband Ka-band 8-device power amplifier based on the slotted-waveguide power dividing/combining circuit was designed and fabricated. In this power amplifier design, the

traveling-wave power dividing/combining technique was first used on the slotted-waveguide power dividing/combining circuit and inductive posts were incorporated in the waveguide to achieve the various levels of power coupling between waveguide and microstrip lines. The designed dividing/combining circuit demonstrates a high power combining efficiency over a wide bandwidth and the resulting structure is still simple to fabricate and can provide the same efficient heat sinking for the active devices as in our previous resonant designs.

A broadband tray based spatial power amplifier that employs dielectrically filled miniature horn arrays is introduced. Bandwidth improvement was achieved by replacing the patch arrays of an earlier X-band perpendiculary-fed patch array for spatial power amplifier with the broadband horn antennas, while all other design parameters in the amplifier remain the same. A 5x5 spatial power amplifier with miniature horn arrays have been designed, fabricated and measured. This amplifier has a peak gain of 15.8 dB at 9.9 GHz. The 3 dB bandwidth is 1.32 GHz (13%), which is 4.5 times larger than the 3 dB bandwidth of the perpendicularly fed patch array spatial power amplifier. The output power was found to be 27 dBm at 1 dB compression. The measured gain and bandwidth agreed reasonably with simulations.

Numerical Tools for Planar-Structure CAD

In the last phase of our research the focus was on the improvement on the numerical stability of the fast integral equation solver for frequencies for which the electrical size of the conducting structures and/or the cell size in its method-of-moments discretization was a small fraction of the operating wavelength (less than one hundredth of the wavelength). The causes of low-frequency breakdown are well-understood and remedies for its prevention in the method-of-moments solution of electromagnetic integral equations have been proposed and implemented. Our efforts focused on the implementation of these methodologies in the adaptive integral equation (AIM) algorithm we have developed for the fast iterative solution of the electric field integral equation. Our implementation begins with the well-known loop-tree decomposition of the unknown current utilizing the roof-top functions the loop-tree decomposition of the unknown current. This change of basis functions from the roof-tops to the loops and branches of the tree allows for explicit separation of the irrotational and solenoidal fields resulting in a stable numerical scheme down to very low frequencies. Subsequently, the AIM iterative algorithm is adjusted to accommodate for the new basis functions in terms of loops and the tree branches such that its $O(N \log N)$ computation complexity and $O(N)$ storage requirements are preserved.

The successful implementation of loop-tree AIM is demonstrated in Figure 2 below, where the reflection coefficient at the input of a four-element patch antenna array is depicted versus frequency. The original method-of-moments solution (without loop-tree current decomposition) breaks down for frequencies below 1 GHz where the geometry size becomes much smaller than the wavelength. Implementation of loop-tree current decomposition remedies the problem, allowing for reliable solution down to very low frequencies. Also shown are the results of the loop-tree AIM implementation, which coincide with those obtained with the results from the loop-tree current decomposition-based method-of-moments solution.

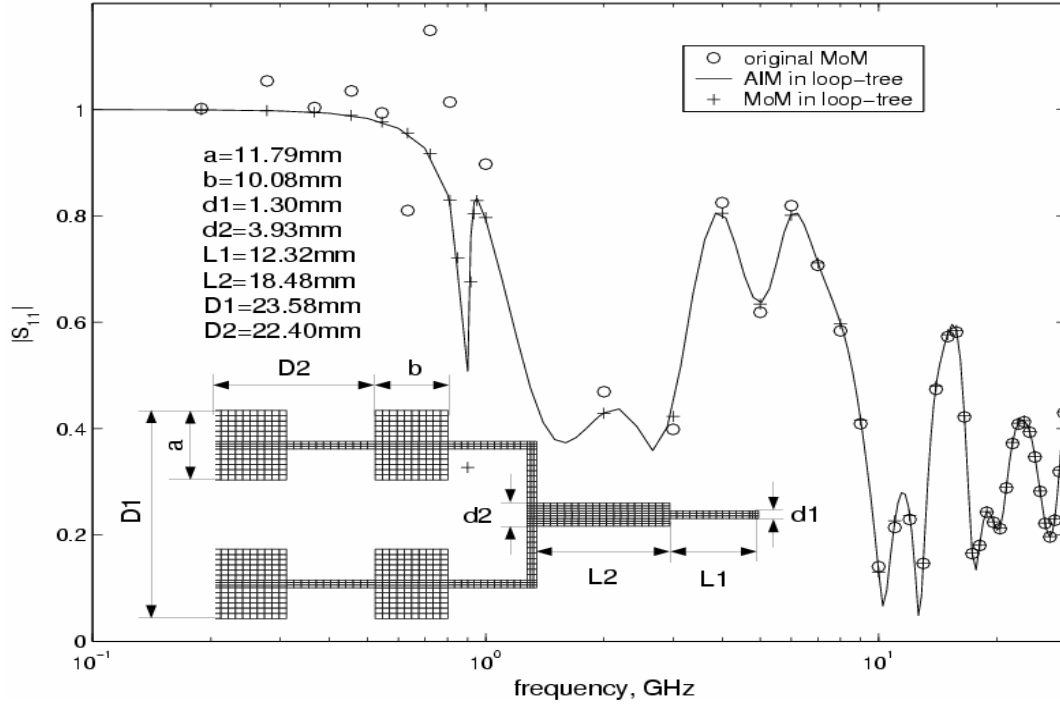


Figure 2. Input reflection coefficient for a four-element patch antenna array.

Unified CAD Modeling for Quasi-Optical Structures

In the final phase of the project NCSU concentrated on the completion of two milestones. The first of these was the development of simulator tools for planar spatial power combiners and the second was on the delivery of a user friendly simulation environment for spatial power combiners.

The modeling environment for the electromagnetic analysis of planar spatial power combining systems was developed in order to understand physical fundamentals and provide a basis for the design process. Two types of planar spatial power combining systems were explored. Propagation in a quasi-optical parallel plate system was investigated with the aim of establishing the mode structure and characteristics of the modes. Theoretical electromagnetic properties of a Gauss-Hermite beammode expansion was developed, and verified experimentally, for the prediction of the resonant frequencies of the structure and dispersion behavior of beammodes. The system was designed, fabricated, tested, and showed good agreement between the experimental and theoretical results. In addition, a spatially distributed parallel-plate stripline-slot amplifier system was designed, tested and compared to an quasi-optical open slab beam waveguide amplifier system with Vivaldi-type antennas. Experimental results verify that a quasi-optical parallel-plate stripline-slot amplifier can be modeled using Gauss-Hermite beammodes. A full-wave electromagnetic model was developed and verified for a spatial power combining system consisting of slotted rectangular waveguides coupled to a strip line. The waveguide-based structure represents a portion of the planar power combiner discussed above. The electromagnetic simulator iwa developed to analyze the stripline-to-slot transitions in a waveguide-based environment. The simulator is based on the method of moments technique to model a power combining array of slotted waveguide modules coupled to a strip line. The

simulator uses Galerkin projection technique with piecewise sinusoidal testing and basis functions in the electric and magnetic surface current density expansions. Electric and magnetic dyadic Green's functions are developed for an infinite rectangular waveguide in the form of partial expansions over the complete system of eigenfunctions of a transverse Laplacian operator. Numerical results are obtained and compared with a commercial microwave simulator for a few representative slot-strip-slot spatial power combining transitions and arrays.

In the second aspect of NCSU's work an integrated design environment consisting of a graphical user interface and electromagnetic and circuit simulation programs for the design and simulation of spatial power combining structures was developed. Surface modes and full nonlinear effects can be studied. Experimental validation was undertaken. The programs for the nonlinear analysis and the interfaces have been defined and documented. The central modeling environment is the circuit simulator fREEDA is a state variable based harmonic balance simulator. Interface program to fREEDA for design and validation of arbitrary structures have been implemented. The simulation environment allows grid amplifier and tray structures to be examined from a holistic point of view. Overlap of structures, design rule check schematic-based entry, multi-layer design can now be done. The simulation environment can be extended to allow what-if studies to be conducted.

Coupled-Oscillator Phased Arrays

Earlier years' work have shown that the keys to reliable designs for coupled oscillator phased arrays are 1) close matching of free running frequencies among all cells in the coupled oscillator array, and 2) achievement of the widest possible locking bandwidth for the unit cell used. This constitutes an unusual set of design goals for oscillators—one never before pursued, to our knowledge, in oscillator design. We have concluded our activities under this MURI program by investigating this design modality.

The investigation of useful oscillator designs was conducted with the expectation that oscillator cells for coupled oscillator arrays will be fabricated as MMICs. With the cooperation of Filtronic Corporation, we were able to purchase 50 LP 7612 transistors that were taken from the same quadrant of the wafer on which they were manufactured. (Filtronic's handling of dies in sawing, sorting, and packaging precludes any closer identification of wafer location for a given die.) These transistors were purchased as packaged devices and were measured in an transistor test fixture. The integrity of the manufacturing process was verified in that the S_{11} , S_{22} , and S_{21} parameters for the devices clustered relatively tightly in the displayed data. The reproducibility of the S_{12} parameter was not so tightly clustered, but this parameter remained quite small, nevertheless.

A design of oscillator cells for a coupled oscillator array was carried out based on the so-called "truth model" for statistical variation among devices. This design achieved maximum locking range based on the optimization of the phase slope for the open-loop equivalent of the oscillator circuit, which had been developed earlier in the MURI activity. A five-cell test-bed was fabricated using this design. The test-bed is shown in Figure 3. The clusters of nylon screws visible on the top serve to hold down packaged transistors into the fixture. Measured performance of the sample of 50 devices showed that 90 percent of the devices showed a free-running frequency that fell within an 80 MHz spread about the nominal design frequency.

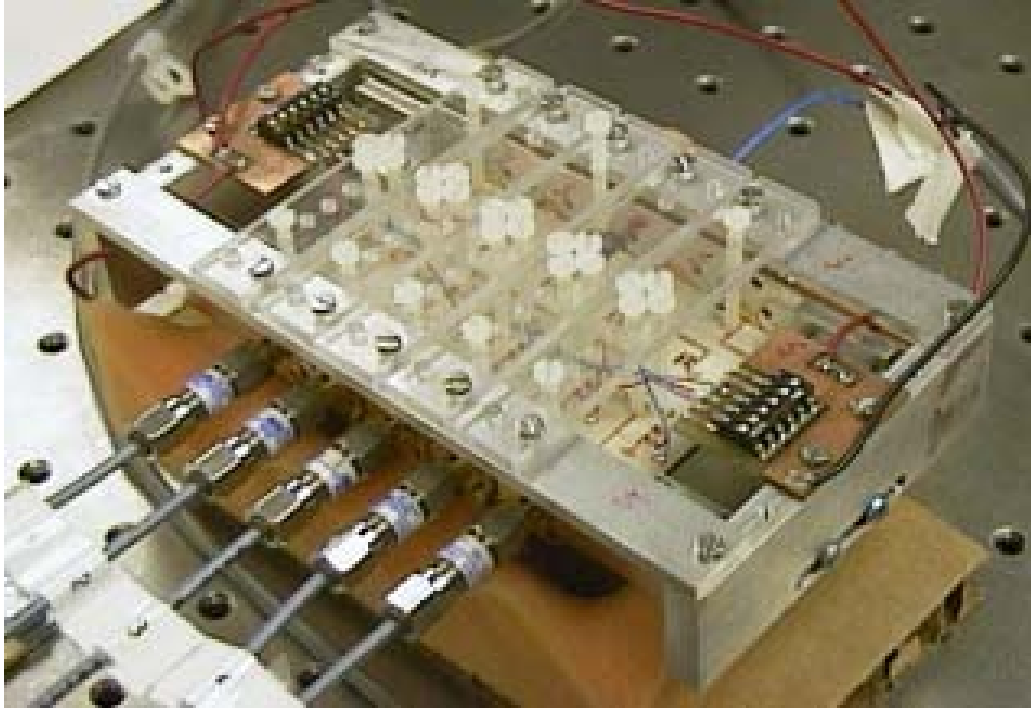


Figure 3. Five cell test bed for evaluating matched transistors in an array

While individual oscillators showed suitably low phase slopes, it was found that for an injection signal of -15 dBm, the best achievable locking range for a five-element array was 2 MHz—small compared with the 80 MHz figure cited above. This leaves us with two conclusions from this study: 1) Careful device matching, such as taking dies from the same region of a wafer, leads to design for dependable free-running frequencies sufficient to ensure that oscillator cells will mutually cohere when placed in a coupled array. 2) The combination of phase slope and frequency agreement attainable is not sufficient to allow an array with a smooth phase front to be fabricated through a simple MMIC process.

We remain sanguine on the potential for coupled oscillator phased arrays. The conclusions stated above simply dictate that a means for trimming the free-running frequencies of the device be built into the MMIC design. A laser-trimmable stub that sets the final frequency would likely prove suitable. This undertaking would have to be a part of a later study of suitable scope to allow the fabrication of custom MMIC components amenable to laser trimming.

Publications

W. Batty and C.M. Snowden, ‘Fully analytical treatment of inhomogeneity, position varying surface heat flux coefficient and non linearity in compact dynamic thermal model construction for complex packages,’ *Proceedings 9th International Workshop on Thermal Investigations of ICs and Systems (THERMINIC 2003)*, Aix-en-Provence, September 2003, to be published.

N.J. Pilgrim, W. Batty, R.W. Kelsall and C.M. Snowden, ‘Nanoscale electrothermal co-simulation: compact dynamic models of hyperbolic heat transport and self-consistent device Monte Carlo,’ *Proceedings 9th International. Workshop on Thermal Investigations of ICs and Systems (THERMINIC 2003)*, Aix-en-Provence, September 2003, to be published.

L. Codecasa, D. D’Amore, P. Maffezzoni and W. Batty, ‘Analytical multi-point moment

matching reduction of distributed thermal networks,' *IEEE Trans. Comp. Packag. Technol.*, 2003, to be published.

W. Batty, C.E. Christoffersen, A.B. Yakovlev, J. F. Whitaker, A. Mortazawi, A. Al-Zayed, M. Ozkar, S.C. Ortiz, R.M. Reano, K. Yang, L.P.B. Katehi, C.M. Snowden and M.B. Steer, 'Global coupled EM-electrical-thermal simulation and experimental validation for a spatial power combining MMIC array,' *IEEE Trans. Microwave Theory and Techniques*, vol. 50, no. 2, pp. 2820-2833, December 2002.

W. Batty, C.E. Christoffersen, A.B. Yakovlev, J.F. Whitaker, A. Mortazawi, A. Al-Zayed, M. Ozkar, S. Ortiz, R. Reano, K. Yang, L.P.B. Katehi, C.M. Snowden and M.B. Steer, 'Electro-thermal simulation a complex design example: the spatial power combining MMIC array,' *Proc. 8th International Workshop on Thermal Investigations of ICs and Systems (THERMINIC 2002)*, Madrid, pp. 210-215, October 2002.

L. Codecasa, D. D'Amore, P. Maffezzoni and W. Batty, 'Multi-point moment matching reduction of distributed thermal networks,' *Proceedings 8th International Workshop on Thermal Investigations of ICs and Systems (THERMINIC 2002)*, Madrid, pp. 231-234, Oct. 2002.

W. Batty, C.E. Christoffersen, C.M. Snowden and M.B. Steer, 'Coupled electro-thermal physical device simulation in global microwave circuit modeling,' *IEEE MTT-S International Microwave Symposium*, Workshop WSG: GHz and THz Solid State Device Simulation, June 2002.

W. Batty, C.E. Christoffersen, A.B. Yakovlev, J.F. Whitaker, M. Ozkar, S. Ortiz, A. Mortazawi, R. Reano, K. Yang, L.P.B. Katehi, C.M. Snowden and M.B. Steer, 'Global coupled EM-electrical-thermal simulation and experimental validation for a spatial power combining MMIC array,' *IEEE MTT-S International Microwave Symposium Dig.*, Paper IF-TH-49, Vol. 3, pp. 2177-2180, June 2002.

S. David, W. Batty, A.J. Panks, R. G. Johnson and C.M. Snowden, 'Simulation of thermally induced intermodulation distortion,' *Proceedings 13th Workshop on Physical Simulation of Semiconductor Dev. (PSSD)*, Ilkley, UK, March 2002.

S. Ortiz, A. Al-Zayed and A. Mortazawi, "A Ka-band Perpendicularly-fed patch array for Spatial power combining," *IEEE MTT-S International Microwave Symposium Dig.*, volume 3, pp. 1519-1522, June 2002.

A. Al-Zayed, S. Ortiz, M. Ozkar, and A. Mortazawi, "Numerical and experimental investigation of losses in a tray based spatial power amplifier," *IEEE MTT-S International Microwave Symposium Dig.*, volume 3, pp. 1867-1870, June 2003.

A. Al-Zayed, S. Ortiz and A. Mortazawi, "Bandwidth Improvement in a Tray Based Spatial Power Amplifier," *IEEE MTT-S Int. Microwave Symposium Dig.*, volume 2, pp. 1313-1316, June 2002.

M. Ozkar, and A. Mortazawi, "Optimization of the array parameters in waveguide-based spatial power combiners with hard horn feeds," *IEEE MTT-S Int. Microwave Symposium Dig.*, volume 2, pp. 1301-1304, June 2002.

M. Ozkar, A. and A. Mortazawi, "Electromagnetic modeling of a waveguide-based spatial power amplifier array with hard horn feeds," *IEEE Antennas and Propagat International Symposium Dig.*, volume 3, pp. 400-403, June 2002.

Xin Jiang; Li Liu; Ortiz, S.C.; Bashirullah, R. and A. Mortazawi, "A Ka-band power amplifier based on a low-profile slotted-waveguide power-combining/dividing circuit," *IEEE Trans. Microwave Theory Tech.*, volume 51, Issue. 1, pp. 144-147, January, 2003.

Xin Jiang; Ortiz, S.C.; Mortazawi, A.; "A Ka-band Power Amplifier Based on the Traveling-Wave Power Dividing/Combining Slotted-Waveguide Circuit"; (Accepted) *IEEE Trans. Microwave Theory Tech*

R.M. Reano, D. Peroulis, J.F. Whitaker, and L.P.B. Katehi, "Electro/thermal measurements of RF MEMs capacitive switches," to appear in *IEEE 2003 MTT-S International Microwave Symposium Digest*.

J.F. Whitaker, K. Yang, R.M. Reano, and L.P.B. Katehi, "Electro-optic probing for microwave diagnostics," invited review paper accepted to the *IEICE Trans. on Electronics*, special issue on "Recent Progress in Microwave and Millimeter-Wave Photonics Technologies." To be published in 2003.

J.F. Whitaker and K. Yang, "Electro-optic sampling and field mapping," book chapter in *Ultrafast Lasers, Technology and Applications*, M.E. Fermann, A. Galvanauskas, and G. Sucha, eds., pp. 473-519, Marcel Dekker AG, New York, 2003.

R.M. Reano, J.F. Whitaker, and L.P.B. Katehi, "Resonant-cavity magnetic-field probe for millimeter-wave frequency-domain spatial field mapping," in *Ultrafast Phenomena XIII*, R.D. Miller, M.M. Murnane, N.F. Scherer, and A.M. Weiner, eds., Springer-Verlag, Berlin, pp. 289-291, 2003.

R. Reano, J.F. Whitaker, and L.P.B. Katehi, "Field-tunable probe for combined electric and magnetic field measurements," *IEEE MTT-S International Microwave Symposium Digest*, New York: IEEE, pp. 1513-1516, pp. 289-291, June 2002.

C. W. Hicks and A. B. Yakovlev and M. B. Steer, "Aperture-coupled stripline-to-waveguide transitions for spatial power combining," *The Journal of the Applied Computational Electromagnetics Society*, volume 19, 2004.

M. V. Lukich, A. B. Yakovlev, A. Z. Elsherbeni, C. E. Smith and M. B. Steer, "Printed antenna design for broadband waveguide-based spatial power combiners," *IEEE Microwave and Wireless Component Letters*, volume 13, March 2003, pp. 125-127.

A. B. Yakovlev, M. V. Lukich, A. Z. Elsherbeni, C. E. Smith and M. B. Steer, "Meander-slot and U-slot antenna arrays for wideband spatial power combiners," *Microwave and Optical Technology Letters*, volume 36, number 5, March 2003, pp. 411-415.

A. B. Yakovlev, S. Ortiz, M. Ozkar, A. M. Mortazawi and M. B. Steer, "Electric dyadic Green's functions for modeling resonance and coupling effects in waveguide-based aperture-coupled patch arrays," *The Journal of the Applied Computational Electromagnetics Society*, volume 17, number 2, July 2002, pp. 123-133.

M. B. Steer, J. W. Bandler and C. M. Snowden, "Computer-aided design of RF and microwave circuits and systems," *IEEE Trans. Microwave Theory Techniques*, March 2002, pp. 996-1005, *invited paper*. (NEOCAD)

- T. Tayag, M. B. Steer, J. F. Harvey, A. B. Yakovlev and J. Davis, "Spatial power splitting and combining based on the Talbot effect," *IEEE Microwave and Guided Waves Letters*, volume 12, Jan. 2002, pp. 9–11.
- C. W. Hicks, A. B. Yakovlev and M. B. Steer, "Slotted waveguide transitions for spatial power combining," *Applied Computational Electromagnetics Society Conference*, March 2003.
- C. W. Hicks, A. B. Yakovlev and M. B. Steer, "Planar aperture coupled waveguide amplifier array for spatial power combining," *IEEE Radar Conference 2003*, May 5-8, 2003.
- W. Batty, C. E. Christoffersen, A. B. Yakovlev, J. F. Whitaker, A. Mortazawi, A. Al-Zayed, M. Ozkar, S. Ortiz, R. Reano, K. Yang, L. P. B. Katehi, C. M. Snowden and M. B. Steer, "Electro-thermal simulation a complex design example: the spatial power combining MMIC array," *6th International Workshop on Thermal Investigations of ICs and Systems (Therminic)*, October 2002.
- J. Suryanarayanan, W. Y. Liu, J. Nath, B. N. Johnson, S. Mohammadi, L. P. B. Katehi and M. B. Steer, "Toroidal inductors for integrated radio frequency and microwave circuits," *2003 IEEE MTT-S International Microwave Symposium*, June 2003.
- M. B. Steer, and J. F. Harvey, "Microwave and RF technology choices and research directions," Plenary Talk, *Mediterranean Microwave Conference*, June 2002.
- M. B. Steer, C. E. Christoffersen, S. Velu and N. Kriplani, "Global modeling of RF and microwave circuits", *Mediterranean Microwave Conference*, June 2002.
- A. B. Yakovlev, M. V. Lukich, A. Z. Elsherbeni, C. E. Smith, and M. B. Steer, "Broadband printed antennas for waveguide-based spatial power combiners," *IEEE AP-S International Symposium and USNC/URSI National Radio Science Meeting*, June 2002
- C. E. Christoffersen, S. Velu and M. B. Steer, "A universal parameterized nonlinear device model formulation for microwave circuit simulation," *2002 IEEE MTT-S International Microwave Symposium*, June 2002.
- W. Batty, C. E. Christoffersen, C. M. Snowden and M. B. Steer, "Fully physical coupled electro-thermal modeling of power devices and circuits," *Proceedings 13th Workshop on Physical Simulation of Semiconductor Devices (PSSD)*, Session 3, Ilkely, UK, March 2002.
- W. Batty, A. J. Panks, C. M. Snowden, C. E. Christoffersen and M. B. Steer, "Coupled electro-thermal physical device simulation in global microwave circuit modeling," *Workshop of the International Microwave Symposium*, June 2002.
- V. I. Okhmatovski and A.C. Cangellaris, "A new approach to the evaluation of the dyadic Green's function in spherical layered media," *Proceedings 2002 Antennas and Propagation Society International Symposium*, pp. 800-803, June 16-21, 2002.
- V. I. Okhmatovski, J. Morsey and A. C. Cangellaris, "An efficient integral equation solver for the electromagnetic modeling of highly-integrated planar RF/microwave circuits," *2002 IEEE International Microwave Symposium Digest*, volume 3, pp. 1897-1900, June 2-7, 2002.

V. I. Okhmatovski and A.C. Cangellaris, "A new technique for the derivation of closed-form electromagnetic Green's functions for unbounded planar layered media," *IEEE Trans. Antennas and Propagation*, volume 50, number 7, pp. 1005-1016, July 2002.

L. Proekt, V. Okhmatovski, B. Karatas, and A. C. Cangellaris, "Investigation of the accuracy of a closed-form expression for the electromagnetic Green's function in planar layered media," *Proceedings 2002 ACES Meeting*, Monterey, CA, March 2002.

W. Wang and L. W. Pearson, "Frequency Stabilization of Power Combining Grid Oscillator Arrays," *IEEE Trans. on Microwave Theory and Techniques*, MTT-50(5), May, 2002, pp. 1400-1407

M. Colwell and L. W. Pearson, "Amplifier-Based Oscillator with Enhanced Locking Range," to be published in *IEEE Microw. Wireless Compon. Lett.*, August, 2003.

J. Shen and L. W. Pearson, "The Phase Error and Beam-Pointing Error in Coupled Oscillator Beam-Steering Arrays," In review, *IEEE Trans. Antennas Propagat.*

J. Shen and L. W. Pearson, "A Design for Two-Dimensional Coupled Oscillator Beam-Steering Antenna Array," *Antennas and Wireless Propagat. Lett.*, September, 2003.

L. W. Pearson, "Reduction of Spatial and Quasi-Optical Power Combining to Engineering Practice," 2002 Government Microelectronics Applications Conference (GOMAC), Moterey, CA, March, 2002.

J. Shen and L. W. Pearson, "How To Increase Locking Range Of Coupled Oscillator Cells Without Lowering Q," 2002 IEEE International Microwave Symposium, Seattle Washington, June, 2002.

C. M. Tompkins, S. Olwen, and L. W. Pearson, "Pattern Deformation due to Substrate Flexing" National Radio Science Meeting, San Antonio Texas, June, 2002.

L. W. Pearson, J. Shen, and X. Wang, Coupled-Oscillator Phased Array Systems for Millimeter Wave Applications, XXVIIth Triennial General Assembly of the International Union for Radio Science, Maastricht, Netherlands, August, 2002.

L. W. Pearson, Spatial and Quasi-Optical Power Combining, GOMAC Tech 2003, Tampa, FL, March, 2003.

C. M. Tompkins and L. W. Pearson, "Achievable Coupled-Oscillator Array Performance," submitted to USNC-URSI National Radio Science Meeting, Columbus, OH, June, 2003.

X. Wang and L. W. Pearson, "Coupled-Oscillator Phased Array Design without *a posteriori* Tuning," in preparation.

X. Wang and L. W. Pearson, "Coupled-Oscillator Phased Array Design based on Statistical Device Characterization," in preparation.

Patent Applications

Pending - "Resonant-cavity magnetic-field probe for millimeter-wave frequency-domain spatial mapping" May 2002.

Pending - "Field-tunable probe for combined electric and magnetic field measurements" May 2002.

Annual Report
Calendar Year 2001

Spatial and Quasi-Optical Power Combining
a
Multidisciplinary University Research Initiative

Contract Number
DAAG55-97-1-0132

2. LIST OF SCIENTIFIC PERSONNEL PERSONNEL

Clemson University

L. Wilson Pearson, PI
Jinjin Shen
Xing Wang
Jabberia Miller
Christopher Tompkins

University of Illinois

Andreas Cangelaris
Jason Morsey
Vladimir Okhmatovski

University of Leeds

Christopher Snowden
William Batty

University of Michigan

Linda P. B. Katehi
John F. Whitaker
Ron Reano

North Carolina State University

Amir Mortazawi
Michael Steer
Carlos Christoferssen
Sean Ortiz
M. Ozkar
Jiang Xin
Lee Liu
Ayman Salazy

3. REPORT OF INVENTIONS

Patent Application:

"Integrated Electro-Thermal Probe," J.F. Whitaker, R. Reano, and L.P.B. Katehi, filed 03/07/02.

4. SCIENTIFIC ACCOMPLISHMENTS

Electro-Optic Sampling

The previously developed electro-optic sampling system was augmented to measure magnetic field, as well. Magneto-optic sampling, which utilizes short-pulse lasers in conjunction with the Faraday effect to sense magnetic-field-induced circular birefringence within certain magneto-optic crystals, has been utilized to investigate spin relaxation and magnetic resonance effects, to measure picosecond current pulses, to sample transient THz beams, and to examine low-frequency RF circuits. However, the signal-to-noise ratio obtained from magneto-optic probes is typically far less than that obtained from electro-optic probes of similar physical dimensions. To improve upon the technique, and to enhance its viability as a microwave diagnostic tool, we have developed a frequency-domain technique that can be used to increase significantly the sensitivity of magneto-optic sampling and magnetic-field mapping. By tuning the probe dimensions to form a resonant cavity at the frequency of interest, the magnetic-field inside of the probe becomes a magnified representation of the sampled field, thereby improving the resulting signal-to-noise ratio. The short-pulse laser is utilized to achieve millimeter-wave operation, thus providing the means to perform internal-node diagnostics on high-frequency circuits and radiating structures. The probe is a Faraday-effect-based sensor consisting of a circular cylinder of terbium gallium garnet (TGG),

Electrothermal CAD Modeling

Part of the work at focused on integrating the various tools that can be used to model quasi-optical systems. This including development of a graphical user interface that can be used to layout a quasioptical system interface and provide the type of information required to do an electromagnetic simulation and an electro-thermal circuit simulation with the results of the EM simulation incorporated.

We have previously used an approach that required much manual manipulation of data but this proved to be a very difficult process that could not be transferred to other groups. The solution was to make modifications to open source software, Electric Editor that already supported the concept of a mixed schematic-layout view. There were problems with the software in that it did not properly support distributed structures. We made the necessary modifications to the code and our changes have been released in the latest version of the software.

The challenge in developing this system is that we needed a solution that was compatible both with VLSI design and our spatial power combining requirements. Issues that evolved including permitting definitions of a quasioptical structure without ground planes. We are working incorporating material properties into the screen capture of the layout editor and also a tighter interface between the graphical layout display and the circuit simulator so that it is not necessary for a user to relate the quasioptical terminal numbers between the layout display of a quasioptical system and the simulator. Thus a user will be able to examine waveforms in the quasioptical display by clicking on the layout. This resolves the last remaining hurdle in a user-friendly simulation environment.

Electrothermal modeling has required extensive interactions with the team at the University of Leeds. The visit by Dr. William Batty to NCSU for three months during the summer speeded the interaction significantly. The work focused considerably on modeling convection and radiation issues which appear to be important in electro-thermal modeling of microwave high power semiconductors as the strong thermal nonlinearities of these structures results in convection and radiation being major means of heat removal. An ongoing effort is directed at electrothermal behavioral modeling, which will lead to the capstone experiments for the MURI.

Coupled Oscillator Phased Arrays

Demonstration and quantification of a frequency doubling (10-20 GHz) 4x4 coupled oscillator array was completed in 2001. Frequency doubling results in phase doubling as well, and scan angles approaching $\pm 30^\circ$ are observed in the scanned pattern data. This brings coupled oscillator systems into the range of useful scanning systems.

Two techniques for widening the locking range of oscillator cells were developed in 2001. One involves direct observation of oscillator parameters and achieves increased locking range through parameter adjustment that does not lower oscillator Q. The second method involves extensive optimization of the phase function in the loop gain of a feedback model of the oscillator. Small experimental arrays have been built on both of these principles and exhibit wider scanning angles before oscillator lock in broken.

Modeling of Planar Open Structures

A closed form Green's function was developed for computing currents on planar conducting surfaces residing on stratified media. The closed-form Green's function shows good accuracy and orders of magnitude in speed improvement over conventional Sommerfeld integral techniques. Efforts are underway to incorporate this Green's functions into the Livermore EIGER planar structure integral equation program.

An adaptive integral equation method (AIM) that exploits block structure of planar arrays was developed. The idea of AIM is to introduce a regular grid of "equivalent sources" that can be used to calculate the product ZI using $O(N \log N)$ -complexity FFTs. Initial computational experiments show that the AIM provides substantial improvement on problems large enough to warrant its use in the first place.

Tray-Architecture Arrays

The FDTD approach was taken here is to calculate the input impedance seen at each antenna port of the input antennas to the tray. Other ports and the feed point of the hard horn with absorbing boundaries in the calculation model used.. A 7x7 element Ka band tray architecture array was completed and demonstrated five watts of output power and a nominal gain of 10 dB. The X-band array that we previously developed has been improved to produce 35 watts of output power.

Performance degradation due to device failures in a spatial power combining system was studied, including analysis and measurement. For this study, a 5x5 amplifier array, employing 17 dBm (P1dB) MMIC amplifiers, has been designed and tested. Individual unit cells have been turned off in order to represent a system with device failures. In

addition, simulated system degradation versus device failure has been studied. Results for both simulated and measured device failures are given for collected and radiated power. The power compression curve of the amplifier array was measured for several cases of device failures. In each case (1 cell, 2 cells, etc.), 5 random combinations of cells were turned off and the output power was measured with the exception of the 1 cell case. For this case, all 25 cells were turned off one at a time. The worst case performance degradation (lowest gain) was plotted for all combinations of the device failure measurements. A full-wave integral equation formulation was developed for the electromagnetic modeling of the waveguide to aperture coupled patch array, resulting in the GSM of the 25 dielectric filled waveguides to the hard horn feed. The GSM for the hard horn feed was obtained using the mode matching technique. All the modules within the power combining system including the amplifier network could then be cascaded to find the overall response of the system. The cascading can be performed within a nonlinear circuit simulator such as *Agilent ADS* in order to use nonlinear models for the amplifiers. Simulated results for the same experiment were compared with the experimental results. In conclusion, simulated and measured power compression curves compared well in predicting the system performance versus device failure, (i.e. 36% loss in power for 20% of the devices failed).

Appendix I Publications

Journal

1. M. Abdullah, and M B. Steer, "Extraction of the network parameters in the electromagnetic analysis of planar structures using the method of moments," *IEEE Trans. Microwave Theory Techniques*, Feb. 2001
2. W. Batty, C. E. Christoffersen, S. David, A. J. Panks, R. G. Johnson, C. M. Snowden and M. B. Steer, "Fully physical time-dependent compact thermal modelling of complex non-linear 3-dimensional systems for device and circuit level electro-thermal CAD," Proc. 17th Annual *IEEE Semiconductor Thermal Measurement and Management Symp.* (SemiTherm XVII), San Jose, March 2001.
3. W. Batty, C. E. Christoffersen, A. J. Panks, S. David, C. M. Snowden, and M. B. Steer, "Electro-thermal CAD of power devices and circuits with fully physical time-dependent compact thermal modelling of complex nonlinear 3-d systems," *IEEE Trans. Components Packaging Technology*, 2001.
4. C. E. Christoffersen and M. B. Steer, "State-variable-based transient circuit simulation using wavelets," *IEEE Microwave and Guided Waves Letters*, vol. 11. 2001.
5. R.M. Reano, K. Yang, J.F. Whitaker, and L.P.B. Katehi, "Simultaneous measurements of electric and thermal fields utilizing an electrooptic semiconductor probe," *IEEE Trans. Microwave Theory Tech.*, Vol. 49, pp. 2523-2531 (Dec. 2001).
6. T. Tayag, M. B. Steer, J. F. Harvey, A. B. Yakovlev and J. Davis, "Spatial power splitting and combining based on the Talbot effect," *IEEE Microwave and Guided Waves Letters*, Vol. 12, Jan. 2002, pp. 9–11.
7. W. Wang and L. W. Pearson, "Frequency stabilization of power combining grid oscillator arrays," to be published in *IEEE Trans. on Microwave Theory and Techniques*, May 2002.
8. W. Wang and L. W. Pearson, "Phase Modulation of A Loop Phase Locked Grid Oscillator Array," *Microwave and Wireless Component Letters*, 11(11) 441, November, 2001.
9. K. Yang, L.P.B. Katehi, and J.F. Whitaker, "Electric-field mapping system using an optical-fiber-based electro-optic probe," *IEEE Microwave and Wireless Components Lett.* April 2001.
10. K. Yang, T. Marshall, M. Forman, J. Hubert, L. Mirth, Z. Popovic, L.P.B. Katehi, and J.F. Whitaker, "Active-amplifier-array diagnostics using high-resolution electro-optic field mapping," *IEEE Trans. Microwave Theory Tech.* (May 2001).
11. A. B. Yakovlev, M. V. Lukich, A. Z. Elsherbeni, C. E. Smith and M. B. Steer, "Meander slot antennas for wideband spatial power combiners," *IEEE Microwave and Wireless Component Letters*, *In Review*.

12. A. B. Yakovlev, S. Ortiz, M. Ozkar, A. M. Mortazawi and M. B. Steer, "Electric dyadic Green's functions for modeling resonance and coupling effects in waveguide-based aperture-coupled patch arrays," *The Journal of the Applied Computational Electromagnetics Society*, July 2002.

Conference Proceedings

1. W. Batty, C. E. Christoffersen, S. David, A. J. Panks, R. G. Johnson, C. M. Snowden and M. B. Steer, "Global electro-thermal CAD of complex nonlinear 3-d systems based on a fully physical time-dependent compact thermal model," *IEEE MTT-S Internat. Microwave Symp. Dig.* Arizona, paper WE1C-2, May 2001.
2. W. Batty, A. J. Panks, S. David, R. G. Johnson and C. M. Snowden, 'Series acceleration of a compact thermal model and fast non linear optimisation of electrothermal device design,' Proc. 7th Internat. Workshop on Thermal Investigations of ICs and Systems (THERMINIC 2001), Paris, September 2001.
3. W. Batty, A. J. Panks, C. E. Christo_ersen, S. David, R. G. Johnson, C. M. Snowden and M. B. Steer, 'Fully analytical compact thermal model of complex electronic power devices and packages in coupled electrothermal CAD,' Proc. 7th Internat. Workshop on Thermal Investigations of ICs and Systems (THERMINIC 2001), Paris, , September 2001.
4. J. Panks, W. Batty, S. David, R. G. Johnson and C. M. Snowden, 'Fully physical electro-thermal CAD for power FET optimisation by non uniform _nger spacing,' Proc. 9th Gallium Arsenide Application Symp. (GAAS 2001), London, paper GAAS/G7 (1), September 2001.
5. W. Batty, C.E. Christofersen, A.J. Panks, S. David, C.M. Snowden and M.B. Steer, 'Electro-thermal CAD of power devices and circuits with fully physical time-dependent compact thermal modelling of complex nonlinear 3-d systems,' *IEEE Trans. Components Packaging Technology*, September 2001.
6. 5. W. Batty, C. E. Christofersen, A. J. Panks, S. David, R. G. Johnson, C. M. Snowden and M. B. Steer, 'Electrothermal circuit modelling of complex non linear systems: generalised multiport thermal Z-parameters,' Proc. 2nd IEEE European MIDAS Workshop: Topical Meeting on Mixed Signal Simulation for Communication Systems, Surrey, July 2001.
7. 8. W. Batty, C. E. Christo_ersen, S. David, A. J. Panks, R. G. Johnson, C. M. Snowden and M. B. Steer, 'Fully physical time-dependent compact thermal modelling of complex non linear 3-dimensional systems for device and circuit level electro-thermal CAD, Proc. 17th Annual IEEE Semiconductor Thermal Measurement and Management Symp. (SemiTherm XVII), San Jose, pp. 71-84, March 2001.
8. C. E. Christoffersen and M. B. Steer, "Comparison of wavelet-and time-marching-based microwave circuit transient analyses," 2001 *IEEE MTT-S Int. Microwave Symp. Digest*. May 2001

9. V. I. Okhmatovski and A. C. Cangellaris "Fast electromagnetic analysis of dense shielded integrated circuits using the adaptive integral method (AIM)," *IEEE MTT-S Internat. Microwave Symp. Dig.* Arizona, May 2001.
10. M. T. Colwell, L. W. Pearson, "A Wide-locking-range MMIC-based oscillator with small footprint," *National Radio Science Meeting*, Boulder, CO, January 2001.
11. S. David, W. Batty, A. J. Panks, R. G. Johnson and C.M. Snowden, "Thermal transients in microwave active devices and their influence on intermodulation distortion," *IEEE MTT-S Internat. Microwave Symp. Dig.* Arizona, May 2001.
12. S. Sean Ortiz, Mete Ozkar, Alexander Yakovlev, Michael Steer, and Amir Mortazawi, "Fault Tolerance Analysis and Measurement of a Spatial Power Amplifier, IEEE Int. Microwave Symp., May 2001, Phoenix, AZ
13. Mete Ozkar, Gianluca Lazzi, and Amir Mortazawi, "Study of Design Parameters in Waveguide-Based Spatial Power Combining Amplifier Arrays Using FDTD," IEEE Int. Microwave Symp., May 2001, Phoenix, AZ
14. L. W. Pearson and C. Tompkins, "Coupled-oscillator phase generation for millimeter-wave RF systems," *2001 Government Microcircuit Applications Conference*, March 2001.
15. R.M. Reano, K. Yang, J.F. Whitaker, and L.P. Katehi, "Integrated electro-thermal probe," *IEEE MTT-S International Microwave Symposium Digest* 2001, New York: IEEE.
16. R. Reano, J.F. Whitaker, and L.P.B. Katehi, "Field-tunable probe for combined electric and magnetic field measurements," submitted to the *IEEE MTT-S International Microwave Symposium Digest*, June 2002.
17. R. Reano, J.F. Whitaker, and L.P.B. Katehi, "Resonant-cavity magnetic-field probe for millimeter-wave frequency-domain spatial field mapping," accepted to the 2002 OSA Topical Meeting on Ultrafast Phenomena.
18. R. Reano, W. Thiel, J.F. Whitaker, and L.P.B. Katehi, " Measured and simulated electric, magnetic, and thermal-field distributions of a patch antenna operating at high power," submitted to the 2002 IEEE International Symposium on Antennas and Propagation.
19. P. J. Rudge, R. E. Miles, M. B. Steer and C. M. Snowden, "Two-tone intermodulation distortion simulations in the time domain using a quasi-2D physical PHEMT Model," 2001 *IEEE MTT-S Int. Microwave Symp. Digest.* May 2001.
20. J. Shen and L. W. Pearson, "A Two Dimensional Coupled Oscillator Array with MMIC Frequency Multipliers," 2001 National Radio Science Meeting, Boston, MA, July 2001.
21. J. Shen and L. W. Pearson, "How To Increase Locking Range Of Coupled Oscillator Cells Without Lowering Q," to be presented at the 2002 IEEE International Microwave Symposium, Seattle Washington, June, 2002.

22. M .B. Steer, C.E Christoffersen, W. Batty and C. M. Snowden, "Electro-thermal modeling of large scale active arrays," *Government Microcircuit Applications Conference*, to be published, March 2001.
23. X. Wang, M. Colwell and L. W. Pearson, "Oscillator Locking-Bandwidth Enhancement for Coupled-Oscillator Applications," Proceedings of 2001 European Microwave Conference, London, October, 2001.
24. A. B. Yakovlev, S. Ortiz, M. Ozkar, A. Mortazawi, and M. B. Steer, "Electric Green's dyadics for modeling resonance and surface wave effects in a waveguide-based aperture coupled patch array," Proc. 2001 *IEEE Antennas and Propagation Symposium*.

Annual Report
Calendar Year 2000

Spatial and Quasi-Optical Power Combining
a
Multidisciplinary University Research Initiative

Contract Number
DAAG55-97-1-0132

2. LIST OF SCIENTIFIC PERSONNEL PERSONNEL

Clemson University

L. Wilson Pearson, PI

Anthony Q. Martin

Jason Keen

Jinjin Shen

Xing Wang

Jabberia Miller

University of Illinois

Andreas Cangelaris

Jason Morsey

Vladimir Okhmatovski

University of Leeds

Christopher Snowden

William Batty

University of Michigan

Linda P. B. Katehi

John F. Whitaker

Kyoung Yang

Ron Reano

North Carolina State University

Amir Mortazawi

Michael Steer

Alexander B. Yakovlev

Sean Ortiz

M. Ozkar

Jiang Xin

Lee Liu

Ayman Salazy

3. REPORT OF INVENTIONS

None

4. SCIENTIFIC ACCOMPLISHMENTS

Electro-Optic Sampling

The electro-optic sampling effort for the last annual period has concentrated on the continued development, characterization, and application of the field-mapping technique and probes. This includes the following areas:

- development of a joint electro-thermal measurement capability
- demonstration of a near-to-far-field transformation technique based on high-resolution electro-optic measurements in extremely close proximity to a radiation source
- detailed investigation of the invasiveness of the probe on a device under test
- temperature calibration of the GaAs electro-optic probe
- calibration of the probe measurements to known electric-field values

We have undertaken an extensive study of the temperature dependent effects associated with GaAs electro-optic probes, demonstrating that it is possible to simultaneously measure both electric and thermal fields with our sensors. This accomplishment takes advantage of two important facts: not all of the laser light sampling the radiated electric field is coherently modulated by this high-frequency field; and the bandgap of GaAs is essentially changing linearly in a large temperature range of interest for our laser wavelength. This allows for the combined electro-thermal examination of active microwave and millimeter-wave circuits with a single probe and the ability to calibrate electric field data that is corrupted when the probe is placed in areas where temperature variations are present. The technique has been applied to the combined electro-thermal examination of an MMIC in a quasi-optical power-combining array.

The temperature dependence of the GaAs probe was discovered in the process of measuring fields of a 5x5 quasi-optic testbed developed during the current year. This testbed is configured with the amplifiers in a brick-array orientation (plane of the circuits perpendicular to the radiating aperture). This array produced substantial temperature increase, which was documented with an infrared camera. Attempts to measure the fields simultaneously with the temperature observation revealed inconsistency in the calibration of the GaAs probe. By revealing the extent of the thermal sensitivity of GaAs, this experiment proved key in the development of the combined measurement described above.

The electro-optic field mapping system has also been used to acquire high-spatial resolution electric-field maps in close proximity to radiating structures for the purpose of demonstrating an improved technique for transforming near-field radiation distributions into far-field patterns. Due to the simultaneous amplitude and phase measurement capability of the electro-optic mapping technique, it was possible to reconstruct far-field patterns from a single two-dimensional near-field scan acquired at a distance approximately 100 μm above the surface of a Ka-band 6x6 quasi-optical amplifier. The high-spatial-resolution capability of the electro-optic near-field-mapping technique simplified the transformation procedure to a far-field calculation from equivalent 2-dimensional magnetic dipole arrays. Furthermore, the high resolution of the near-field mapping made it possible to isolate the field excited around specific sections of the radiating structure, and as a result, different spatial filters were introduced to isolate and

investigate the contributions from the various antenna elements. Also, due to the high sensitivity of the electro-optic field mapping system and the ability to scan the electro-optic probe in very close proximity to the array, surface waves were observed, and their contribution to the far-field formation was analyzed.

We have also begun to successfully address two issues involving the development of the probe that have not as yet been fully considered: absolute field calibration and invasiveness. Utilizing a rectangular waveguide structure with a well-understood field pattern as a calibration device, and accounting for the effects of the permittivity of the electro-optic probe on the field being sensed, we have found for our system a minimum detectable electric field of 1.24 V/m with a 300 ms bandwidth. This should allow us to directly measure absolute values of the electric field within a field map instead of relative field strengths. In addition, the invasiveness of the probe has been initially quantified by examining the change in the characteristic impedance and capacitance per unit length of a planar transmission line. Measured and simulated data show that the effect the probe has on the line is equivalent to a lumped shunt capacitance on the order of a few femtofarads.

Electrothermal CAD Modeling

The Leeds thermal impedance matrix model structure has been completed, and efforts during the past year have shifted toward integration of the thermal model into the TRANSIM quasi-optical system simulator. Initial coupled electro-thermal studies have been made for planar MMIC grid arrays and for tray/card spatial power combining architectures. The thermal model has been validated by thermal imaging and wafer probe testing.

Notable achievements are as follows:

- The first treatment in coupled electro-thermal CAD of thermal nonlinearity due to temperature dependent diffusivity has been constructed. This requires a time variable transformation of the nonlinear time dependent heat diffusion equation, if time constants are to be calculated accurately. This time-variable transformation has now been implemented in TRANSIM for one thermal element. This is in addition to the Kirchhoff transformation for accurate steady-state temperatures, already implemented in TRANSIM.
- Implementation of surface flux nonlinearity in TRANSIM has been studied. These studies show that such a description can be implemented using the state variable approach, without requiring construction of additional error functions beyond those already employed in the existing linearized surface flux description.
- Analytical series acceleration techniques have been developed for thermal subsystem solutions, based on the Watson transformation and Poisson summation formula. These will combine rapid precomputation with high spatial resolution.
- A generalized multiport network parameter description has been constructed for arbitrarily complex and piecewise inhomogeneous three-dimensional systems. This allows transient and steady-state time-dependent simulations of any system that can be represented in terms of composite rectangular subvolumes. This fully analytical 3-dimensional solution, with all device detail, contrasts with existing thermal solutions, which commonly base component descriptions on approximate numerical discretization of the heat diffusion equation; simplification of the heat

diffusion equation to one-dimensional form; and neglect of structural detail such as die surface metallization.

- The electrical RF subroutine from the Leeds Physical Model has been extracted and demonstrated (the electrical DC subroutines already functional), for eventual combination with TRANSIM. The Leeds Physical Model with electro-thermal coupling has been demonstrated to work when embedded in an amplifier circuit.
- Joint theoretical and experimental studies have been made of thermal IMD in power FETs, using the RF Leeds Physical Model subroutines described above. These include
 - experimental two-tone tests of power FET response using a spectrum analyzer.
 - physical model simulation of time constants in GaAs dice and correlation with IM3 dispersion measurements.
 - physical simulation of pulsed IV characteristics; experimental validation ongoing.
 - physical simulation of electrical down conversion to IM2 and corresponding simulation of steady-state time dependent thermal response at difference frequency, $f_2 - f_1$, in two-tone harmonic balance.
 - physical simulation of two-tone and multitone thermal IMDs ongoing.
- The main experimental development consists of transient thermal imaging making comparison of theory and experiment for a passive grid array at turn-on. This comparison illustrates the importance of thermal effects for power combiner operation. Turn-on transient on the order of 1,000 ns in large systems is especially relevant to pulsed and intermittent operation.

Implementation of the Leeds thermal impedance matrix model in TRANSIM, has produced a modular and hierarchical netlist description of thermal subsystems. Transient, single-tone and multi-tone HB analysis have been performed using MMIC one-port, two-port and MMIC array N-port elements. Linearized radiation and convection has been treated fully, with the nonlinear treatment on-going. Temperature dependent conductivity is treated by Kirchhoff transformation, and diffusivity by time variable transformation (though only a partial implementation, so far)

- Example simulations have been performed in TRANSIM illustrating:
- decay of drain current at turn-on due to mobility reduction with increasing temperature under the action of a step input in drain-source voltage.
- small amplitude thermal oscillations at microwave frequencies suggesting the possibility of a previously unconsidered source of classical thermal noise.
- thermal intermodulation distortion simulated by two-tone HB,
- spectral regrowth and ACPR due to thermal effects simulated by multitone HB,
- electrothermal coupling in a 3x3 power FET array,

- coupled electro-thermal/EM operation of a 2x2 amplifier array.

Initial numerical simulations have been performed of the thermal operation of the quasi-optical testbed described in the previous section. The testbed is modeled as an Al block nominally 12x9x5 cm in dimension, cooled purely by radiation and convection, so that emissivity and external fluid flow are key issues. Based on a simplified description of fluid flow as laminar convection over a vertical flat plate, convective losses were calculated to vary from 5, 10, 15 W, when average surface emissivity varied from 1.0, 0.3 to 0.1, with corresponding average steady-state surface temperatures of 350 K, 380 K, 410 K, reached after 4, 10 and 16 hours, respectively. These simulations complement experimental characterization of the testbed structure obtained in the electro-optical scanning system.

Measured, suggested, and predicted effects based on the Leeds program of thermal modeling and measurement, now include:

- possible beam distortion from MMIC gain variation due to temperature non uniformity across a MMIC array.
- grid array temperature non uniformity due to natural convection.
- potential beam impact of long turn-on transients, ~1,000-10,000 s.
- potential spectral regrowth due to weak thermal nonlinearity and impact on ACPR of thermal design.
- possible noise source due to classical thermal response at RF frequencies.
- surface emissivity and external fluid flow as issues for coupled EM/electrical/thermal response of quasi-optical systems.

Coupled Oscillator Phased Arrays

Work has continued to reduce the coupled-oscillator phased array to a practical system that can be used as a millimeter wave array requiring application of control only on the perimeter of the array. In calendar year 1999, we identified the useful parameter range for which coupled oscillator arrays can be made practical. Namely, the locking bandwidth (roughly inversely proportional to the quality factor, Q) of oscillator elements in the array must be large, and the coupling factor between elements must be high. This choice of parameters leads to an array design that is relatively insensitive to cell-to-cell variation in the the cells' free-running frequency. It further provides the widest possible beamsteering range.

In the year 2000, we have conducted further experiments to validate York's theoretical models that lead to the conclusion about parameter range stated above. We did experiments with a 2.5 GHz array whose parameters are precisely adjustable. By intentionally skewing the set of free-running frequencies in this six-element array, we were able to generate precise array states whose phase fronts and associate radiation patterns fit the York mathematical model quite precisely.

Previous experiments have focused on controlling the phase of an injected signal at the end elements as the means for phase control. In 2000, we built a three-element array for which the end-element control was introduced through a stub-loading to skew the free-running frequency of the elements at the end of the linear array. This experiment

validated this second means of phase control. The monotonicity of the beamshift with applied phase control was investigated with this array. The observed monotonicity suggests that a “prewarping” of applied phase signals from calibrated array performance provides a means of producing an array with precise beam pointing.

In work supported by NASA funds, we demonstrated that a coupled-oscillator system can be used to generate phases for a modulated carrier signal through cell-by-cell mixing. This mixing scheme suggests the possibility of employing harmonic mixing so that the frequency, and concomitantly the phase, of oscillator cells is multiplied. The phase multiplication can extend the scanning range of the array. Based on the successful NASA result and the potential for harmonic mixing, we have begun experiments with a 4 x 4 array in which the outputs of a 12 GHz oscillator array are delivered to 2X frequency multiplier/amplifier MMICs and then radiated. This array has been successfully operated and is undergoing refinement and adjustment before a final test program is conducted.

The wide locking range mentioned in the introductory paragraph of this section takes us into an unexplored regime of oscillator design. We have demonstrated with a feedback loop on a MMIC amplifier that proper loading of the feedback transmission line can stagger tune the oscillator so that its locking range can be extended. Building on this result, we are engaged in developing discrete-device designs that can employ the same principle for increase of locking range.

Appendix I Publications

Journal

1. M. Abdullah, and M B. Steer, "Extraction of the network parameters in the electromagnetic analysis of planar structures using the method of moments," *IEEE Trans. Microwave Theory Techniques*, Feb. 2001, In Press (MURI).
2. R. Bashirullah and A. Mortazawi, "A slotted waveguide power amplifier for spatial power-combining applications," *IEEE Trans. Microwave Theory and Techniques*, vol. MTT-48, pp. 1142-1147, July 2000.
3. W. Batty, C. E. Christoffersen, S. David, A. J. Panks, R. G. Johnson, C. M. Snowden and M. B. Steer, "Fully physical time-dependent compact thermal modelling of complex non-linear 3-dimensional systems for device and circuit level electro-thermal CAD," Proc. 17th Annual *IEEE Semiconductor Thermal Measurement and Management Symp.* (SemiTherm XVII), San Jose, to be published, March 2001.
4. W. Batty, C. E. Christoffersen, A. J. Panks, S. David, C. M. Snowden, and M. B. Steer, "Electro-thermal CAD of power devices and circuits with fully physical time-dependent compact thermal modelling of complex nonlinear 3-d systems," *IEEE Trans. Components Packaging Technology*, to be published, 2001.
5. W. Batty and C. M. Snowden, "Electro-thermal device and circuit simulation with thermal non linearity due to temperature dependent diffusivity," *Electron. Lett.* vol. 36, no. 23, pp. 1966 –1968, 2000.
6. C. E. Christoffersen, U. A. Mughal, and M. B. Steer, "Object oriented microwave circuit simulation," *Int. J. on RF and Microwave Computer Aided Engineering*, Vol. 10, Issue 3, 2000, pp. 164- 182. (MURI).
7. C. E. Christoffersen and M. B. Steer, "State-variable-based transient circuit simulation using wavelets," *IEEE Microwave and Guided Waves Letters*, vol. 11. 2001, In Press.
8. M. Ozkar and A. Mortazawi, "Analysis and design of an inhomogeneous transformer with hard wall waveguide sections," *IEEE Microwave and Guided Wave Letters*, vol. 10, no. 2, pp. 55-57, February 2000.
9. W. Wang and L. W. Pearson, "Frequency stabilization of power combining grid oscillator arrays," to be published in *IEEE Trans. on Microwave Theory and Techniques*.

10. A. B. Yakovlev, A. I. Khalil, C. W. Hicks, A. M. Mortazawi and M. B. Steer, "The generalized scattering matrix of closely spaced strip and slot layers in waveguide," *IEEE Trans. Microwave Theory Techniques*, Vol. 48, Jan. 2000, pp. 126-137. (MURI).
11. A.B. Yakovlev, S. Ortiz, M. Ozkar, A. Mortazawi, and M.B. Steer, "Electric dyadic Green's functions for modeling resonance and coupling effects in waveguide-based aperture-coupled patch arrays," *IEEE Transactions on Microwave Theory and Techniques*
12. A. B. Yakovlev, S. Ortiz, M. Ozkar, A. Mortazawi, and M.B. Steer, "A waveguide-based aperture-coupled patch amplifier array—full-wave system analysis and experimental validation," *IEEE Transactions on Microwave Theory and Techniques*, Vol. MTT-48, pp. 2692-2699, Dec. 2000.
13. K. Yang, L.P.B. Katehi, and J.F. Whitaker, "Electric-field mapping system using an optical-fiber-based electro-optic probe," to appear in *IEEE Microwave and Wireless Components Lett.* April 2001.
14. K. Yang, L.P.B. Katehi, and J.F. Whitaker, "Electro-optic field mapping system utilizing external gallium arsenide probes," *Appl. Phys. Lett.* vol. 77, pp. 486-488 (Jul. 2000).
15. K. Yang, T. Marshall, M. Forman, J. Hubert, L. Mirth, Z. Popovic, L.P.B. Katehi, and J.F. Whitaker, "Active-amplifier-array diagnostics using high-resolution electro-optic field mapping," *IEEE Trans. Microwave Theory Tech.* (May 2001).
16. K. Yang, J.F. Whitaker, and L.P.B. Katehi, "Far-field transformation using high-resolution near-field data obtained by electro-optic field mapping," submitted to *IEEE Trans. On Antennas and Propagation*, May 2000.

Conference Proceedings

17. W. Batty, C. E. Christoffersen, S. David, A. J. Panks, R. G. Johnson, C. M. Snowden and M. B. Steer, "Predictive microwave device design by coupled electro-thermal simulation based on a fully physical thermal model," 8th *IEEE International Symposium on Electron Devices for Microwave and Optoelectronic Applications*, Nov. 2000.
18. W. Batty, C. E. Christoffersen, S. David, A. J. Panks, R. G. Johnson, C. M. Snowden and M. B. Steer, "Steady-state and transient electro-thermal simulation of power devices and circuits based on a fully physical thermal model," 6th *International Workshop on Thermal Investigations of ICs and Systems (Therminic 2K)*, September 2000.

19. W. Batty, C. E. Christoffersen, S. David, A. J. Panks, R. G. Johnson, C. M. Snowden and M. B. Steer, "Global electro-thermal CAD of complex nonlinear 3-d systems based on a fully physical time-dependent compact thermal model," *IEEE MTT-S Internat. Microwave Symp. Dig.* Arizona, paper WE1C-2, to be published, May 2001.
20. W. Batty, A. J. Panks, R. G. Johnson and C. M. Snowden, "Electro-thermal modelling of monolithic and hybrid microwave and millimeter wave IC 's," *VLSI Design*, vol. 10, no. 4, pp. 355–389, 2000.
21. W. Batty, A. J. Panks, S. David, R. G. Johnson and C. M. Snowden, "Electro-thermal modelling and measurement of thermal time constants and natural convection in spatial power combining grid arrays," *IEEE MTT-S Internat. Microwave Symp. Dig.* vol. 3, pp. 1937–1940, June 2000.
22. C. E. Christoffersen and M. B. Steer, "Comparison of wavelet-and time-marching-based microwave circuit transient analyses," 2001 *IEEE MTT-S Int. Microwave Symp. Digest.* May 2001 (MURI).
23. M. T. Colwell, L. W. Pearson, "A Wide-locking-range MMIC-based oscillator with small footprint," *National Radio Science Meeting*, Boulder, CO, January 2001.
24. S. David, W. Batty, A. J. Panks, R. G. Johnson and C. M. Snowden, "Electro-thermal modelling of microwave transistors and MMICs for optimised transient and steady-state performance," Proc. 8th *IEEE Intrnat. Symp. Electron. Dev. for Microwave and Optoelectron. Appl.* (EDMO 2000), Glasgow, November 2000.
25. S. David, W. Batty, A. J. Panks, R. G. Johnson and C. M. Snowden, "Fully physical coupled electro-thermal modelling of transient and steady-state behavior in microwave semiconductor devices," Proc. 8th *Gallium Arsenide Application Symp.* (GAAS 2000), paper GAAS/P1 (3), Paris, October 2000.
26. R. G. Johnson, W. Batty, A. J. Panks and C. M. Snowden, "Fully physical, coupled electro-thermal simulations and measurements of power FETs," *IEEE MTT-S Internat. Microwave Symp. Dig.* vol. 1, pp. 461–464, Boston, June 2000.
27. S. David, W. Batty, A. J. Panks, R. G. Johnson and C.M. Snowden, "Thermal transients in microwave active devices and their influence on intermodulation distortion," *IEEE MTT-S Internat. Microwave Symp. Dig.* Arizona, to be published, May 2001.
28. W. Y. Liu, M. B. Steer and D. P. Steenson, "Characterization of the nonlinear device capacitance in frequency domain," 8th *IEEE International Symposium on Electron Devices for Microwave and Optoelectronic Applications*, Nov. 2000.

29. J. D. Morsey and L. W. Pearson, "Array evaluation at millimeter wavelengths employing planar near-field scanning," 2000 *IEEE International Symposium on Antennas and Propagat.* Salt Lake City, UT, July, 2000.
30. A. Ortiz, J. Hubert, E. Schlecht, L. Mirth and A. Mortazawi, "A 25 watt and a 50 watt Ka-band quasi-optical amplifier," *IEEE International Microwave Symp.* June 2000, Boston, MA.
31. S. Ortiz, M. Ozkar, A. Yakovlev, A. Mortazawi and M. Steer, "Spatially combined fault tolerant millimeter-wave power amplifiers," 2001 *Government Microcircuit Applications Conf.*, March 2001.
32. L. W. Pearson, "Coupled-Oscillator Phase Generation— A useful millimeter wave phasing scheme," *DoD Workshop on Beamforming Technology and Applications*, Huntsville, AL, July 26-27, Huntsville, AL.
33. L. W. Pearson, J. Shen, and C. Tompkins, "Coupled-oscillator arrays: beamsteering without phase shifters," *IEEE International Conference on Phased Array Systems and Technology*, Dana Point, CA, May 20-26, 2000.
34. P. J. Rudge, R. E. Miles, M. B. Steer and C. M. Snowden, "Two-tone intermodulation distortion simulations in the time domain using a quasi-2D physical PHEMT Model," 2001 *IEEE MTT-S Int. Microwave Symp. Digest.* May 2001.
35. J. Shen and L. W. Pearson, "Beam pointing errors in coupled oscillator active arrays," *National Radio Science Meeting*, Boulder, CO, Jan. 5-8, 2000.
36. J. Shen and L. W. Pearson, "Oscillator reproducibility consideration in coupled oscillator phase-steering arrays," *IEEE International Microwave Symposium*, June 11-16, 2000.
37. M. B. Steer, C. E. Christoffersen, W. Batty and C. M. Snowden, "Electro-thermal modeling of large scale active arrays," *Government Microcircuit Applications Conference*, to be published, March 2001.
38. A. B. Yakovlev, S. Ortiz, M. Ozkar, A. Mortazawi, and M. B. Steer, "Electromagnetic modeling and experimental verification of a complete waveguide-based aperture-coupled patch amplifier array," 2000 *IEEE MTT-S Int. Microwave Symp. Digest.* June 2000 (MURI).
39. A. B. Yakovlev, S. Ortiz, M. Ozkar, A. Mortazawi, and M. B. Steer, "Electromagnetic modeling of an aperture-coupled patch array in the N-port layered waveguide for spatial power combining Applications," to be presented at the *IEEE AP-S International Symposium and USNC/URSI National Radio Science Meeting Dig.* Salt Lake City, UT, July 2000.

40. A. B. Yakovlev, S. Ortiz, M. Ozkar, A. Mortazawi, and M. B. Steer, "Electric Green's dyadics for modeling resonance and surface wave effects in a waveguide-based aperture coupled patch array," Proc. 2001 *IEEE Antennas and Propagation Symposium*, (MURI).
41. K. Yang, J. D. Morsey, L. W. Pearson, J. Whitaker, L. P. B. Katehi, "Far field analysis of a Ka-band patch antenna array using high-resolution electro-optic near-field mapping," 30th *European Microwave Conference*, Paris, October, 2000.

Annual Report
Calendar Year 1999

Spatial and Quasi-Optical Power Combining
a
Multidisciplinary University Research Initiative

Contract Number
DAAG55-97-1-0132

March 30, 2001

4. SCIENTIFIC ACCOMPLISHMENTS

Electro-Optic Sampling

The electro-optic sampling system at the University of Michigan has been used to evaluate several different quasi-optical system and system components. A partial lists includes the following.

- ◆ Hard horns employed in the Lockheed-Martin MAFET Thrust III design
- ◆ QO Amplifier System (Colorado—Popovic)
- ◆ Slot Antenna Array at 31 GHz (model for amplifier system)
- ◆ Cornell Power Combiner
- ◆ Patch Antenna Array (NCSU—Mortazawi)
- ◆ The utility of the system has been further established through the uncovering of several system difficulties, which were subsequently corrected. Viz:
- ◆ Ladder network effect in bias network that resulted in non-uniform amplification by an array
- ◆ Surface-wave launching from slot-antennas
- ◆ Phase asymmetry in slot combiner due to bias conditions

Of course, in the evaluation of any system, even when there is no need for correction, one gains confidence in the system from observing that performance is in line with expectations.

The current system employs free-field (lens) optics, which proves to be somewhat cumbersome in configuring a given test. There is special difficulty in arranging absorber to eliminate all reflections from the motion-control elements for the lens system. In 1999, we began development of a GaAs probe element that attaches to the end of an optical fiber, thereby obviating the lens system and accompanying motion components. The fiber fed probe has proven viable, and we expect to implement a next-generation scanner in the coming year employing the fiber-fed GaAs probe.

Spatially Combining Amplifiers

In 1999, we have opened exploration one new amplifier configurations based on existing architectural principles. This amplifier is designed at 10 GHz, but is structurally suited to operation at millimeter wavelengths through proper scaling. The concept was developed jointly between Amir Mortazawi at North Carolina State University and Bruce Wallace at the Army Research Laboratories. This amplifier achieved a combining efficiency of 69 percent, with 14 W output power from eight devices in a waveguide-fed/waveguide-combined array. The device exhibited 6.8 dB gain. Theoretical predictions were made for the gain of the array and agreed with measurement within 0.1 dB.

Evaluation of two alternative waveguide combiner designs has been carried out at K_a band. This evaluation includes theoretical modeling of the electromagnetic coupling within the configuration. Passive models of key sections of the structure were fabricated and measured, as well.

A design of a QO amplifier array in which the amplifying devices are oriented perpendicular to the plane of the antennas (brick configuration in phased array parlance) has been initiated.

This amplifier is envisioned to provide the team with an amplifier testbed that can be employed for a variety of studies. For example, it can be populated with MMIC amplifier elements with a variety of gains to achieve different power levels and concomitantly presenting different thermal dissipation loads for thermal studies.

Hard horn geometries have been studied with the finite-difference time-domain modeling method (FDTD) with an eye for optimizing the horn design. A stepped-wall hard horn design has been developed and shortens the length of the horn compared with flared horn walls.

We have begun to develop a hybrid method that combines mode matching and FDTD calculations in order to deal with the geometrical complexity interior to spatial combining arrays. The FDTD can be used in complex, material-loaded regions, while mode matching is used to splice the FDTD solutions to modal solutions in waveguide regions and Floquet representations that characterize patch arrays.

Coupled Oscillator Systems

We have gained considerable understanding of the operation of coupled oscillator systems in 1999. A Runge-Cutta differential equation solver has been developed for the coupled differential equation system developed by York and his associates. This solver has been used extensively to understand the operation of coupled oscillator systems in phase transition. Pogorzelski has recently contributed a small-phase approximate analytical solution for the coupled differential equation system. His approximation reduces to a diffusion equation, thereby demonstrating that phase changes are communicated across a coupled-oscillator array through a diffusion process. We have studied systems that do not conform to the small-phase approximation using the exact differential equation model and have shown that both the diffusive character of the solution and the transit times provided by Pogorzelski stand up even when his approximations are violated.

We have identified a key design sensitivity that is revealed through the coupled differential equation system. Namely, the phase of individual elements is sensitive to the departure of the free-running frequency of individual oscillators from the actual operating frequency (*i.e.*, the ensemble average of the free-running frequencies). The key factor in this sensitivity is Q/κ , where Q is the quality factor of the resonators in the oscillators and κ is the coupling factor between adjacent elements. By keeping the Q/κ ratio low, one is able to limit this sensitivity. This is a significant finding, because it defines unequivocally the useful region of the parameter space for coupled oscillator systems. Quantitative studies suggest that phase errors comparable with current phased-array practice are achievable, but require that we design oscillators with low Q (order 10) and large coupling coefficients (>1.0). The design of low- Q oscillators with reproducible operating frequencies is a previously unexplored possibility within oscillator design.

The potential for coupled oscillators is encouraging for millimeter wave applications. A coupled oscillator array can be controlled from its perimeter, only, thereby obviating the cell-by-cell phase shifter approach that is ubiquitous in phased array practice today.

Global Modeling

In 1999 we built upon the development of the linear circuit modeling program, TRANSIM, that was developed under Thrust 3 of the MAFET program. Specifically, we incorporated

electromagnetic modeling capability into TRANSIM for both open QO structures and for waveguide power combiners. TRANSIM, as developed under the MAFET program, comprises a linear circuit modeling function, a nonlinear modeling function, and a thermal analysis capability. Modeling is state-variable based, in contrast to typical node-voltage-based circuit modeling programs. This state-variable formulation obviates the need for a single ground node in the circuit. This feature is important for incorporation with electromagnetic models, because one cannot define a conservative scalar potential in complete electrodynamic system. Thus TRANSIM is the first circuit modeling tool formulated in such a way that dynamic systems can be directly coupled to circuit components.

Open-region electromagnetic models have been developed for a slot-stripline-slot QO amplifier structure, for CPW-Slot QO amplifier structure, as well as for a Cartesian grid structure appropriate to amplifiers and grid oscillators. The electromagnetic modeling functionality includes near and far field calculation, calculation of circuit parameters at defined ports, and field-circuit interaction.

Closed-region electromagnetic models employ the so-called generalized scattering matrix (GSM) formulation in conjunction with the method of moments. The GSM formulation facilitates the cascading of layers to characterize multilayered structures, which are typical in closed-region QO systems. As in the open region modeling, port definition is supported, thereby providing the interface with circuit models. Thus the TRANSIM circuit solver can be run with full electrodynamic effects of the closed-region “radiating” structures taken into account.

The thermal modeling capability in the original incarnation of TRANSIM used a commercial thermal analysis tool targeted to semiconductor device modeling. The incumbent modeling capability was not especially compatible with TRANSIM, and the computational load was heavy. An electrothermal CAD modeling tool for eventual incorporation into TRANSIM is being developed in parallel within our MURI effort.

Electrothermal CAD Modeling

Work in electrothermal CAD modeling has proceeded on two fronts. Theoretical activity involves the construction of a technique for fully physical, global, coupled electro-thermal simulation of complex systems on CAD time scales. Experimental activity comprises a program of thermal and electrical measurement, for model validation and development and for exploration of fundamental thermal issues.

The Leeds physical modeling capability combines the pre-existing, electro-thermally self consistent, Leeds Physical Model (LPM) of individual MESFETs and HEMTs, with a newly developed, ‘thermal impedance matrix’ approach to the problem of coupled heat flow. The result is a physical (hence fully predictive) description of complex 3-dimensional electro-thermal systems, such as spatial power combining arrays, on time scales suitable for electro-thermal CAD.

The coupled, global electro-thermal model developed at Leeds has been constructed to encompass the full range of architectures under consideration, including single-sided grid arrays on AlN substrate (Lockheed Martin, Popovic), double-sided grid arrays with thick metal ground plane and through-thick-plate coupler (Lockheed Martin, Mortazawi), and

tray/card mounted spatial power combining architectures (Robert York).

Electrical measurements and high resolution Thermal imaging have been carried out to demonstrate some key thermal considerations for such architectures, from the individual device, though MMIC to the grid array level. In particular, experimental studies have been made of: amplifier gain dependence on temperature; the impact on beam formation of MMIC base temperature variation across a grid array substrate; and the orientation dependence of spatial power combiner operation due to the effects of natural convection. Simultaneous modeling efforts have highlighted the importance of surface metalization for heat spreading, the relevance of substrate thermal conductivity for temperature uniformity, and the significance of radiative and convective surface flux losses for large area grid array substrates. More recently, joint theoretical and experimental studies have been undertaken of thermal time constants at varying length scales in spatial power combining arrays.

While electrothermal work has concentrated on the thermal management issues central to the realization of inexpensive, efficient, high power quasi-optic millimeter wave sources, model development has proceeded in the knowledge that fundamental understanding of spatial power combining systems must combine electromagnetic (EM), electrical circuit and thermal descriptions. The thermal impedance matrix approach has therefore been designed from the outset to be fully compatible with electrical network based EM-electrical circuit simulators, notably TRANSIM (NCSU). While the studies listed above make clear the value and importance of purely electro-thermal simulation and measurement for spatial power combiner optimization, the combination of the Leeds global electro-thermal model with the NCSU coupled EM-electrical circuit capability, will allow the first explicit theoretical demonstration of the importance of thermal effects for spatial power combiner circuit performance. The impact of thermal nonlinearity on intermodulation distortion might reasonably be expected to be amongst the first circuit level thermal phenomena to be demonstrated by the fully integrated simulations.

The Leeds thermal model development began with construction of the thermal time-independent solution, as this was the simplest case, but with the intention that this solution should generalize naturally to describe the thermal time-dependent case, both steady-state and transient. The full time-dependent thermal solution is still under development, but is now sufficiently advanced that integration of the thermal impedance matrix model with TRANSIM is underway.

Ultimately it is also intended to couple the LPM to TRANSIM, but this requires a fully algebraic realization of the LPM for compatibility. Such an implementation is non trivial, as time derivative information is essential to the LPM in the form of the displacement current. Putting this current contribution to zero is of no value physically, as it removes all transistor capacitance information. The best solution to this problem seems to be to reformulate the LPM in the frequency domain, giving a fully algebraic description. However, this will be a time consuming task, as it requires major changes to the core model. (In contrast, the thermal impedance matrix approach was designed so as to require no modification to the LPM at all, while still supplying an accurate and fully physical global electro-thermal solution). Integration of the LPM is, however, considered secondary to immediate integration of the thermal model, as algebraic (though not fully physical) device models already exist in TRANSIM.

Appendix I Publications

Journal Publications

1. W. Batty, A. J. Panks, R. G. Johnson, and C. M. Snowden, "Electrothermal modeling and measurement for spatial power combining at millimeter wavelengths," *IEEE Transactions on Microwave Theory and Techniques*, vol. 47, no. 12, pp.2574-2585, December 1999.
2. W. Batty, A. J. Panks, R. G. Johnson and C. M. Snowden, "Electro-thermal modelling of monolithic and hybrid microwave and millimeter wave IC's," *VLSI Design*, 10 (4) to be published 2000.
3. R. M. Reano, J. F. Whitaker, L. P. B. Katehi, "Near-field characterization of parasitic and slotline mode coupling in a Quasi-optical unit cell via electro-optic sampling,"
4. W. Wang and L. W. Pearson, "Frequency stabilization of power combining grid oscillator arrays," paper prepared for submission to the *IEEE Transactions on Microwave Theory and Techniques*, November 1999.
5. K. Yang, G. David, J-G. Yook, I. Papapolymerou, L.P.B. Katehi, and J.F. Whitaker, "Electrooptic mapping and finite-element modeling of the near-field pattern of a microstrip patch antenna," *IEEE Transactions on Microwave Theory and Techniques*, vol. 48, no. 2, pp.288-294, February 2000.
6. K. Yang, T. Marshall, M. Forman, J. Hubert, L. Mirth, Z. Popovic, L.P.B. Katehi, and J.F. Whitaker, "Active-amplifier-array diagnostics using high-resolution electro-optic field mapping," submitted to *IEEE Transactions on Microwave Theory and Techniques*.
7. K. Yang, J. F. Whitaker, and L.P.B. Katehi, "Far-field transformation using high-resolution near-field data obtained by electro-optic field mapping," submitted to *IEEE Microwave and Guided wave Letters*.

Conference Proceedings

8. W. Batty, A. J. Panks, S. David, R. G. Johnson and C. M. Snowden, "Electro-thermal modelling and measurement of thermal time constants and natural convection in spatial power combining grid arrays," submitted to the *2000 IEEE MTT International Microwave Symposium*.

9. W. Batty, A. J. Panks, S. David, R. G. Johnson and C. M. Snowden, "Electro-thermal physical modeling and measurement of MMICs and MMIC grid arrays with thermal transients due to turn-on, pulsed operation and modulation," submitted to the *IEEE Microwave Theory and Techniques-International Microwave Symposium*.
10. W. Batty, C. E. Christoffersen, S. David, A. J. Panks, R. G. Johnson, C. M. Snowden and M. B. Steer, "Steady-state and transient electro-thermal simulation of power devices and circuits based on a fully physical thermal model," submitted to the *Therminic 2000 Workshop*.
11. W. Batty, A. J. Panks, C. M. Snowden, "Fully coupled electro-thermal simulation of MMICs and MMIC arrays based on a physical model," 1999 *IEEE International Microwave Symposium*.
12. S. David, W. Batty, A. J. Panks, R. G. Johnson and C. M. Snowden, "Fully physical coupled electro-thermal modelling of transient and steady-state behavior in microwave semiconductor devices," submitted to the *European Microwave Conference (GAAS 2000)*
13. R. G. Johnson, W. Batty, A. J. Panks and C. M. Snowden, "Fully physical, coupled electro-thermal simulations and measurements of power FETs," submitted to the *IEEE International Microwave Symposium 2000*.
14. J. D. Morsey and L. W. Pearson, "Array evaluation at millimeter wavelengths employing planar near-field scanning," submitted to the *2000 IEEE International Symposium on Antennas and Propagation*.
15. L. W. Pearson and J. Shen, "Coupled-oscillator arrays: Beamsteering without phase shifters," *IEEE International Conference on Phased Array Systems and Technology*, May 20-26, 2000
16. J. Shen and L. W. Pearson, "Beam pointing errors in coupled oscillator active arrays," *National Radio Science Meeting*, Boulder, CO, Jan. 5-8, 2000
17. J. Shen and L. W. Pearson, "Oscillator reproducibility consideration in coupled oscillator phase-steering arrays," submitted to the *2000 IEEE International Microwave Symposium*.
18. C. M. Snowden, "Electro-thermal microwave transistor models for large-signal CAD," proceedings *Integrated Nonlinear Microwave and Millimeter Wave Circuits Conference*, Duisburg, October 1998.
19. K. Yang, J. D. Morsey, L. W. Pearson, J. Whitaker, L. P. B. Katehi, "Far field analysis of a Ka-band patch antenna array using high-resolution electro-optic near-field mapping," submitted to the *Thirtieth European Microwave Conference*.

Spatial and Quasi-Optical Power Combining

A

Multidisciplinary University Research Initiative

ARO Grant No. DAAG 55-97-0132

Interim Progress Report

L. Wilson Pearson, Principal Investigator
Department of Electrical and Computer Engineering
Clemson University
Clemson, SC 29634-0915

January, 1999

Team Members

Linda P.B. Katehi
University of Michigan

Amir Mortazawi
North Carolina State University

Christopher M. Snowden
University of Leeds

Michael Steer
North Carolina State University

Approved for Public Release
Distribution Unlimited

TABLE OF CONTENTS

I. KEY TASKS	4
II OVERVIEW OF ACCOMPLISHMENTS.....	5
III. SUMMARY OF ACCOMPLISHMENTS BY TOPIC	6
<u>1. ENRICHMENT OF QUASI-OPTICAL DESIGN ENVIRONMENT</u>	<u>6</u>
<u>2. ELECTRO-OPTICAL NEAR-FIELD SCANNING</u>	<u>6</u>
<i>Introduction.....</i>	<i>6</i>
<i>Patch Antenna.....</i>	<i>7</i>
<i>Grid Oscillator.....</i>	<i>7</i>
<i>Ka-Band Quasi-Optical Amplifier Arrays.....</i>	<i>8</i>
<i>Horn Measurements.....</i>	<i>8</i>
<i>Slot Antenna Array, Type 1: Improper DC bias network.....</i>	<i>9</i>
<i>Slot Antenna Array, Type 2: Improved DC Bias Network.....</i>	<i>11</i>
<i>Surface Wave Observation.....</i>	<i>17</i>
<i>Amplifier Array Utilizing Patch Antennas.....</i>	<i>18</i>
<i>Electro-Optic Mapping System utilizing GaAs Probes.....</i>	<i>21</i>
<u>3. AMPLIFIER ARRAYS.....</u>	<u>24</u>
<i>Performance of a Slotted Waveguide Power Divider.....</i>	<i>24</i>
<u>4. OSCILLATOR-BASED POWER COMBINING.....</u>	<u>26</u>
<u>5. CHARACTERIZATION ISSUES</u>	<u>28</u>
<u>6. THERMAL CHARACTERIZATION</u>	<u>31</u>
<i>Theory</i>	<i>31</i>
<i>Experiment</i>	<i>31</i>
<i>Joint Theory/Experiment.....</i>	<i>31</i>
<i>1 Validity of linear radiation b.c.....</i>	<i>32</i>
<i>2 Radiative loss variation with area.....</i>	<i>32</i>
<i>Grid Arrays: Hierarchical Treatment.....</i>	<i>33</i>
<i>Near Exact” Interface Matching.....</i>	<i>33</i>
<i>Non Linear Interface Matching.....</i>	<i>34</i>
<i>Fully Nonlinear Electro-Thermal Problem.....</i>	<i>35</i>
<i>Thermal Impedance Matrix.....</i>	<i>35</i>
<i>Experimental Measurements</i>	<i>36</i>
<i>Experimental Measurements</i>	<i>36</i>
JOURNAL PUBLICATIONS.....	41
CONFERENCE PUBLICATIONS	41
APPENDIX PUBLICATIONS STEMMING FROM MURI ACTIVITY	44

LIST OF FIGURES

Fig. 2.1: Electro-optic measurement results for various horn antennas at $f_{in} = 31$ GHz....	9
Fig. 2.2: Photograph of 6×6 quasi-optical amplifier array type A as DUT.....	10
Fig. 2.3: Electro-optic field mapping of the quasi-optical array with improper dc bias network.....	11
Fig. 2.4: Schematic of type 2A and type 2B array measurement.....	12
Fig. 2.5 shows the electro-optic mapping results for both the type 2A and type 2B arrays.	12
Fig. 2.5: Electro-optic field mapping of array type 2A and type 2B.....	13
Fig. 2.6: Electro-optic mapping result of a unit cell.....	14
Fig. 2.7: Isolation measurement setup picture for array type 2A and 2B.	15
Fig. 2.8: Isolation measurement results of array types 2A and 2B.	16
Fig. 2.9: Isolation measurement results of array type 2A and 2B.....	17
Fig. 2.10: Substrate propagation mode wave measurement result (amplitude, in linear scale) of type 2B array for center feeding.	18
Fig. 2.11: Measurement setup for the Lockheed-Martin array utilizing patch antennas. .	19
Fig. 2.12: Electro-optic mapping result for the array.....	19
Fig. 2.13: Comparison of electro-optic mapping results obtained by BSO/LiTaO ₃ and (100)/(110) GaAs-based system.	22
Fig. 2.14: Electro-optic mapping result for coplanar waveguide structure – normal component.	23
Fig. 2.15: Electro-optic field mapping results from a 6× frequency multiplier for the dominant component.	23
Fig. 3.1. Feed mechanism of slot array.	25
Fig. 4.1 Mortazawi’s array design with tuning modification.....	27
Fig. 5.1. Millimeter wave anechoic chamber under construction. Copper shielding.....	28
Fig. 4.2. Millimeter-wavelength Scanning System with Absorber Removed.....	30
Linearizations.....	32
Fig. 6.2. Generic Cuboid.....	33
Fig. 6.3. 3-stage, 38 GHz, balanced amplifier array.....	36
Fig. 6.4. Thermal image of substrate reverse side.....	37
Fig. 6.5. Simulation of FR-4 front side (below Cu).	37
Fig. 6.6. Simulation of FR-4 reverse side.	37
Fig. 6.7. Forward gain of 38 GHz MMIC amplifier.	38
Fig. 6.8. 10×10 resistive array, frestanding, horizontal, dissipating 10 W over area 5×5 cm ²	39
Fig. 6.9. Same array as in Fig. 6.8, but cooled by small fan.....	39
Fig. 6.11. Same array as in Fig. 10, but cooled by a small fan.	39
Fig. 6.10. 10×10 resistive array, edge mounted, horizontal, dissipating 10 W over area 5×5 cm ²	39
Fig. 6.12. 10×10 resistive array, frestanding, vertical, dissipating 10 W over area 5×5 cm ²	39
Fig. 6.13. Same array, offset by 45°. (Thermal hotspot at top of array, top right.	39

I. KEY TASKS

This MURI activity is directed toward gaining a fundamental understanding of the effects that come to play in spatial and quasi-optical power combining through both theoretical and experimental means. A significant part of the experimental activity involves development of both classical and innovative assay methods so that they are applicable to spatial and quasi-optical combining systems and enable precise characterization of performance and phenomena present in these systems. Key activities pursued during calendar year 1998 include the following.

1. Enrichment of the quasi-optical design environment whose development was begun by Steer under Thrust 3 of the MAFET program.
2. Continued development and application of electro-optical near-field scanning methodology for assay of both the radiation field and the quasi-static fields present in combining arrays.
3. Development of a general understanding of the phenomenology that ultimately limits the performance of amplifier arrays.
4. Development of an improved understanding of coupled-oscillator combining systems, including issues pertaining to signal quality and the capacity for an oscillator-derived field to carry information content.
5. Development of classical near-field scanning and pattern measurement principles for use with combining systems at millimeter wavelengths.
6. Development of thermal models for microwave electronic components (discrete devices and MMICs) suitable for coupling with the electromagnetic simulator development discussed in 1. above.

II OVERVIEW OF ACCOMPLISHMENTS

- The Generalized Scattering Matrix has been extended with the Method of Moments to provide a modeling tool for multilayered structures lying in a cross-sectional plane to a waveguide. The formulation accounts for field interactions between layers, as well as coupling through defined ports in a metallic barrier.
- The Michigan electro-optic nearfield scanning system has been employed in evaluating a number of different spatial combining systems from both this MURI program and from the MAFET Thrust 3 program.
- A GaAs electro-optic transducer has been developed suitable for measurement of tangential field components, as well as the (previously achieved) normal component. Gallium Arsenide is preferable to previous BSO and LiTaO₃ transducers, because of its substantially lower dielectric constant.
- A slotted waveguide power divider has been perfected for comparison with Wilkinson divider feeding and spatial feeding of spatially combined amplifier arrays.
- A coupled electrical/thermal model has been constructed. The electrical component is based on the Leeds quasi-2D HEMT model. This couples a Schrodinger-Poisson charge control model, to a hydrodynamic description of in-plane transport with hot electron effects. Temperature dependence enters the model via the description of mobility. The thermal component is based on analytical solution of the heat diffusion equation, with adoption of a thermal resistance matrix approach for electrical iteration.

III. SUMMARY OF ACCOMPLISHMENTS BY TOPIC

1. Enrichment of Quasi-Optical Design Environment

The achievements under this task are provided by way of the references in the Appendix.

2. Electro-Optical Near-Field Scanning

Introduction

Activity on the electro-optical near-field scanning system has been balanced between application of the system to analyze the fields radiated by a number of different spatial combining systems and system components, and the further development of the system toward a second-generation configuration.

Structures that have been analyzed include a 4-GHz microstrip patch antenna, a 4.7-GHz phase-locked grid oscillator, and two 30-GHz grid amplifier arrays. Simulations using a finite-element model have also been carried out for the patch antenna and compared to the experimental near-field maps. The transition between near and far field radiation patterns has been characterized in the electro-optic measurements, and near-field patterns have been utilized to compute far-field patterns. The field maps have also allowed the diagnosis of an insufficient bias condition for one of the active arrays, which has led to an 8-dB improvement in gain for the amplifier, and evidence of the presence of surface waves in some structures has also been found.

In addition to the array measurements, the output field patterns for several conventional, tapered feed horns were characterized, along with a number of large and small dielectric-loaded hard horns. We have also determined that there is no problem with extending our electro-optic field-mapping system out to W-band frequencies, as we have measured the output from the rectangular aperture of an active 6X multiplier while using a 17-GHz input. Finally, the initial strides toward producing a compact, fiber-based probe system have been made, as free-space-coupled probes fabricated from both (100) and (110)-oriented GaAs exhibited a high degree of performance for electro-optic sensing of x-y-z orthogonal field components.

One paper has appeared in the *IEEE Trans. On Microwave Theory and Techniques* in the past year with support from this MURI [2]. This was on the topic of electro-optic field mapping for guided-wave structures, and the essence of the work appeared in last year's report. This work was also presented at the 1998 IEEE MTT-S International Microwave Symposium, and the paper that appeared in the conference digest [28] was expanded to produce [2]. Another conference paper appeared in the digest of the 1998 European Microwave Conference, on the topic of electro-optic field mapping for the Clemson 4x4 phase-locked grid oscillator [27]. The results are summarized below, but the complete paper is attached to provide all of the relevant details. We have also submitted a paper to the *IEEE Trans. On Microwave Theory and Techniques* on our comparison of electro-

optic field-mapping measurements of a 4-GHz patch antenna with a Finite-Element-Model simulation. A copy of this submitted paper is also attached. In addition, we have two papers in preparation, one on the near-field characterization of quasi-optic power combining amplifiers, and one on the use of GaAs as a low-permittivity electro-optic field sensor for capturing three orthogonal field components.

Part of the work that is described in the following pages has been undertaken as a part of collaborations, essentially with visitors bringing quasi-optic arrays that could be probed with the electro-optic near-field measurement system. As mentioned, we have worked with Wilson Pearson from Clemson to measure the amplitude and phase of each of the elements of a 4x4 oscillator array. We have also commenced an effort with MURI team member Amir Mortazawi from North Carolina State Univ. to characterize a passive quasi-optic array, as well as the electric field right at the aperture of a Ka-band hard horn that had both dielectric-covered walls and a dielectric lens. This project has produced only preliminary, exploratory measurements, and they are not being described in this report. Two interactions peripheral to the MURI program have also produced fruitful results that are included in this report. The first has helped MAFET researchers at Lockheed-Martin observe the near-field pattern of several Ka-band active arrays employing patch antennas. The second effort has examined a number of active arrays from the group of Zoya Popovic at the University of Colorado at Boulder. A combination of experiments has demonstrated that electro-optic field mapping can diagnose deficiencies with an array, which were then corrected so that both electrical and electro-optic measurements substantiated the improvements.

Patch Antenna

As stated, measurements of all three orthogonal electric field components have been demonstrated for a microstrip patch antenna that is designed to have a 4-GHz resonance frequency. Measurements include a near- to far-field transition, as well as near-field amplitude and phase measurements of the complete patch antenna radiation pattern. For comparison, a three-dimensional Finite Element Method (FEM) simulation has been performed for the investigated antenna structure. We feel the electro-optic measurement results are superior to the FEM simulation results in terms of spatial resolution and data/result acquisition time. Plus, the measurement and simulation show good agreement. In addition, the scattering parameter S_{11} of the antenna has been calculated from the electro-optic field map data revealing the standing wave characteristics of the structure at different frequencies. Finally, these results extracted from the electro-optic field measurements have been compared with the S_{11} from a conventional network analyzer. All of this is covered in the submitted MTT paper that is attached.

Grid Oscillator

Experimental results for a grid oscillator consisting of 16 radiating elements [27] have been obtained to illustrate the capabilities of the measurement technique and to help diagnose potential problems with the relative phase across the array. Two-dimensional scans of the amplitude and phase of each of the orthogonal field components (typically

two tangential as well as the normal field component) have been made in different planes of the radiation pattern above the grid. The results demonstrate the usefulness of this scheme especially for the characterization of arrays of passive or active radiators. All details may be found in the attached digest paper for the European Microwave conference.

Ka-Band Quasi-Optical Amplifier Arrays

Finally, numerous electro-optic near-field measurements on quasi-optical amplifier arrays have been performed. The electro-optic measurements presented demonstrate the technique's usefulness for improving the performance of the structures described, providing detailed information that cannot otherwise be obtained by conventional measurement methods. Among other discoveries, a substrate mode propagation wave was detected experimentally for the first time.

Horn Measurements

Before testing the arrays, it was necessary to measure the output field pattern of the feeding horns, since the output near-field pattern of an array can depend strongly on the input field pattern (*i.e.*, output of the feeding horn). A standard WR-28 tapered horn and two different types of hard horns were used to feed the various quasi-optic arrays. One of the hard horns (type A) utilized a WR-28 standard horn. Hard horn type B used a customized horn body. Dielectric layers and lenses were used for both hard horns to achieve plane wave outputs at only a short distance from the output plane of the horn [M. A. Ali, *et. al.*, *IEEE Trans. Microwave Theory and Tech.*, vol. 46, pp. 1469-1473]. Figure 2.1 shows electro-optic measurement results for the dominant electric field component (the y-component) of all three horns. Each horn is operated at a frequency of 31.043 GHz, which is a combination of a 31.04 GHz rf signal and a 3 MHz IF signal. Due to the limit of the rf synthesizer used in the measurement, it was necessary to employ a frequency doubler between the rf synthesizer output port and the input port of the horn antennas. The frequency doubler generated 30.043 GHz output from a 15.5215-GHz input. Figure 2.1 (a) and (b) show the normalized amplitude and phase of the dominant electric field component for the standard WR-28 horn. The phase measurement result displays a 180 degree phase variation from the center to edge of the aperture, which agrees well with theoretical predictions for this horn output. Figure 2.1 (c) and (d) display the normalized amplitude and phase of hard horn type A. In comparison with a standard horn, the results show significant improvement of the uniformity of the phase (Fig. 2.1 (d)). The phase variation of hard horn type A is around 50 degrees. The hard horn type B shows the best results for both amplitude and phase distribution (Fig. 2.1 (e) and (f)). It shows an excellent 20 degree phase variation and the most uniform amplitude distribution among the three horn antennas.

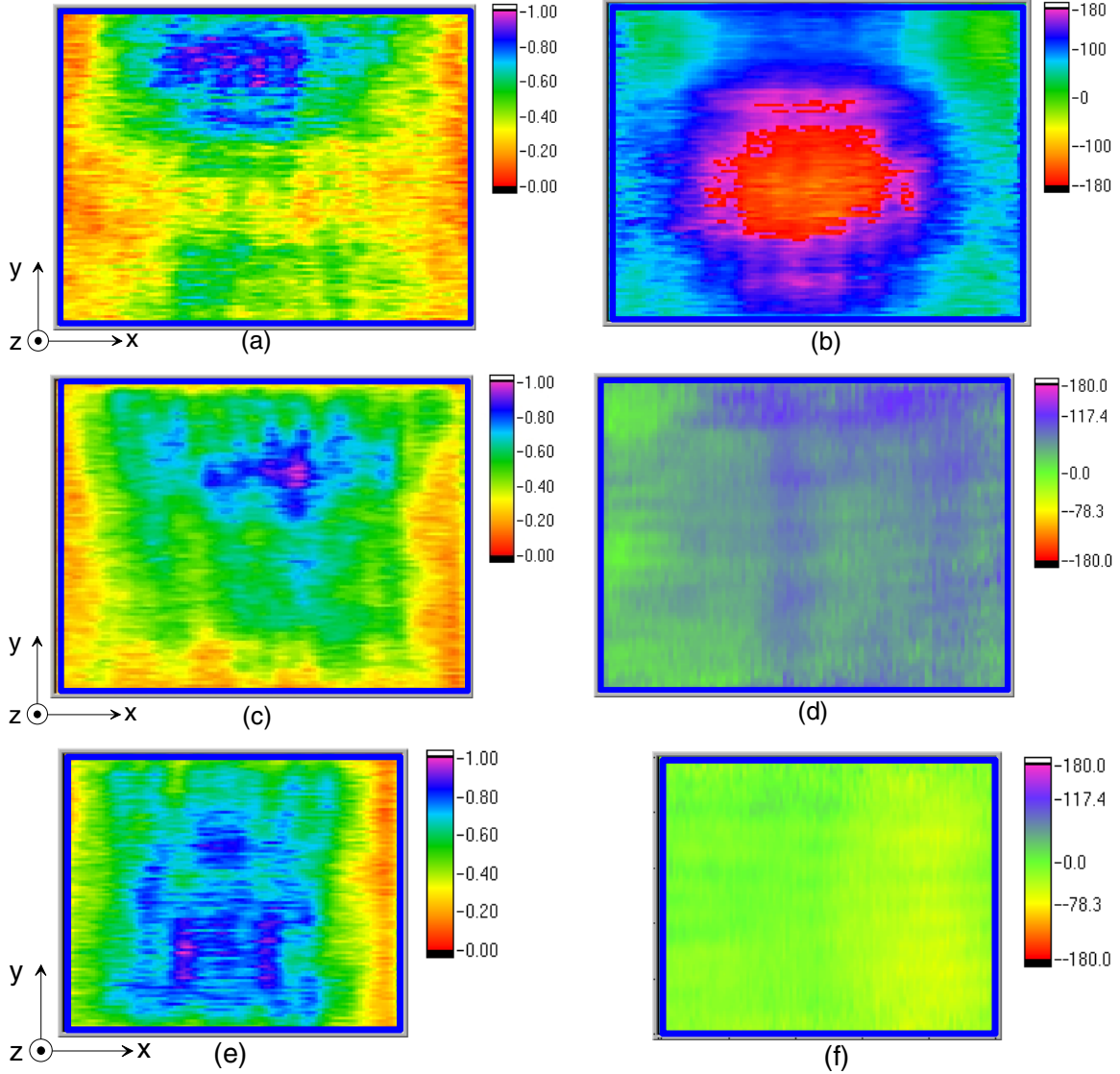


Figure 2.1: Electro-optic measurement results for various horn antennas at $f_{in} = 31$ GHz (a) normalized amplitude for standard WR-28 horn and (b) phase in degrees; (c) normalized amplitude and (d) phase in degrees for hard horn type A; (e) normalized amplitude and (f) phase in degrees for hard horn type B. The metal boundaries of the horn apertures are overlaid with a bold blue line.

From the results for the three different types of horn antenna measurements, it is clear that the two hard horns have superior characteristics in terms of uniformity of phase, which is a critical factor for generating a plane wave.

Slot Antenna Array, Type 1: Improper DC bias network

A photograph of a 6×6 quasi-optical amplifier (from the University of Colorado) mounted as the DUT is shown in Fig. 2.2. Each input slot antenna receives power from the horn feed antenna. The received power is coupled onto a $50\text{-}\Omega$ coplanar waveguide

(CPW) transmission line and is then amplified by an Alpha AA0028P3-00 MMIC amplifier. The amplified power is re-radiated after 90-degree polarization rotation with respect to the input field. Isolation and stability are provided by orthogonal input and output antennas [7].

Figure 2.3 shows the electro-optic field map results for this array. The unit step size for the scanning is $500\ \mu\text{m} \times 450\ \mu\text{m}$ and the total scanning area is $6.25\ \text{cm} \times 4.8\ \text{cm}$. The total elapsed time for the scan is around 1 hour and 10 minutes. Figure 2.3 (a) clearly shows that most of the functioning elements are concentrated around the dc bias point. From the results, several possible diagnoses were suggested. The first possibility was that most of the amplifier MMICs were malfunctioning, except for those in an area around the dc bias point. However, this analysis is not reasonable because the MMICs around the dc bias point are less protected to external disturbances such as static charge effects or abrupt bias changes than are those far away from the dc bias point. The second possibility is an improper dc bias network. In other words, the bias lines failed to supply a uniform bias across the whole array area due to a distributed ohmic loss. The latter

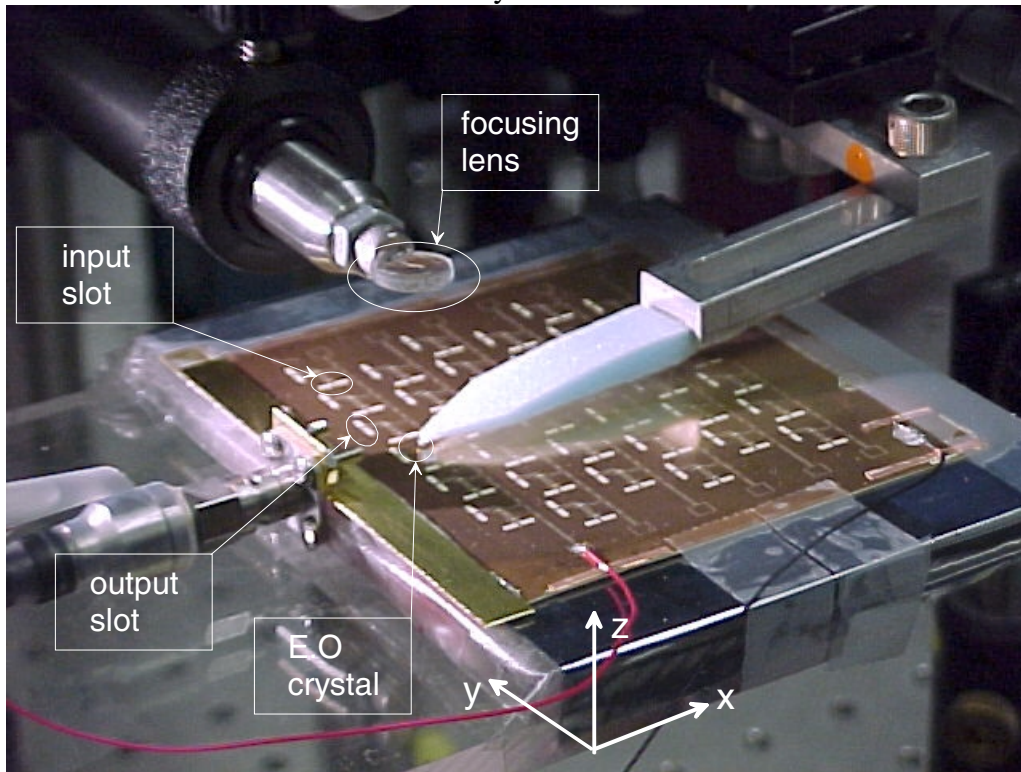


Figure 2.2: Photograph of 6x6 quasi-optical amplifier array type A as DUT. The input slots are aligned along the x-direction (y-direction polarization), while output slots are aligned along the y-direction (x-direction polarization). A LiTaO3 electro-optic probe is mounted at the end of a Styrofoam arm.

explanation agrees well with the measurement results. Also, an accurate voltage distribution calculation performed in Boulder has revealed that array type 1 has a noticeable dc voltage variation along the bias network [M. Forman, *et. al.*, 1999 *IEEE*

International Microwave Symp.] To reduce the ohmic loss of the dc network, which is critical for the uniform bias of a large number of MMICs, an improved array that utilizes thicker metal line as dc bias network was developed.

Slot Antenna Array, Type 2: Improved DC Bias Network

In response to the electro-optic field-mapping results, two different arrays have been assembled, with each having an improved dc bias network design (array type 2A

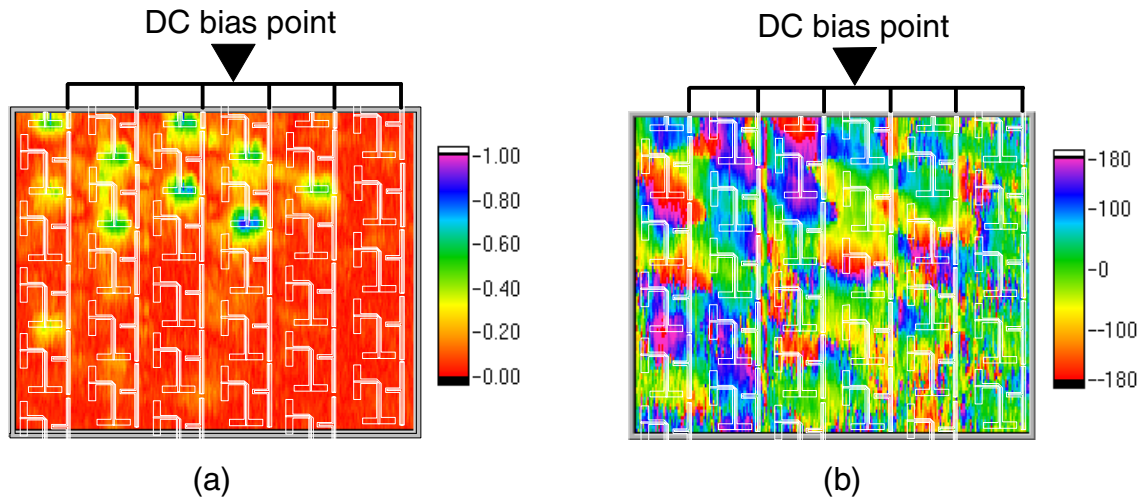


Figure 2.3: Electro-optic field mapping of the quasi-optical array with improper dc bias network. (a) normalized amplitude and (b) phase in degrees. Circuit outline is overlaid.

and type 2B). Both arrays share the same physical design as array type 1. Array type 2A has an improved bias network utilizing thick copper tape for the main bias line and the type 2B array utilizes a thick metal plating process to reduce the ohmic loss. Also, a number of capacitors have been mounted along the bias line to block rf cross-talk between each element throughout the bias network. For the measurements, both the type 2A and type 2B arrays were mounted face-down toward the feeding horn to improve the accessibility of the electro-optic probe to the radiating slot antennas (Fig. 2.4). Furthermore, this setup makes it possible to measure the propagation wave through the substrate (*i.e.*, the substrate propagation mode), due to the proximity of the electro-optic crystal to the substrate. The individual scanning step size is $500 \mu\text{m} \times 450 \mu\text{m}$ and the total scanning area covers $63 \text{ mm} \times 54 \text{ mm}$. The total scanning time is again around 1 hour, 10 minutes. The hard horn type B (Fig. 2.1 (e), (f)) was used as the feeding horn antenna because it displayed superior performance to the standard horn or the type A hard horn.

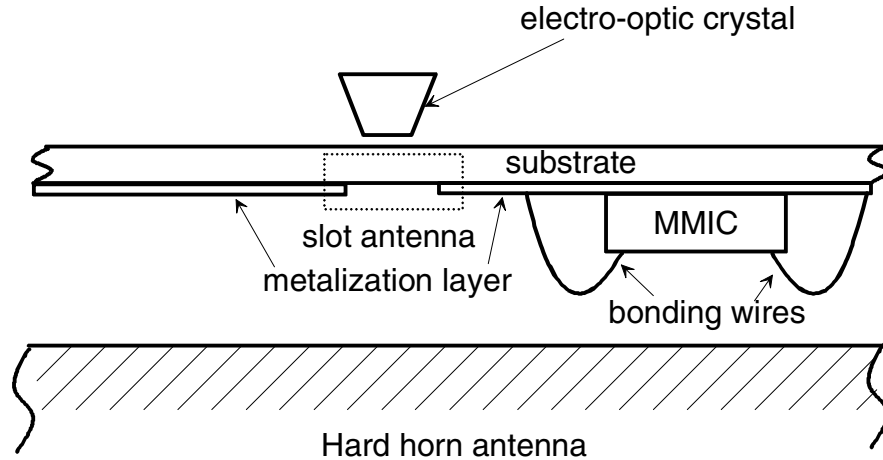


Figure 2.4: Schematic of type 2A and type 2B array measurement; LiTaO₃ is used as the electro-optic crystal.

Figure 2.5 shows the electro-optic mapping results for both the type 2A and type 2B arrays. The normalized amplitude of the type 2A array shows an uneven distribution (Fig. 2.5 (a)), even though it exhibits an improved pattern with respect to the array type 1 (Fig. 2.3 (a)). The electro-optic mapping results from array type 2B display significant improvement of output field distribution both in amplitude and phase (Fig. 2.5 (c) and (d)).

Since array type 2A and type 2B share the same layout design, the discrepancy of the performance between the two arrays can best be explained as rf cross talk between individual elements. As mentioned above, both arrays type 2A and type 2B utilize an improved bias networks. However, only the type 2B array has rf blocking capacitors on the bias line. The results show that suppressing cross talk between each element is another important factor to enhance the performance of amplifier arrays along with achieving uniform dc bias distribution.

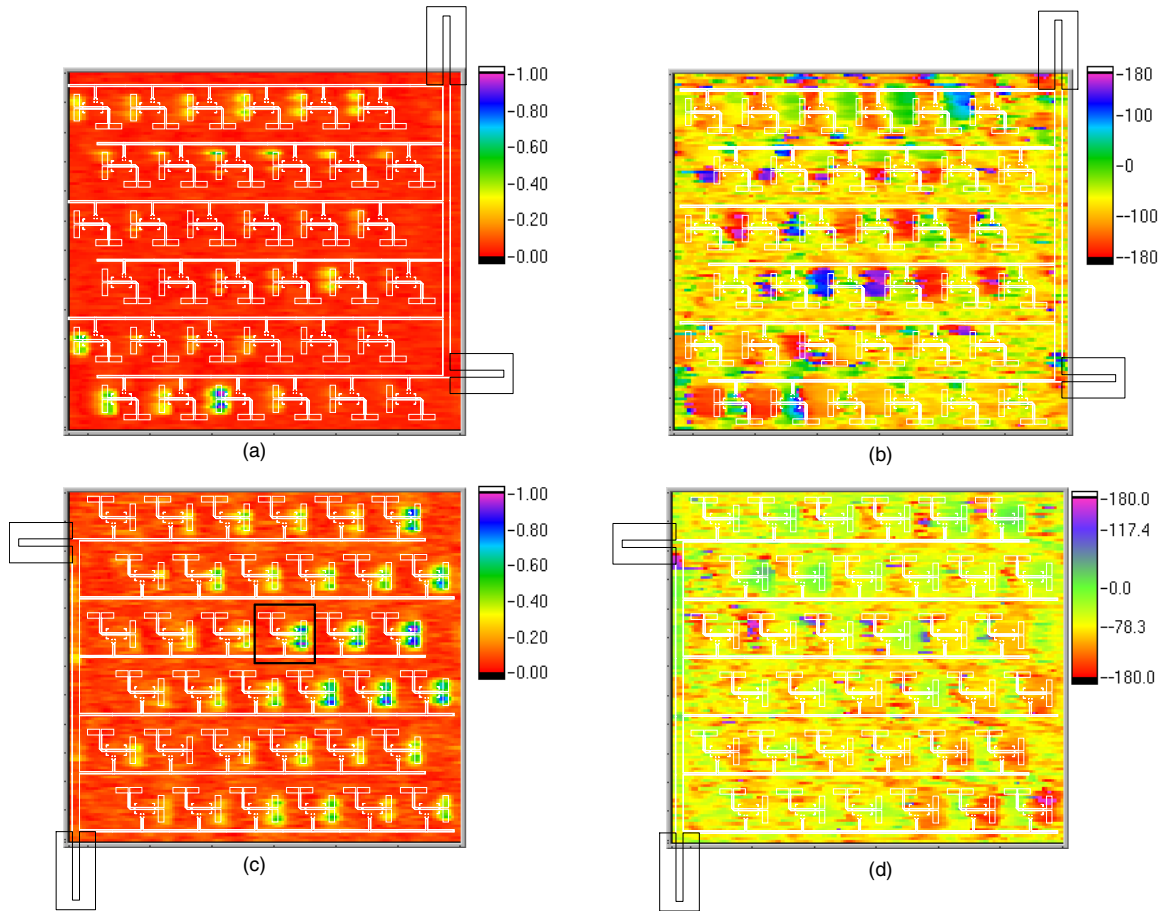


Figure 2.5: Electro-optic field mapping of array type 2A and type 2B. (a) normalized amplitude and (b) phase in degrees of array type 2A; (c) normalized amplitude and (b) phase in degrees of array type 2B. Square box in (c) shows position of the cell used for unit cell measurement. Circuit outline is overlaid.

To examine detailed information on the array, a unit cell is selected (shown in the box in Fig. 2.5 (c)) and measured. The normalized amplitude and phase are shown in Fig. 2.6 (a) and (b). Figure 2.6 (a) displays an excellent symmetry in the amplitude in the output slot antenna. Also, the measured phase in the output slot antenna shows a very uniform distribution, which is, of course, desirable. To obtain a higher resolution result for the unit cell mapping, the scanning step size was reduced to $93 \mu\text{m} \times 100 \mu\text{m}$ and the total scanning area covered $9.3 \text{ mm} \times 10 \text{ mm}$.

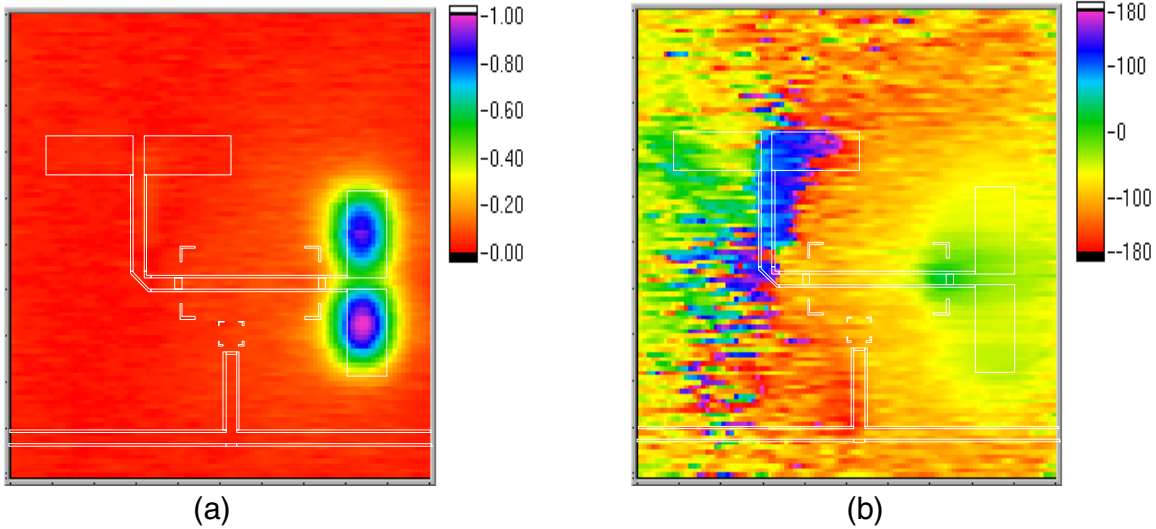


Figure 2.6: Electro-optic mapping result of a unit cell (square box shown in Fig. 2.5 (c)). (a) normalized amplitude and (b) phase in degrees.

Another important measurement for the array would help to determine its rf isolation properties. As shown in Fig. 2.5 (a), poor rf isolation between the unit cells can degrade the performance of the array significantly. It is impossible to feed a single element with the hard horn due to its large aperture. Thus, WR-28 waveguide was used to feed a single element. Also, to examine the position dependence of the isolation performance, unit cells around both the center and the corner of the arrays were selected and fed separately. Figure 2.7 shows the setup for the isolation measurement, including an L-bend connector, the frequency doubler, and the WR-28 waveguide. To confine the output field of the waveguide into one cell, the waveguide was placed directly below the desired unit cell of an array.

To examine the isolation properties, our scanning still covered the full array area, even though only one cell was fed as shown in Fig. 2.7. Figure 2.8 shows the measured amplitude and phase results of array types 2A and 2B when the waveguide was placed under a unit cell in the center of the array. The blue rectangle in the figure represents the position and size of the aperture of the feeding waveguide.

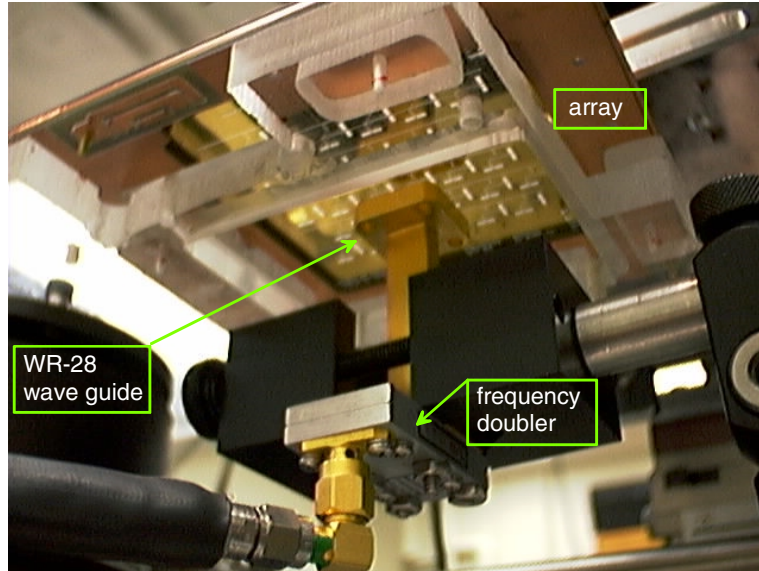


Figure 2.7: Isolation measurement setup picture for array type 2A and 2B. WR-28 waveguide was used to feed one element in the arrays. The frequency doubler generates 31.003 GHz output signal from a 15.5215 GHz input.

As shown in Fig. 2.8 (a), the type 2A array shows a stronger signal in some elements that are far away from the feeding point. One of the possible explanations for this strong cross talk is that the dc bias line behaves as an rf signal wave guide. In other words, the output signal generated by the element fed by the waveguide was transmitted to other elements through the dc bias lines. This transmitted signal acted like an input signal for elements that were isolated from the waveguide feeding. Because the transmitted signal was already amplified by the MMIC of the element that was being fed, the outputs of elements activated by cross talk could be even stronger than the output of the excited element. In Fig. 2.8 (a), several elements show much stronger output signals than the element that was directly fed from the waveguide. Array type 2B (Figs. 2.8 (c) and (d)) shows superior characteristics in terms of rf cross talk suppression. As expected, capacitors mounted along the dc bias lines exhibited excellent performance in suppressing cross talk between individual cells.

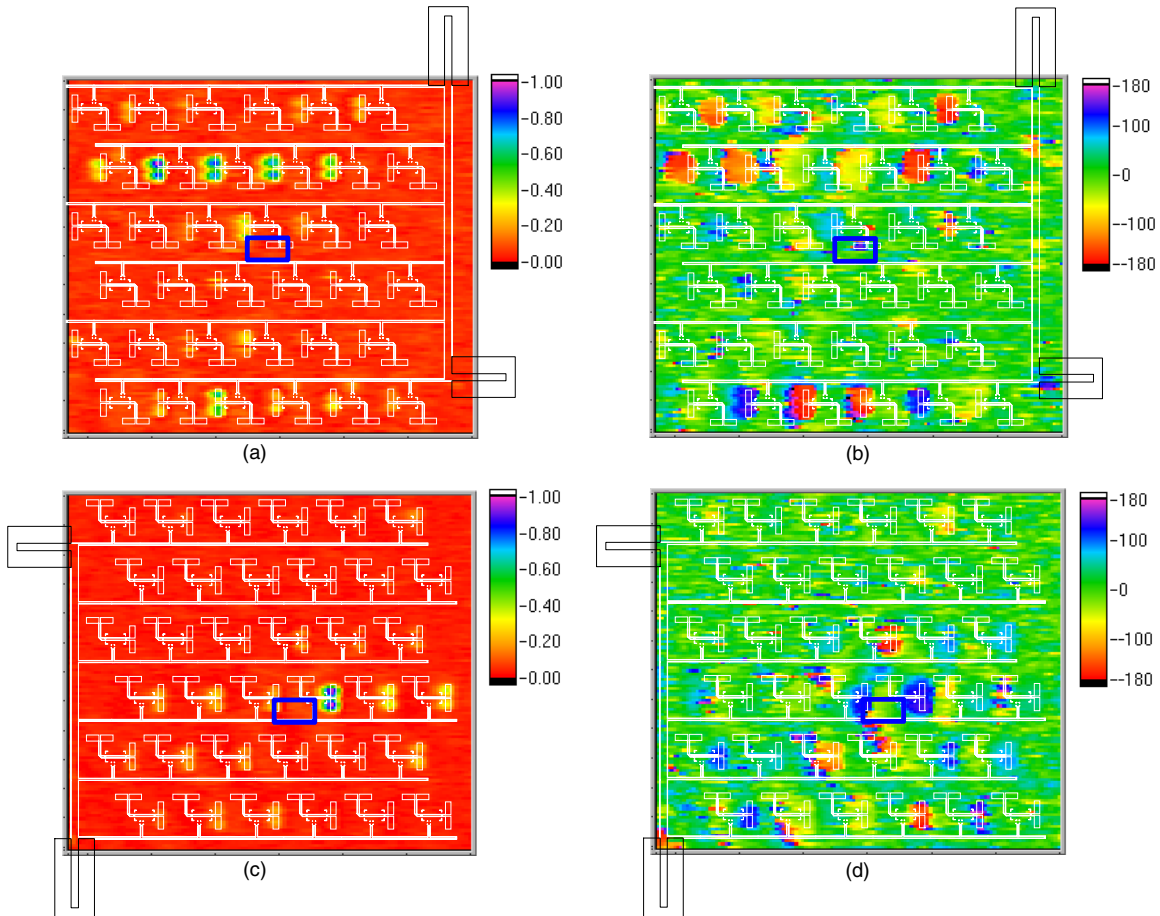


Figure 2.8: Isolation measurement results of array types 2A and 2B. (a) normalized amplitude and (b) phase (in degrees) of array type 2A; (c) normalized amplitude and (d) phase (in degrees) of array type 2B. The blue rectangle represents the position and relative size of the feeding waveguide.

To examine the position dependence of the cross talk property, the feeding point was also positioned around one of the corner unit cells (Fig. 2.9). As shown in Fig. 2.9 (a), the type 2A array measurement result exhibited better isolation characteristics when it was fed near its corner. However, Fig. 2.9 (a) shows a strong output from one element in the bottom row. On the other hand, the measurement result from array type 2B demonstrates a gradually decreasing output signal as the distance from the feeding point increased.

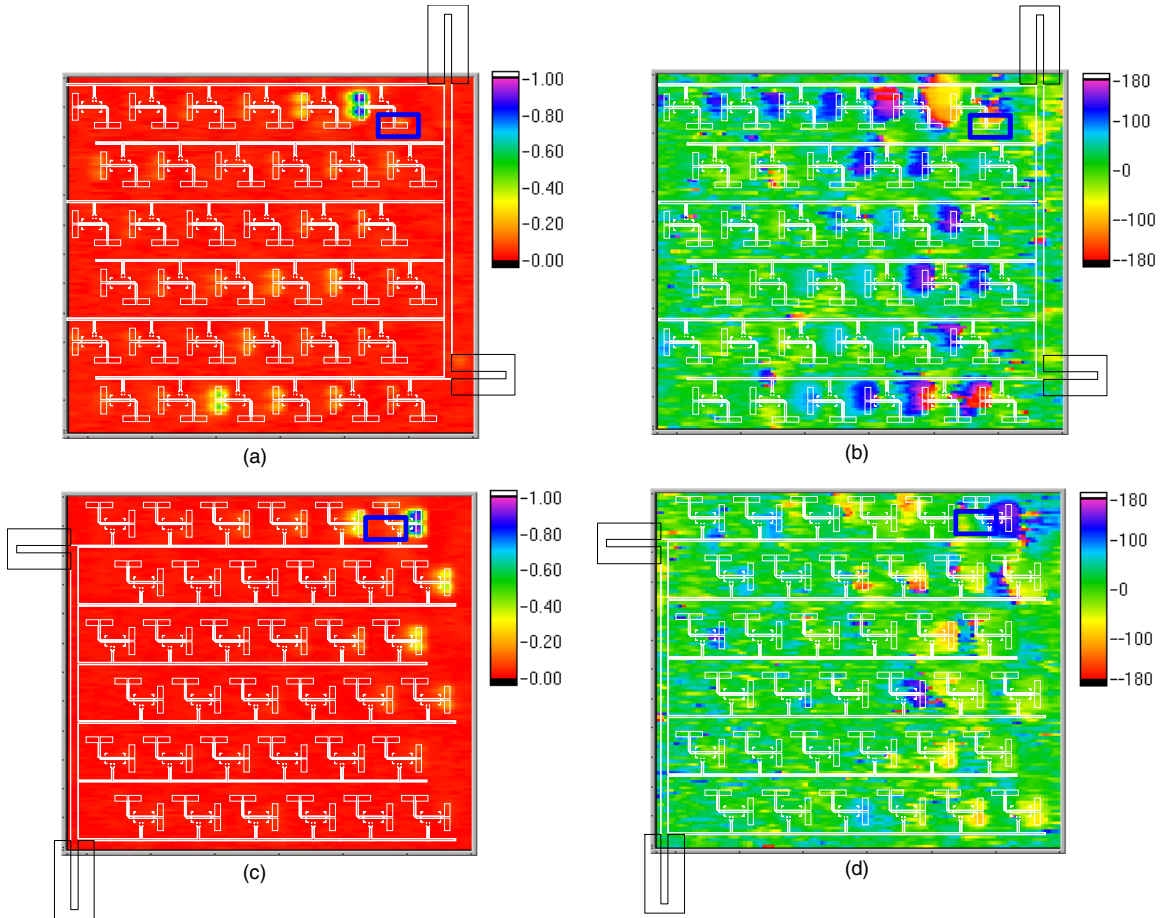


Figure 2.9: Isolation measurement results of array type 2A and 2B. (a) normalized amplitude and (b) phase (in degrees) of array type 2A; (c) normalized amplitude and (d) phase (in degrees) of array type 2B; The blue rectangle represents the position and relative size of the feeding waveguide.

Surface Wave Observation

One new capability, and a distinct advantage of the electro-optic measurement technique with respect to conventional field measurement methods is the capability to capture substrate-propagation-mode waves. Due to the proximity of the electro-optic crystal to the substrate and its high sensitivity, it is possible to detect an electric field traveling through the substrate. Figure 2.10 shows a magnified 2-dimensional amplitude mapping result obtained from the center-feed measurement of array type 2B (Fig. 2.8 (c)). The picture is captured from a real-time animation of the time-varying electric field at one point in space. Also, the amplitude scale is adjusted to enhance the substrate mode wave visibility.

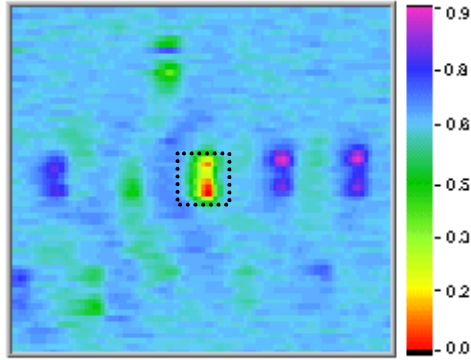


Figure 2.10: Substrate propagation mode wave measurement result (amplitude, in linear scale) of type 2B array for center feeding. The picture is captured during real-time animation. The element that is excited directly by the waveguide feed is shown in the dotted box.

The element that is directly fed from the waveguide is inscribed within the dotted box. The result clearly displays the existence of substrate-mode propagation by concentric peak wave fronts that are displayed in the periodic green areas. This result suggests that the electro-optic measurement system can be a powerful tool for observing real substrate propagation waves, which are very difficult to detect by other conventional measurement techniques. We will continue to explore these important effects and our ability to extract them.

Amplifier Array Utilizing Patch Antennas

Another type of quasi-optic amplifier array that used microstrip patch structures for the input and output antennas has also been measured with the electro-optic field-mapping technique to examine the characteristics and performance of the array. This is the Lockheed-Martin MAFET array. Figure 2.11 shows a picture of the measurement scheme with the array in place. The Lockheed-Martin array has five columns of active cells, and three of those columns have four elements while the other two columns have three elements. The array has two amplifier MMICs per unit cell, one to amplify the input signal before its coupling through the substrate and the other one mounted right before the output patch antenna. Because the main purpose of the measurement is to examine the active cells, scanning has been performed over the active area. The actual scanning area is enclosed by the dotted line in Fig. 2.11.

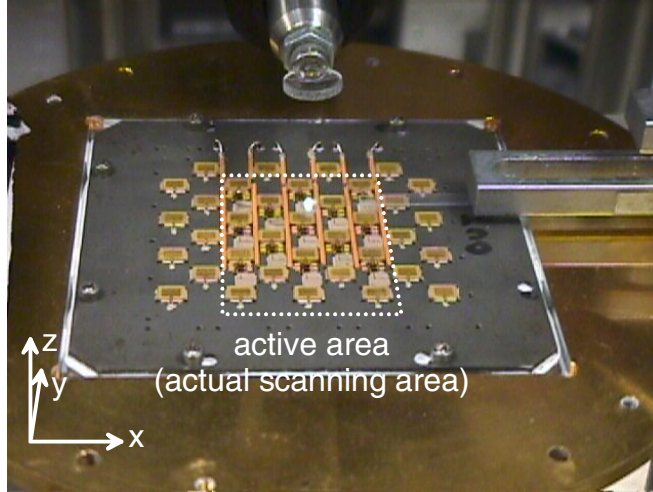


Figure 2.11: Measurement setup for the Lockheed-Martin array utilizing patch antennas. The active area (actual scanning area) is enclosed by a dotted line.

For the measurement, hard horn type B was used as the feeding antenna. The unit step size for the scanning was $284 \mu\text{m} \times 341 \mu\text{m}$, and 100 steps were taken for both the x- and y-directions. Thus the total scan covers $28.4 \text{ mm} \times 34.1 \text{ mm}$ ($x \times y$, area enclosed by dotted box in Fig. 2.11). The total scanning time is around 45 minutes for one complete field map, a time that was reduced when a new, dc-servo x-y translation stage was added to the probe station. Two different types of crystals - BSO for the z component and LiTaO_3 for the x and y components – were again used to sense the three orthogonal field components.

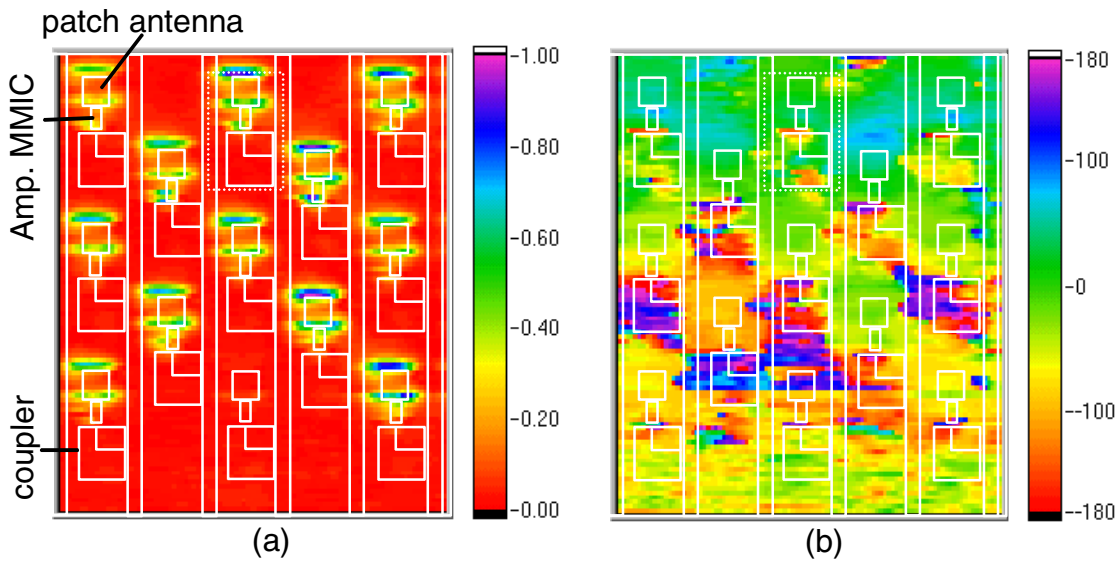


Figure 2.12: Electro-optic mapping result for the array. (a) normalized amplitude and (b) phase (in degrees) of the Lockheed array for the y component.

Figure 2.12 shows one of the measurement results obtained from the electro-optic mapping. Figure 2.12 (a) and (b) display the normalized amplitude and phase (in degrees) of the y component, which is the dominant field component propagating away from the array. Due to the high-resolution of the electro-optic measurement technique, two radiating edges for each of the individual patch antenna are easily distinguished in Fig. 2.12(a). Also the results show a good agreement with the single-patch-antenna measurements that were discussed earlier.

It is quite obvious that one element at the bottom of the middle column was malfunctioning. Also, this element appears to disturb the phase distribution significantly (Fig. 2.12 (b)). However, most of the individual patch antennas show quite a uniform phase distribution. The measurement results demonstrate the usefulness of the electro-optic field mapping technique for the diagnosis and fault isolation of array structures.

This work with Lockheed-Martin is intended to continue, and we should be able to demonstrate field mapping for a high-power amplifier array in the future. We have already assembled a crude anechoic chamber that encloses the device under test, the electro-optic probe, and the microscope and other optical hardware. As such the chamber is designed to protect the environment from high microwave power.

One issue that the interaction with Lockheed has revealed is that when we work at Ka-band frequencies using the passive doubler at ~15-20 GHz, we have very little power available to use at the input to the array under test. It appears that there are two critical locations where we need to add gain to our input rf system: at the Ku-band input to our doubler (to increase its efficiency), and at the Ka-band output of the doubler. This gain must also be from a solid-state source in order to maintain our low phase noise and synchronization to the laser source. Not only do we need this gain to saturate a typical Ka-band quasi-optic amplifier, but it appears that we may suffer from insufficient signal for effective electro-optic measurements at numerous areas at the output of the horns, in the intermediate spaces away from the output radiators of active arrays, and within passive arrays. It seems entirely possible from our work with the Lockheed array that when the signal drops too low, our phase may not track accurately. This is an issue that we are working to address, although we may need to identify additional equipment support to solve the problem completely.

Electro-Optic Mapping System utilizing GaAs Probes

In spite of the many advantageous features of the existing electro-optic field-mapping system, improvements will be necessary. The first controversial issue regarding the system is the invasiveness of the electro-optic crystals to the DUT. To minimize the invasiveness, the electro-optic crystals are polished to a very small area. The smallest crystal has a $20 \times 10 \mu\text{m}$ footprint. Even though miniaturization of the crystals is possible, there are certain limits on the size because of the fact that the polishing relies totally on a mechanical process. Furthermore, the dielectric constants of conventional electro-optic crystals are usually quite large, which can cause distortion of the local electric field distribution.

Fortunately, gallium arsenide (GaAs) is one material that can be used as an electro-optic crystal. GaAs has several advantages over BSO or LiTaO_3 . First of all, it is more convenient to miniaturize, since standard solid-state fabrication processes such as photolithography and various etching techniques can be employed. Also, GaAs has a relatively small dielectric constant (around 12) as compared to BSO or LiTaO_3 . A number of groups have reported the use of GaAs as an electro-optic sensor crystal, although only for normal-field-component detection up to now.

The electro-optic field measurement technique is a practical application of the characteristics of crystal structures that change their optical properties in the presence of electric fields. Thus, the sensitivity of the electro-optic crystal strongly relies on the crystal structure. It is very well known that (100) orientated GaAs has sensitivity to the normal field component (perpendicular direction to (100) surface). However, in spite of the advantages mentioned above, it would not be sufficient to replace conventional electro-optic crystals that can detect three orthogonal field components with GaAs that could only detect one field component. Thus, it is very important to achieve tangential field sensitivity with GaAs for the implementation of a GaAs probe in an electro-optic measurement system.

In order to accomplish this, we have fabricated two different GaAs electro-optic probes. Because the main purpose of this experiment was to examine the possibility of using GaAs as an electro-optic probe that has sensitivity to three orthogonal field components, a simple mechanical cleaving process is used to fabricate the GaAs probe tips instead of microfabrication. For the detection of the field that is perpendicular to the surface of the DUTs (the normal component), a GaAs wafer that has (100) orientation with $600 \mu\text{m}$ thickness is selected and cleaved into a cube that has $1 \text{ mm} \times 1 \text{ mm}$ facets on the bottom and top. For the fabrication of the probe that has tangential field sensitivity, a (110) GaAs wafer with $400 \mu\text{m}$ thickness is selected and also cleaved to a cube that has $1 \text{ mm} \times 1 \text{ mm}$ facets.

To demonstrate the performance of the GaAs probes, the 4-GHz microstrip patch antenna that was used earlier was employed as the DUT. The measurement setup is nearly identical to that used for the other crystal probes, except that the laser must be tuned to wavelengths greater than 900 nm to minimize absorption in the GaAs. Figure 2.13 shows a comparison of the mapping result on the patch when using the GaAs and the BSO/ LiTaO_3 probes. Figure 2.13 (a) and (b) show normalized amplitude and phase results. For the scanning, a $250 \times 200 \mu\text{m}$ unit step size and 80×80 total steps were used.

The total scanning time was ~ 30 minutes. Figure 2.13 shows excellent agreement between the results obtained by the two systems. In the y-component maps, both results show very low amplitude on the impedance matching slots. However, the phase measurement results obtained on both systems display virtually identical abnormal phase distributions around the upper slot that is possibly caused by the same small defect. This y-component comparison reveals the accuracy and repeatability of both systems. Also, the GaAs (110) probe shows superior results to the BSO crystal probe in terms of high definition for both amplitude and phase mapping. The GaAs electro-optic probes show excellent performance and successfully demonstrate three-orthogonal-component measurement capability.

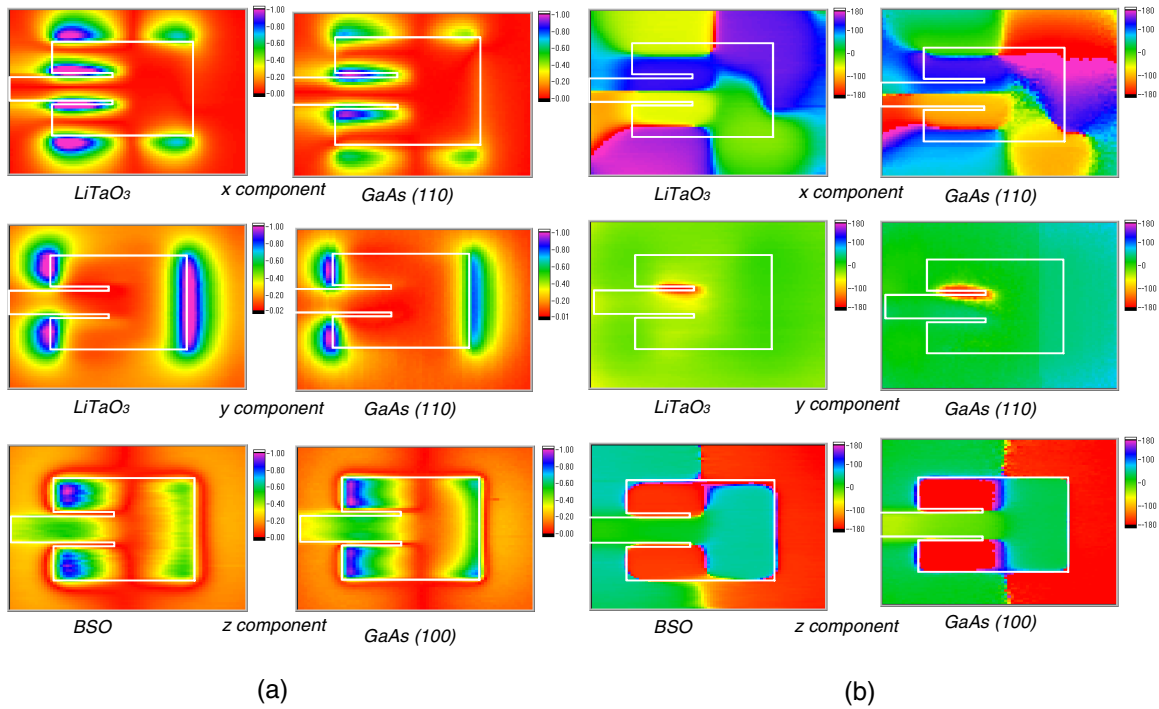


Figure 2.13: Comparison of electro-optic mapping results obtained by BSO/LiTaO₃ and (100)/(110) GaAs-based system. (a) normalized amplitude; (b) phase in degrees.

Figure 2.14 shows electro-optic measurement results from a CPW structure for the normal component using the (100) GaAs probe. The widths of the center conductor, gap, and ground plane are $16 \mu\text{m}$, $35 \mu\text{m}$, and $106 \mu\text{m}$, respectively. The normalized amplitude map clearly shows the peak amplitude occurs on the center conductor (Fig. 2.14 (a)). Also, a good symmetric amplitude distribution can be observed on the center conductor, which implies that the resolution of the measurement is at least $8 \mu\text{m}$ (half width of the center conductor). The phase result shows a 180 degree phase difference on the center conductor and ground plane due to the direction change of the normal field component.

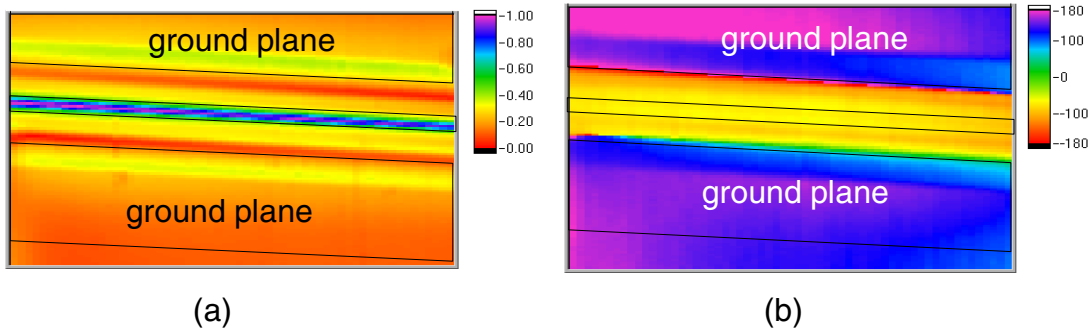


Figure 2.14: Electro-optic mapping result for coplanar waveguide structure – normal component. (a) normalized amplitude; (b) phase in degrees. The (110) GaAs probe was used for the measurement.

The final DUT measured with the GaAs-based electro-optic probes was a frequency multiplier that has a 6X multiplication factor. The input frequency for the multiplier is 16.7205 GHz, and the resultant output signal has a frequency of 100.323 GHz at the output waveguide opening. This output signal includes the 3-MHz IF signal. Figure 2.15 exhibits a 2-dimensional field mapping result of the output opening of the multiplier for the dominant field component. The actual scanning area is 3 mm \times 2 mm, which includes the 2.3 mm \times 1 mm output waveguide openings. Because the dominant component should be parallel to the aperture plane of the waveguide, the (110) GaAs probe was used to detect it. The result shows a reasonable amplitude shape in the output opening. However, the phase distribution is slightly asymmetric. This asymmetric phase distribution can be explained by the fact that the measurement point is too close to the output source. In spite of an asymmetric distribution of phase, the result shows only a small amount of variation over the whole aperture. It also demonstrates that there will not be phase noise problems between the laser and the rf source for frequencies up to W-band, and we are confident that we will be able to characterize quasi-optic power combining devices at these frequencies.

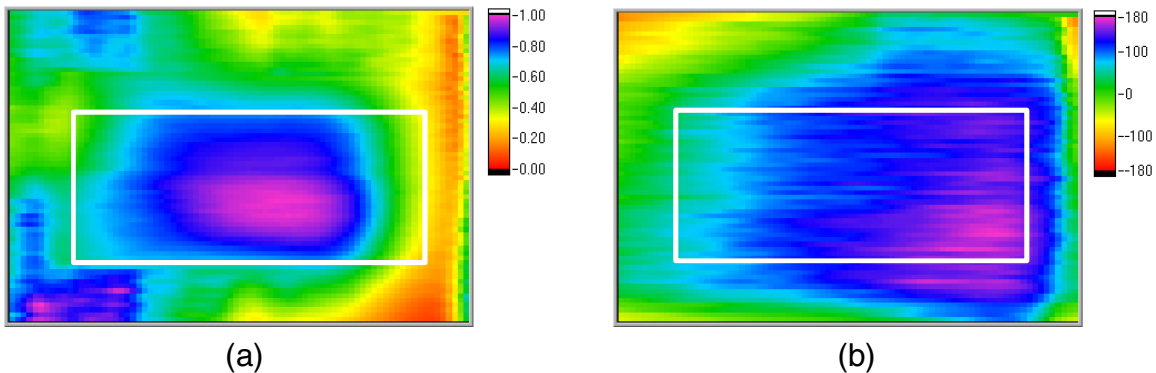


Figure 2.15: Electro-optic field mapping results from a 6 \times frequency multiplier for the dominant component. Input frequency: 16.7025 GHz; output frequency: 100.323 GHz. (a) normalized amplitude; (b) phase in degrees.

3. Amplifier Arrays

Finite Difference Time Domain Simulation of a Microstrip Array in Hard Horn

The use of hard horns in power combining was reported in [T. Ivanov, and A. Mortazawi, *IEEE Microwave and Guided Letters*, vol. 6, pp. 88-90, 1996.]. By applying a uniform field across the microstrip patch antennas that feed the active devices, efficient power combining can be achieved. The goal of this project is to be able to simulate and analyze such structures to improve power combining efficiency and output power. For simulation purposes, coaxial fed microstrip patch antennas are considered. Finite difference time domain (FDTD) technique is chosen to simulate the structure consisting of coaxial fed microstrip patch antennas inside a hard horn. The aim is to calculate the input impedance seen from the antenna ports at the inputs of each amplifier so that the amplifiers can be matched for maximum power. Also, other issues such as resonance frequency shifts, coupling and spacing among the antennas will be investigated.

The FDTD approach taken here is to calculate the input impedance seen at each antenna port by applying a Gaussian pulse to each port while terminating the other ports and the feed point of the hard horn with absorbing boundaries. Since FDTD is a time domain method, FFT will be used to get the required information in the frequency domain. One advantage of FDTD compared to other techniques such as method of moments and FEM, modal decomposition is not required to calculate the total reflection coefficients at the antenna ports, since the solution is done in the time domain.

The FDTD simulations are going to be used to predict the correct placement of antennas for minimum reflections and maximum power absorption from the hard horn. The effect of having microstrip antennas in the transverse plane of the hard horn and how they disturb the predicted uniform field across the horn aperture will be investigated. Uniform field is required to simultaneously saturate all the amplifiers.

Performance of a Slotted Waveguide Power Divider

As part of studying different approaches for feeding spatial amplifiers, we designed and constructed a 14W X-band slotted waveguide array [14]. We are engaged in understanding and comparing this feeding technique with Wilkinson based power dividing and hard horn feeds. The basic feed mechanism is shown in Fig. 3.1. Each slot is coupled to an open circuited microstrip line extended beyond the slots. It is a well known fact that the microstrip line appears as a series impedance to the slot; and looking from the input port of the waveguide, the slots appear as shunt elements joined with transmission lines. The slot behaves as an impedance transformer, effectively transforming the impedance seen in the waveguide to that of the microstrip line to achieve transfer of power.

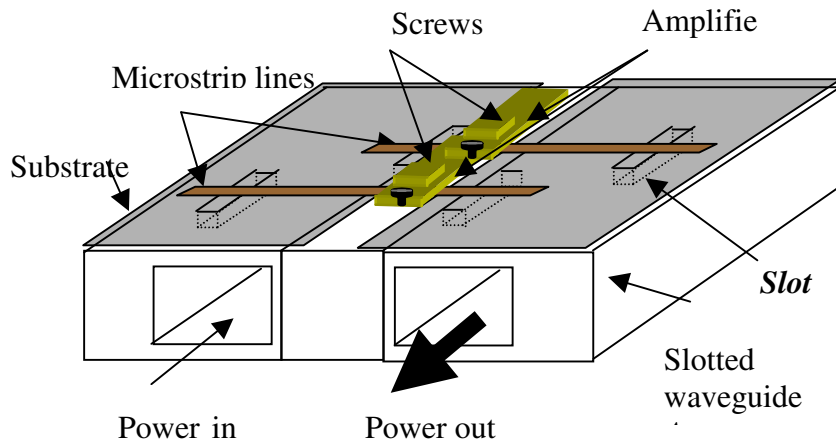


Fig. 3.1. Feed mechanism of slot array.

To understand the overall tolerance of the power amplifier due to active device parameter variation and imperfections of the power combining/dividing distribution circuit, we must focus on the inaccuracies that cause degradation in power combining efficiency. The resonant nature of this power amplifier implies that the combining efficiency is dependent on the phase deviation introduced due to imperfections in slot to slot separation in the power distribution circuit. The equivalent circuit for the slotted waveguide is given by shunt elements separated with transmission lines of an electrical length of 180 degrees. The phase of the input signals to the slots must satisfy certain conditions to achieve perfect power combining. Thus, the phase deviation of the slotted waveguide and its effect on the fractional bandwidth and power combining efficiency can be analyzed by introducing phase errors for an N-way divider/combiner.

The slot admittance seen at the waveguide port is of importance to achieve input match. Since the slot behaves as a transformer, the admittance loading due the input and output device parasitics will affect the slot admittance. Thus, the device parasitics variation and its effect on the slot admittance and the overall combining efficiency can be taken into account. The effect of device failure and gain variation can be analyzed by applying proper signals to the microstrip input/output ports. Furthermore, to better represent the gain variation under different input power levels, nonlinear models can be used to characterize the active elements, instead of the small signal S-parameters provided by the manufacturer.

The analysis was carried out for an eight way slotted waveguide divider (Fig. 3.2). A phase deviation $\Delta\phi$ (± 20 degrees) from 180 degrees was introduced in slots. In addition to the phase variation of the last 3 slots, the slot susceptance was also varied randomly from $\pm j20$ Ohms. The effect on the return loss is more prominent in the ± 2 degrees region of the depicted curves.

In summary, we are in the process of combining the results from Ka band amplifier array measurements with field-circuit simulations to be able to determine the tradeoffs in various feeding techniques for the excitation of quasi-optical amplifiers. Furthermore, we are determining the performance dependence of these arrays to the amplitude and phase variation across them.

4. Oscillator-Based Power Combining

In 1997 and early 1998, Clemson University sustained an activity on grid-oscillator power combining. The principal result of this work was the locking of the grid to a reference source and the application of the phase-locked loop for phase modulation of the radiated signal. These results are summarized in an IMS publication, that is included in the Appendix. The essence of the result is that the oscillator was locked to a microwave synthesizer so that the field radiated from the oscillator displayed a phase noise characteristic comparable with that of the reference to which it was locked. PSK modulation was achieved at 1 MHz, and is clearly sustainable at higher frequencies. (The limitation on modulation frequency excludes *slow* modulation. The frequency of the modulating signal has to be high compared with the 10 kHz bandwidth of the PLL.

Results of amplitude distribution measurements of a 4×4 grid in the Michigan electro-optic scanner were not as encouraging. A substantial phase gradation across the radiating aperture is observed, with concomitant skewing of the main beam direction in the radiation pattern. These results were reported in our previous annual report. In 1998, Clemson University workers fabricated an 6×6 version with the same cell design employed in the earlier work. It was intended that this device be measured in the Michigan facility so that results could be related to those on the 4×4 grid. However, the tuning of this device proved quite problematic. Although all cell features and devices were the as in the 4×4 design it is highly prone to exhibit multiple independent resonances. It can be tuned so that all oscillators couple at a single resonant frequency and phase lock can be achieved for this resonance. However, the stability of this oscillation is marginal. For this reason, time and effort was not invested in the near-field measurement. Modeling at North Carolina State University has corroborated the phase shift phenomenon. It is possible to suppress all but a cophasal operating mode in coupled oscillators with so-called “mode killer” resistors. Grid oscillators are not amenable to mode killing, however. We have discontinued further pursuit of grid geometries.

Mortazawi and his proteges have demonstrated a MESFET oscillator loaded by a circular patch antenna that is amenable to mode killing and has demonstrated particularly impressive combining efficiency results. This design is realized in microstrip with the design control incumbent therewith. Clemson University has begun to explore coupled oscillator systems based on Mortazawi’s cell. We have reproduced Mortazawi’s results and have extended the array design to include tuning transmission line sections in edge elements. When arrays are built with identical units of this oscillator cell, we observe some propensity toward multiple independent oscillations. However, the edge-trimming lines can be used to trim edge elements and achieve a single coherent oscillation.

Figure 4.1 shows the layout of the modified version of this oscillator. The adjustable tuning stubs are noted on the layout, as are the coupling gaps across which mode-killing

resistors are mounted. The high impedance meander lines serve to pass DC bias around the resistors. (Inability to place such a line on a grid design precludes the use of mode-killing resistors in grids.) One noteworthy feature of this design has come to the surface in the course of our realizations of this design. Namely, the coupling from one cell to another, which occurs along the path with the resistor gaps, is sensitive to the width of the gap. This indicates that capacitance between the edges of the gap dominates any coupling through the (50 Ohm) mode-killing resistors in coupling adjacent cells. Mortazawi indicates that the gap size in the original design was chosen strictly on the basis of the size of the resistor to be mounted there. We began our work employing a larger resistor package with concomitantly wider gap. Reducing the gap width so that the lines project under the resistors a modest distance restores the original coupling and the system oscillates coherently. Preliminary results suggest that this design is readily amenable to both injection locking and phase locking.

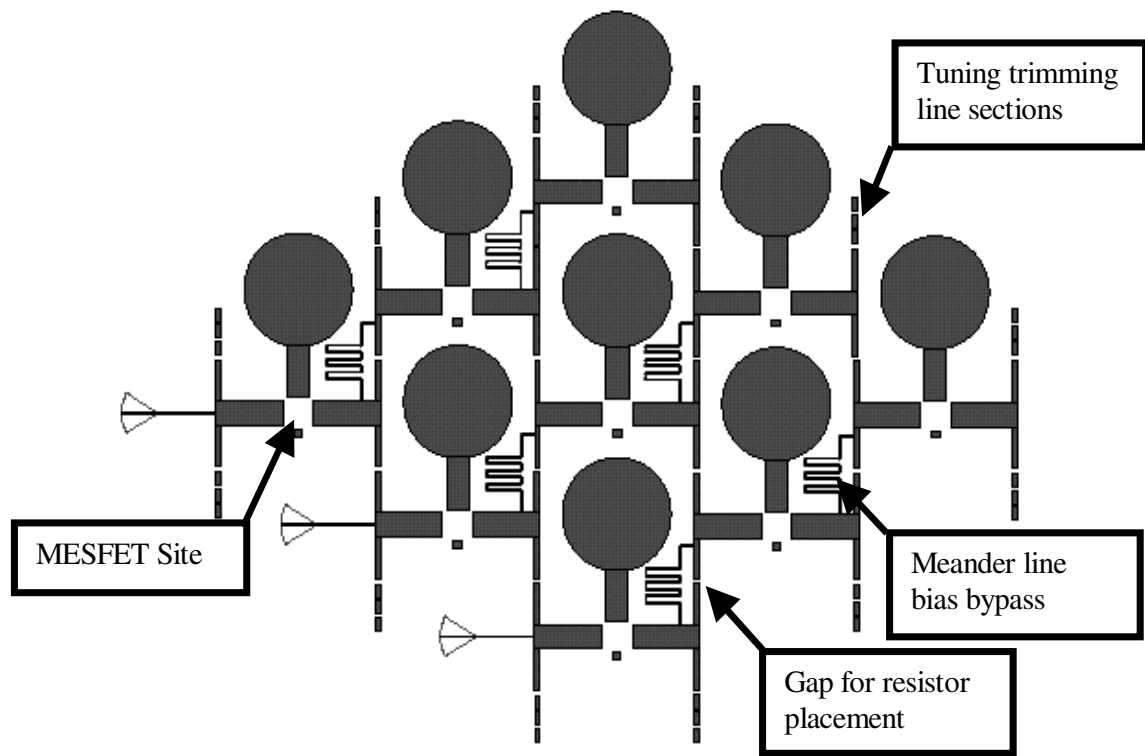


Fig. 4.1 Mortazawi's array design with tuning modification

We expect to employ the array design discussed above as a preliminary design for the study of electronic scanning through control of edge elements only, as proposed by York and developed theoretically by Pogorzelski, *et. al.*

5. Characterization Issues

Accurate characterization of radiation performance of spatial combining systems is essential to placing the technology on a sound scientific footing. A key performance measure in any power-radiating system is efficiency. Efficiency cannot be determined accurately without an accurate knowledge of total radiated power. Virtually all system evaluations, to date, have been characterized in terms of an *ad hoc* assumption regarding the directivity in the radiation field, and indeed the entire lobe structure of the radiation pattern. The efficiency thus obtained is an *estimate* that depends critically on the quality of the assumption about radiation pattern.

To the end of accurate power characterization, we are developing a small anechoic chamber capable of accurate pattern measurement and thereby enabling the evaluation of the pattern integral to obtain total radiated power. The chamber is designed for operation between 10-110 GHz and is RF shielded to ensure the safety of operating personnel in the measurement of systems with significant output power levels.

Shield-to-shield dimensions of the structure are 4×4×10 feet. The chamber is to be lined with Rantec EHP-3 (3 inch tall) absorber. Rantec has performed limited reflectivity tests on this absorber through W-band in an installation at Ohio State University. By employing this absorber *without paint*, they have obtained monotonic improvement of reflectivity through W-band with reflectivity decreasing from -45 dB at X-band to -64 dB at W-band. Standard painting of the absorber results in an initial decrease in reflectivity that returns to -44 dB in W-band. A photograph of the structure for the chamber with copper foil shielding in place is shown in Fig. 5.1.



Fig. 5.1. Millimeter wave anechoic chamber under construction. Copper shielding is in place. Graduate student Jabberia Miller is responsible for this activity.

The chamber will be equipped with Newport positioning equipment designed for precision optical measurements, thereby providing positioners of a size and accuracy

suites for millimeter-wave measurements. The device under test can be rotated in azimuth and polarization, while the “source” antenna rotates in polarization. These degrees of freedom allow measurement of the DUT over 4π steradians, both in the principal- and cross-polarized field components. The azimuth positioner is stacked with a translational positioner so that free-space VSWR measurements can be made to characterize the errors present due to reflections from the chamber walls.

The electrooptical system described in subsection 2 above is well suited to research characterization of electromagnetic systems, both radiating apertures and monolithic circuits. An alternative approach to the characterization of a radiating aperture is that of RF holography. The field of a radiating aperture is scanned with a probe antenna—typically an open-ended waveguide—across a measurement aperture several wavelengths away. Because the probe antenna is electrically large, the data are corrected for the spatial receiving properties of the waveguide and then transformed from the measurement plane to the aperture plane. The computed aperture plane data constitute a holographic image of the aperture plane. Through standard Fourier-transform aperture-radiation calculations, the far field pattern over the hemisphere above the imaging plane can be computed, also.

It is instructive to compare and contrast the holographic imaging method with the electro-optic nearfield scan. The holographic method implicates only radiation fields, a consequence of the placement of the scanning plane several wavelengths from the aperture of the device under test. Thus, the so-called invisible spectrum, which carries the detailed quasi-static fields existing in the aperture, is lost. The image of the aperture is somewhat coarse in resolution as a result. In balance, however, this measurement uses standard laboratory RF equipment. Apart from a servo system for positioning the probe, no unusual equipment is required. This recommends the method for production assay of radiating apertures and for adjustment oriented measurements.

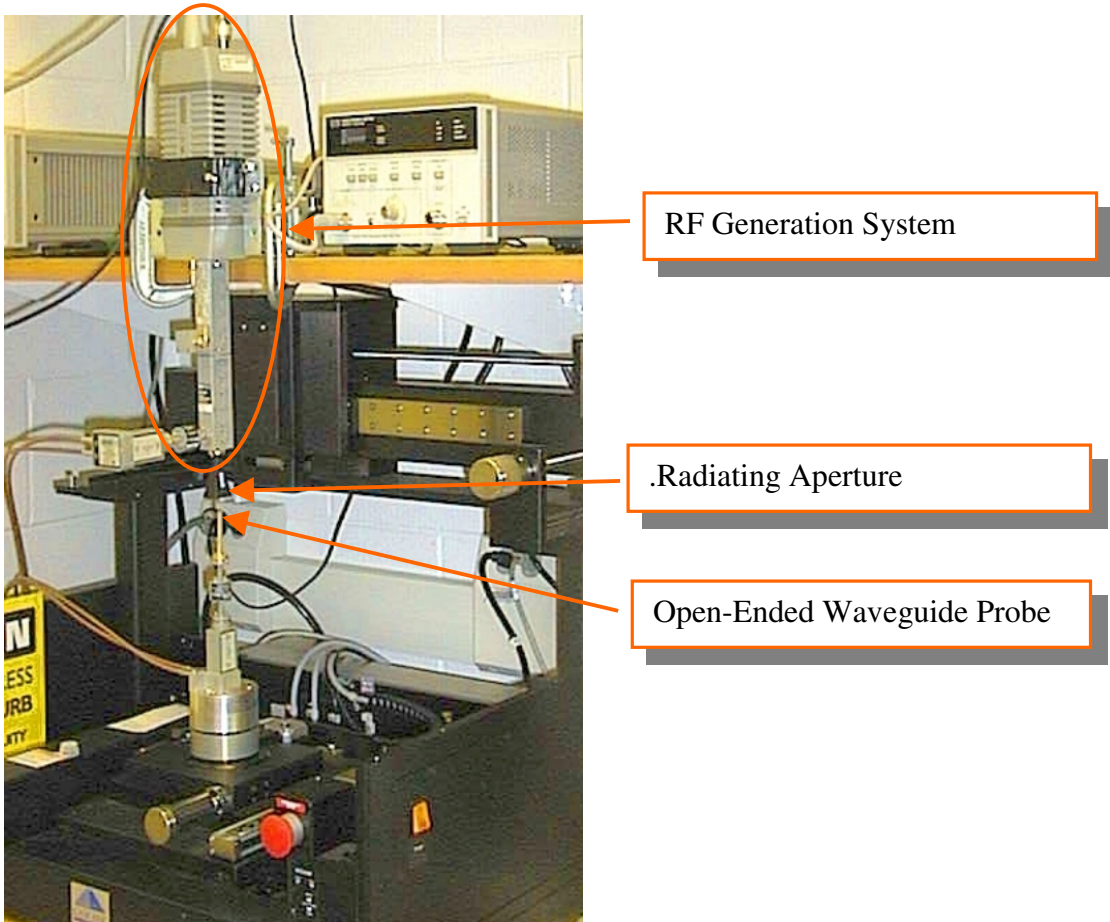


Fig. 4.2. Millimeter-wavelength Scanning System with Absorber Removed. An HP W-band source drives a pyramidal horn, which is scanned by an open-ended waveguide.

Clemson University received DURIP funding from the Ballistic Missile Defense Organization to purchase a Cascade wafer-probing station that is adapted to serve as the scanner robot for a nearfield system for millimeter wave systems. The system, as modified is picture in Fig. 4.2. In the figure, one can identify overhead an HP W-band multiplier signal source that feeds a pyramidal horn antenna (black with small white label). An open-ended waveguide probe (gold) is fixed below. The source is fixed and the waveguide scans the measurement plane under control of the Cascade Probe Station. RF absorber is in place when measurements are underway to remove the surrounding reflecting surfaces from the measurement. Data is captured by an HP receiver and the control computer (not shown).

6. Thermal Characterization

Milestones achieved

A coupled electrical/thermal model has been constructed. The electrical component is based on the Leeds quasi-2D HEMT model. This couples a Schrodinger-Poisson charge control model, to a hydrodynamic description of in-plane transport with hot electron effects. Temperature dependence enters the model via the description of mobility. The thermal component is based on analytical solution of the heat diffusion equation, with adoption of a thermal resistance matrix approach for electrical iteration.

Key features of the electro-thermal model include: treatment of arbitrary layouts of surface heating elements; incorporation of non linear conductivity (Kirchhoff Transformation); generation of a thermal equivalent circuit model for CAD; treatment of heat shunts, multilayers, ...; and treatment of radiative and convective surface cooling. On the experimental side, experimental imaging equipment and MMICs have been specified and obtained.

Theory

The analytical thermal resistance matrix approach has been extended to include a (linear) radiation boundary condition. This means that nonlinear surface fluxes are now only a perturbation on the linear analytical solution, improving solution stability. The case of purely radiative and convective cooling can now be treated, without the need to assume heat sink cooling. The thermal resistance matrix concept has been generalized to allow 'near exact' flux and temperature interface matching by discretizing the interfaces. Hierarchical treatment of MMIC-on-substrate grid arrays has been implemented and fully coupled electrothermal simulations performed. Full treatment of nonlinear surface boundary conditions and non linear interface matching has been achieved, within the framework of the linear thermal resistance matrix approach. This leads to formulation of a non linear system of equations for the coupled electro-thermal model, soluble by Newton methods. The steady-state thermal resistance matrix approach has been generalized to treat the time-dependent case in Laplace transform space, i.e. a thermal 'impedance' matrix approach has been developed containing description of capacitive and transient effects. The Laplace transform approach means that all features of the steady-state approach immediately carry over to the time-dependent case.

Experiment

An Inframetrics ThermaCAM PM280 has been installed. Passive grid arrays have been constructed and a 38 GHz balanced amplifier MMIC obtained for thermal studies. Thermal measurements have been performed to study the effects of radiation, convection and heat sink mounting.

Joint Theory/Experiment

The first fully-coupled electrothermal calculations of a single 38 GHz balanced amplifier MMIC, mounted on freestanding FR-4 substrate, have been performed for model validation against thermal measurements.

IV. Theoretical developments

A. Radiation Boundary Condition

Steady-state problem for $0 < x < L$; $0 < y < W$; $0 < z < D$

$$\nabla \cdot [n(T)\nabla T] = 0 \quad (1)$$

subject to adiabatic b.c.'s on side walls (simple, but not necessary)

$$\left. \frac{\partial T}{\partial x} \right|_{x=0,L} = \left. \frac{\partial T}{\partial y} \right|_{y=0,W} = 0 \quad (2)$$

and “radiation b.c.” at top and bottom surfaces $z = 0; D$

$$\alpha_{0,D} \kappa(T) \left. \frac{\partial T}{\partial z} \right|_{0,D} + H_{0,D} (T - T_{0,D}) + p_{0,D}(x, y) = 0 \quad (3)$$

$\alpha_{0,D}$, $H_{0,D}$ and $p_{0,D}$ can each be zero. $\alpha_{0,D}$, $H_{0,D}$ and $T_{0,D}$ can all be functions of $(x; y)$. $p_{0,D}$ corresponds to power density due to surface heating elements. $H_{0,D} (T - T_{0,D})$ corresponds to imposed temperature (for $\alpha_{0,D} = 0$), or ‘radiative’ flux (for $\alpha_{0,D} \neq 0$).

1 Validity of linear radiation b.c.

Radiative fluxes vary as $(T^4 - T_0^4)$, fluxes due to natural convection as $(T - T_0)^{5/4}$, forced convection as $(T - T_0)$.

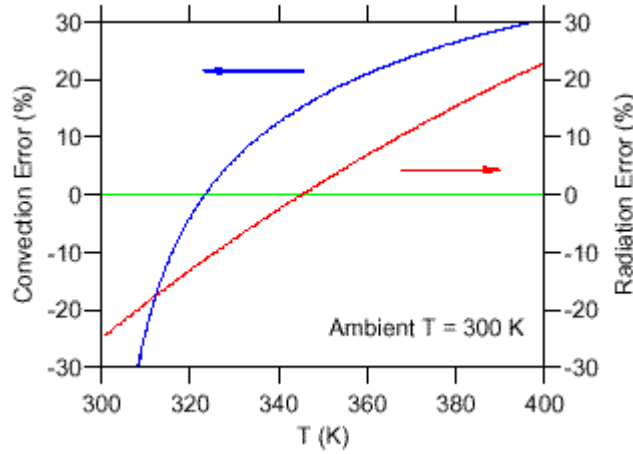


Fig. 6.1. Typical Linearizations

Remaining non linear flux contributions, not fully included in the linear “radiation” term, provide a non linear perturbation which is treated iteratively. Figure 6.1 shows that the relative magnitude of the nonlinear perturbation is typically ~10 % in thermally well managed systems. Absolute magnitudes can be much smaller than this, if the majority of heat flow is by conduction.

2 Radiative loss variation with area

Total power dissipation due to black-body radiation is given by

$$P_{rad} = A \epsilon \sigma (T^4 - T_0^4) \quad (4)$$

and is dependent on surface area A.

For a typical transistor finger, $A \sim 200 \times 50 \mu\text{m}^2$ and $T \sim 500^\circ\text{K}$, so that $P_{rad} < 4 \times 10^{-5} \text{W}$. This means $P_{rad} \ll 1 \text{W}$ corresponding to typical power dissipation.

For a typical MMIC, $A \sim 1 \times 1 \text{mm}^2$ and $T \sim 400 \text{K}$, so that $P_{rad} < 10^{-3} \text{W}$. This means $P_{rad} \ll 1 \text{W}$ corresponding to typical power dissipation.

Finally, for a typical grid-array substrate, $A \sim 10 \times 10 \text{cm}^2$ and $T \sim 350 \text{K}$, so that $P_{rad} < 8 \text{W}$ (for radiative loss from two sides). This means $P_{rad} \sim 10\text{-}100 \text{W}$ corresponding to typical power dissipation. So only in the case of large area substrates are black-body losses significant in absolute terms. Similar arguments for convective losses mean adiabatic boundary conditions are a good approximation for small elements such as MMICs, simplifying the corresponding thermal resistance matrix description.

Grid Arrays: Hierarchical Treatment

Analytical solution of the steady state heat diffusion gives an expression for R_{TH} based purely on geometrical information. Then surface temperature rises $\Delta\theta_i$ over elementary areas D_i are related to corresponding surface power densities P_j , $j = 1, \dots, N$, by

$$\Delta\theta_i = \sum_j R_{TH_{ij}} P_j \quad (5)$$

In a hierarchical solution, R_{TH}^{MMIC} for the MMICs and R_{TH}^{subs} for the substrate are both constructed.

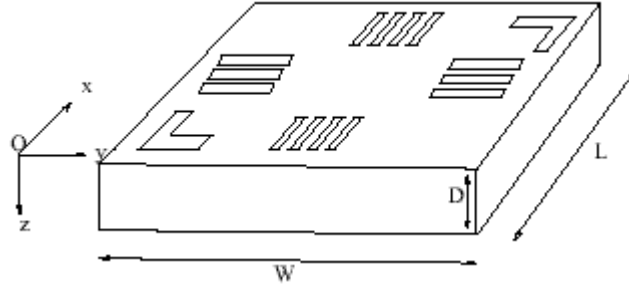


Fig. 6.2. Generic Cuboid

The generic cuboid of Figure 6.2 represents both individual MMICs, with heating by active and passive devices, and the grid array substrate with surface heating by MMIC bases.

“Near Exact” Interface Matching

Interface matching currently assumes uniform flux and temperature over the interface. Discretizing the interface, to match (average) temperatures θ_k^{int} , over elementary areas D_k , Eq. (5) becomes

$$\theta_i = \sum_j R_{TH_{ij}} P_j + \sum_k Z_{ik} \theta_k^{int} \quad (6)$$

where Z_{ik} is constructed analytically and interface matching is exact in the limit of infinitely fine discretization. A corresponding equation holds for matching of flux at the discretized interface, P_l^{int} ,

$$P_l^{\text{int}} = \sum_j S_{TH_{lj}} P_j + \sum_k T_{lk} \theta_j^{\text{int}} \quad (7)$$

Non Linear Interface Matching

When the temperature dependence of the thermal conductivity differs between matched layers, say substrate and MMIC base, matching of linearized temperatures involves a nonlinear relation

$$\theta_i^{\text{sub}} = NL(\theta_i^{\text{MMIC}}) \quad (8)$$

In matrix notation, Eqns. (6) and (7) for MMICs $n = 1; \dots; N$ of a grid array, become

$$\underline{\theta}_n = \underline{R}_{TH}^{\text{MMIC}} \underline{P}_n + \underline{Z} \underline{\theta}_n^{\text{int}} \quad (9)$$

$$\underline{P}_n^{\text{int}} = \underline{S}_{TH} \underline{P}_n + \underline{T} \underline{\theta}_n^{\text{int}} \quad (10)$$

Then the thermal resistance matrix equation for the substrate gives rise to the nonlinear system for the interface temperatures

$$NL(\underline{\theta}_n^{\text{int}}) = \sum_m \underline{R}_{TH_m}^{\text{sub}} (\underline{S}_{TH} \underline{P}_m + \underline{T} \underline{\theta}_m^{\text{int}}) \quad (11)$$

in terms of the surface ux densities P_m , so that Eq. (9) provides a nonlinear relation between surface temperatures $\underline{\theta}_n$ and surfaces fluxes \underline{P}_m for the MMIC grid array. Substrate thermal resistance matrix R_{TH}^{sub} is partitioned into submatrices $R_{TH_m}^{\text{sub}}$. This is the extension to the nonlinear hierarchical case, of the standard linear thermal resistance matrix equation, Eq. (5).

Nonlinear Surface Boundary Conditions

Use of the linear radiation boundary condition, Eq. (3), does not fully describe non linear surface fluxes. The remaining nonlinear perturbation can be treated by including it as an additional flux in the imposed flux term $p_{0,D}(x, y)$ of Eq. (3). This requires discretization of the whole of both faces of the grid-array substrate (surface losses are negligible over smaller areas, Sec. IV-A.2). This gives immediately the following nonlinear relation for the surface temperature rises $\Delta\theta_i$

$$\Delta\theta_i = \sum_j R_{TH_{ij}} P_j - \sum_r Q_{TH_{ir}} nl(\theta_r) - \sum_s V_{TH_{is}} nl(\theta_s^{\text{rev}}) \quad (12)$$

in terms of the imposed surface fluxes P_j . The substrate surface temperatures on the front, θ_r , and reverse sides, θ_s^{rev} are given by similar equations in terms of the surface flux nonlinearity, $nl(\theta)$, and thermal resistance matrices such as $Q_{TH_{ir}}$ and $V_{TH_{is}}$. This system of nonlinear equations provides the nonlinear relation between the surface temperature rises, $\Delta\theta_i$, and surface flux densities, P_j , corresponding to the standard thermal resistance matrix equation, Eq. (5), in the case of the linear radiation boundary condition, Eq. (3).

This approach then provides a full treatment of surface flux nonlinearity based on the purely linear thermal resistance matrix description.

Fully Nonlinear Electro-Thermal Problem

The results of Sections IV-D and IV-E, together with the Leeds Physical Model, provide a description of the coupled electro-thermal problem giving a full treatment of thermal and electrical non linearity. The coupled electro-thermal problem can be expressed

$$\theta_i(P_1, \dots, P_N) - \phi_i(P_i) = 0 \text{ for } i = 1, \dots, N \quad (13)$$

Here, the non linear function $\theta_i()$ returns device channel temperatures θ_i as a function of device power dissipations P_j , $j = 1, \dots, N$, in a fashion determined by the thermal resistance model, as described previously. The term $\phi_i(P_i)$ states that channel temperature ϕ_i is related uniquely to the corresponding power dissipation P_i as determined by the Leeds transistor model.

The full nonlinear electro-thermal equation, Eq. (13), is amenable to solution by Newton methods, for which non linear function evaluations reduce to small thermal resistance matrix multiplications, and simple nonlinear function evaluations, $NL(\theta)$ for interfaces, and $nl(\theta)$ for surfaces. Solution of the corresponding linear problem is immediate and provides a good first guess to the iterative Newton solution. Economical nonlinear function evaluation, availability of a good first guess, and reduction of the thermal nonlinearity to a small perturbation by linearization about the radiation boundary condition, imply stable, rapid solution.

By generation of the $\phi_i(P_i)$ (at a given bias) for a finite range of P_i over the expected range of iteration, storage of the results and physically based interpolation, the nonlinear electrical description based on the Leeds Physical Model becomes computationally economical. It reduces to evaluation of near-analytical function and derivatives, $\phi(P)$, so is rapid and storage requirements are modest. The accuracy and fully predictive nature of the physical electrical model are retained.

The thermal resistance matrix approach therefore offers an efficient treatment of the fully nonlinear coupled electro-thermal problem.

Thermal Impedance Matrix

The time-dependent heat-diffusion equation is

$$\nabla \cdot [\kappa(T) \nabla T] = \rho C \frac{\partial T}{\partial t} \quad (14)$$

Making the Kirchhoff transformation for linearized temperature θ , then taking the Laplace transform, $\mathcal{L}[\{\theta(t)\}] = \bar{\theta}(s)$, the thermal resistance matrix description immediately generalizes to give

$$\bar{\theta}_{av_i} - \frac{\theta_0}{s} = \sum_j R_{TH_{ij}}(s) \bar{P}_j \quad (15)$$

where θ_0 is initial temperature, $R_{TH_j}(s)$ is almost identical to the steady-state case, and P_j is now the transform of the time-dependent surface flux over elementary area D_j .

This relation can be employed directly in s -space, or converted back to the time-domain by use of the inversion formula

$$\theta(t) = \frac{1}{2\pi i} \int_{\gamma-i\infty}^{\gamma+i\infty} e^{st} \bar{\theta}(s) ds \quad (16)$$

where the contour integral is evaluated as $2\pi i \times$ sum of residues). This thermal impedance matrix approach will allow treatment of “turn-on” thermal transients and pulsed operation. The direct similarity between the steady-state and Laplace transform space solutions, means that all features of the steady-state solution transfer almost directly to the time-dependent case in Laplace transform space. Where analytical inversion is impractical, the increased cost of treating time-dependence translates into the need to solve repeatedly for different values of transform parameter s .

Experimental Measurements

1. Thermal Measurements: 38 GHz MMIC

Figure 6.3 shows a 3-stage, 38 GHz, balanced amplifier array, measured using an Inframetrics PM280 Thermacam with a 15 μm resolution ZnSe microscope lens. Center temperature is 87 $^{\circ}\text{C}$; edge temperature 80 $^{\circ}\text{C}$. Figure 6.4 shows the thermal image of reverse side of the freestanding FR-4 substrate. The MMIC was attached by Ag epoxy onto a Cu strip, 2 μm thick. The MMIC was slightly non central. Center temperature 77 $^{\circ}\text{C}$; edge 30 $^{\circ}\text{C}$.

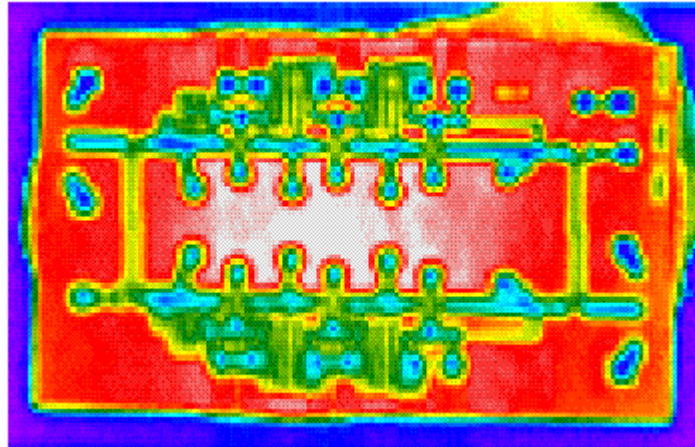


Fig. 6.3. 3-stage, 38 GHz, balanced amplifier array

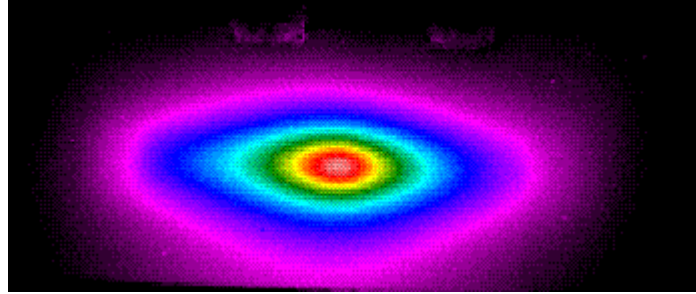


Fig. 6.4. Thermal image of substrate reverse side

2. Electrothermal simulation

Figures 6.5 and 6.6 show simulated temperature profiles for the front and back surfaces of the FR-4 mount. (The front view shows the temperature under the Cu layer.) Temperatures vary from 87 °C (center) to 30 °C (edge) on the front surface, and from 77 °C (center) to 30 °C (edge) on the reverse surface. The electrical model assumed a DC bias point $(V_{ds}, V_{gs}) = (3.0 \text{ V}, -0.55 \text{ V})$, as used experimentally, for a single transistor finger with gate width chosen to reproduce total MMIC power dissipation of 0.54 W. The $.2 \mu\text{m}$ thick Cu strip had to be modeled explicitly, otherwise simulated contours were too localized about the position of MMIC. The model assumed cooling purely by radiation and convection, i.e. no heat sink mounting. In the absence of a model of external fluid flow (natural convection), the term “ H ” in the radiation boundary condition was used as a fitting parameter. Fitting the single scalar parameter H , reproduced reasonably the temperature over the reverse surface and the central temperature difference between front and reverse sides. The chosen H corresponded to convective:radiative fluxes of $\sim 4:1$.

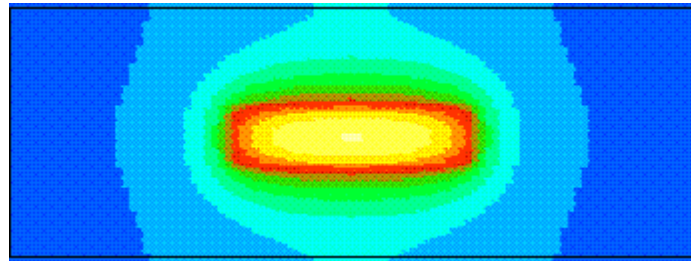


Fig. 6.5. Simulation of FR-4 front side (below Cu).

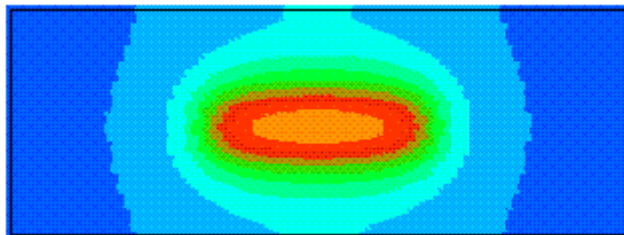


Fig. 6.6. Simulation of FR-4 reverse side.

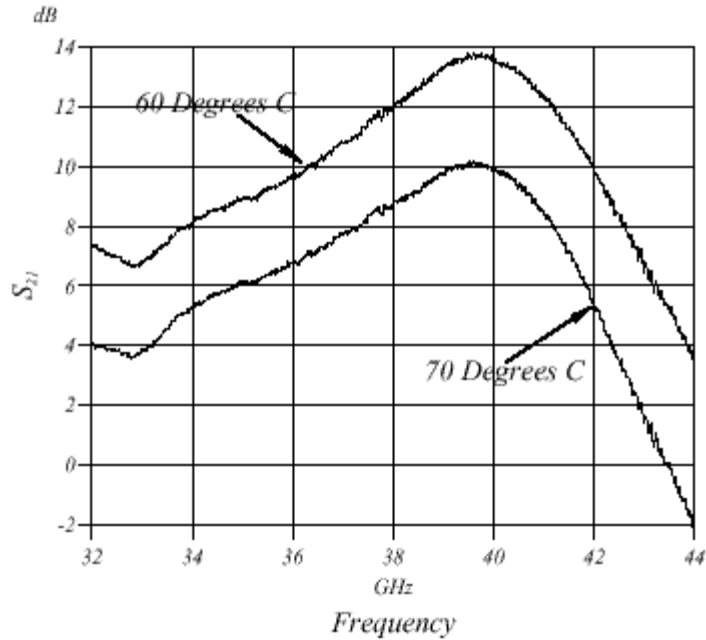


Fig. 6.7. Forward gain of 38 GHz MMIC amplifier.

3. Electrical Measurements: 38 GHz MMIC

A thermal wafer probe station was used to measure the forward gain of the 38 GHz MMIC amplifier at two distinct substrate temperatures. The temperature difference of 10 °C produces a 4 dB difference in S_{21} . This would have a profound effect on the beam pattern of spatial power combining grid amplifier.

4. Thermal Measurements: Passive Arrays

Figures 6.8 and 6.9 show measured temperature profiles of a passive 10×10 array, of area 5×5 cm², dissipating 10 W. The array is freestanding and horizontal. In Figure 6.9 the array is cooled by forced convection from a small fan. Measured temperature variations are: uncooled - high 85 °C, low 30 °C; cooled - high 55 C, low 28 °C.

Figures 6.10 and 6.11 show measured temperature profiles with the 10×10 array heat sink mounted at the edges of one face. In Figure 6.11 the array is cooled by forced convection from a small fan. Measured temperature variations are: uncooled - high 72 °C, low 28 °C. cooled - high 48 °C, low 26 °C.

Figures 6.12 and 6.13 show measured temperature profiles with the 10×10 array freestanding and vertical. In Figure 6.13 the array is offset by 45°. A thermal hotspot is observable at the “top” of the array, top right in the Figure.

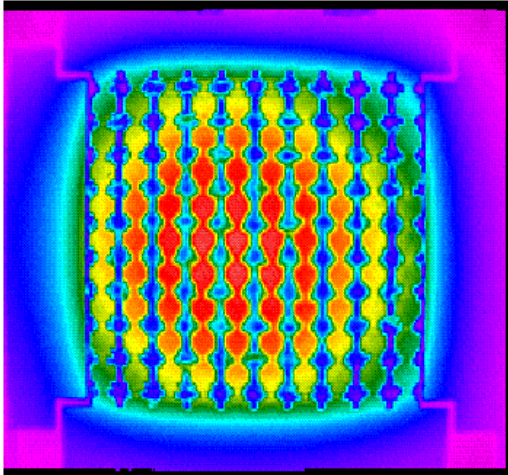


Fig. 6.8. 10×10 resistive array, freestanding, horizontal, dissipating 10 W over area 5×5 cm².

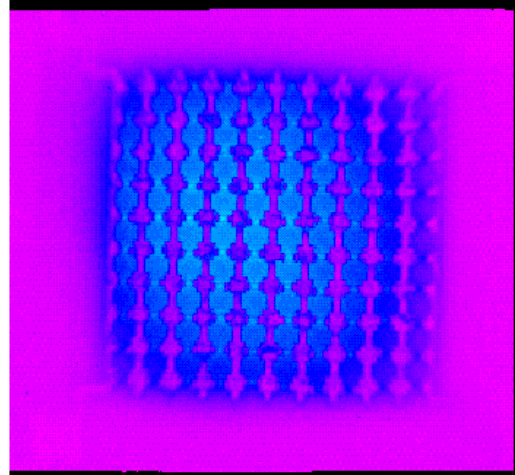


Fig. 6.9. Same array as in Fig. 6.8, but cooled by small fan.

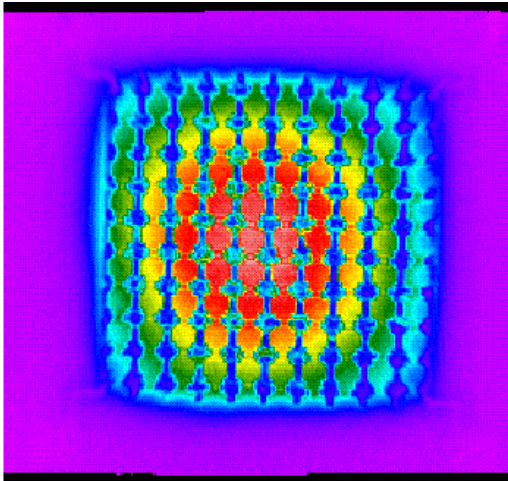


Fig. 6.10. 10×10 resistive array, edge mounted, horizontal, dissipating 10 W over area 5×5 cm².

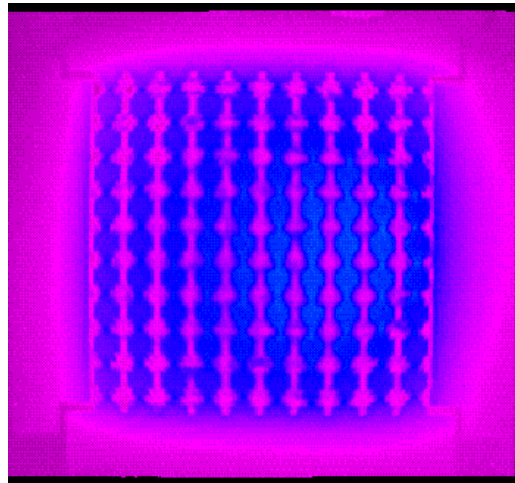


Fig. 6.11. Same array as in Fig. 10, but cooled by a small fan.

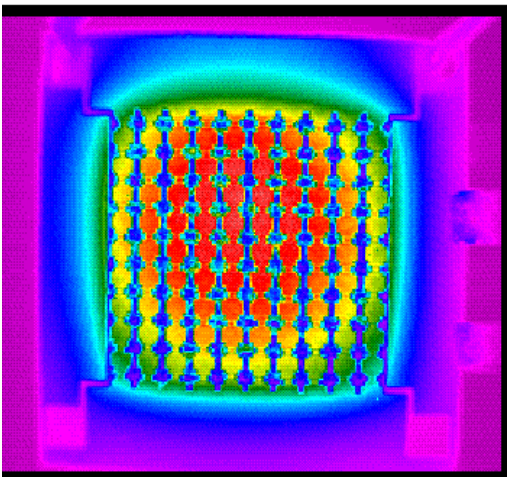


Fig. 6.12. 10×10 resistive array, freestanding, vertical, dissipating 10 W over area 5×5 cm².

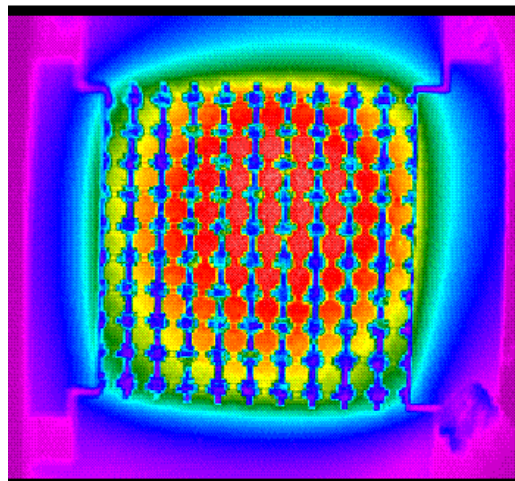


Fig. 6.13. Same array, offset by 45°. (Thermal hotspot at top of array, top right.)

The passive 10×10 arrays, on 5 cm × 5 cm FR-4 substrate, and dissipating a total 10 W, show peak temperature rises of 40-60 °C above ambient. Temperature contours for horizontal arrays are radially symmetric and do not show hotspots at grid positions of resistive heat sources. Edge mounted arrays exhibit lower temperatures than freestanding arrays, due to additional heat sinking, and the area over which significant temperature rises occur is reduced in the edge mounted case. Forced convective cooling by a small fan significantly reduces the peak temperatures of arrays. When mounted vertically, arrays show asymmetric contours with the tops of the arrays up to 10 °C hotter than the bases of the arrays, due to the effects of natural convection.

It should be noted that the thermal conductivity of FR-4, .0.3 W/(K.m), is 3 orders of magnitude smaller than that of AlN, ~180 W/(K.m) and Cu, ~400 W/(K.m). Hot spots are therefore far more localized on FR-4 substrates than on AlN. Also, even very thin layers of Cu on FR-4 act as efficient heat spreaders, significantly distorting temperature contours. Simulations of grid arrays on FR-4, without surface metallization, exhibit grid arrays of hot spots, unlike thermal measurements. Resistance matrix simulations for AlN grid array substrates, either heat-sink mounted, or predominantly cooled by convection (and radiation), indicate almost uniform temperature over the AlN substrate, so that individual MMICs of an AlN grid array experience very similar thermal environments.

JOURNAL PUBLICATIONS

1. M. Abdullah, and M B. Steer, "Extraction of the network parameters in the analysis of planar structures using the method of moments," submitted to *IEEE Trans. Microwave Theory Techniques*.
2. K. Yang, G. David, S. Robertson, J. F. Whitaker and L. P. B. Katehi, "Electro-Optic mapping of near-field distributions in integrated microwave circuits," *IEEE Trans. On Microwave Theory and Techniques*, Vol. 46, No. 12, pp. 2338-2343, December, 1998.
3. I. Khalil, A. B. Yakovlev and M. B. Steer, "A generalized scattering matrix method using the method of moments for electromagnetic analysis of multilayered structures," submitted to *IEEE Trans. Microwave Theory Techniques*.
4. I. Khalil and M. B. Steer, "A Generalized Scattering Matrix Method using the Method of Moments for Electromagnetic Analysis of Multilayered Structures in Waveguide," *IEEE Trans. Microwave Theory and Tech.*, July, 1999, (IN PRESS)
5. I. Khalil, A. B. Yakovlev, and M. B. Steer, "Efficient Method of Moments Formulation for the Modeling of Planar Conductive Layers in a Shielded Guided-Wave Structure," *IEEE Trans. Microwave Theory and Tech.*, August, 1999. (IN PRESS)
6. I. Khalil, A. B. Yakovlev, and M. B. Steer, "An Electric Field Integral Equation Formulation for the Modeling of Planar Conductive Layers in a Shielded Guided-Wave Structure," submitted to *IEEE Trans. Microwave Theory and Tech.*
7. Z. Popovic and A. Mortazawi, "Quasi-Optical Transmit/Receive Front Ends," *IEEE Trans. Microwave Theory and Tech.*, Vol. 46, No. 11, November, 1998, pp. 1964-1975. (INVITED PAPER)
8. M. B. Steer, J. F. Harvey, J. W. Mink, M. N. Abdulla, C. E. Christoffersen, H. M. Gutierrez, P. L. Heron, C. W. Hicks, A. I. Khalil, U. A. Mughal, S. N. Nakazawa, T. W. Nuteson, J. Patwardhan, S. G. Skaggs, M. A. Summers, S. Wang, and A. B. Yakovlev, "Global Modeling of Spatially Distributed Microwave and Millimeter-Wave Systems," *IEEE Trans. Microwave Theory and Tech.*, June, 1999. (IN PRESS)
9. W. Wang and L. W. Pearson, "Experimental Study of Planar Finite Grid Oscillator Arrays," to be published in *International Journal of Infrared and millimeter Waves*.
10. B. Yakovlev, A. I. Khalil, C. W. Hicks, A. M. Mortazawi and M. B. Steer, "The generalized scattering matrix of closely spaced strip and slot layers in waveguide," submitted to *IEEE Trans. Microwave Theory Techniques*.
11. K. Yang, G. David, J.-G. Yook, I. Papapolymerou, L.P.B. Katehi, and J.F. Whitaker, "Electro-Optic Mapping and Finite Element Modeling of the Near-Field Pattern of a Microstrip Patch Antenna," submitted to *IEEE Trans. Microwave Theory and Tech.*

CONFERENCE PUBLICATIONS

12. M. N. Abdulla, U. A. Mughal, and M. B. Steer, "Network Characteristics of a Finite Array of Folded-Slot Antennas for Spatial Power Combining Application," to be presented at 1999 International Microwave Symposium, Anaheim, CA, June 1999.
13. M. N. Abdulla, U. A. Mughal, H-S. Tsai, M. B. Steer, and R. A. York, "A Full-Wave System Simulation of a Folded-Slot Spatial Power Combining Amplifier Array," to be presented at 1999 International Microwave Symposium, Anaheim, CA, June 1999.
14. R. Bashirullah and A. Mortazawi, "A Slotted Waveguide Quasi-Optical Power Amplifier," to be presented at 1999 International Microwave Symposium, Anaheim, CA, June 1999.
15. W. Batty, R. G. Johnson, and C. M. Snowden, "Electro-Thermal HEMT Modelling for Microwave and Millimeter wave Circuit Design," Proc. IOP Condensed Matter and Materials Physics Conference, Exeter, Paper SSb.P2.15, p. 133, 1997.
16. W. Batty, A. J. Panks, and C. M. Snowden, "Fully Coupled Electro-Thermal Simulation of MMICs and MMIC Arrays Based on a Physical Model", IEEE MTT-S International Microwave Symposium Digest, Anaheim, Paper TU4C-5, to be presented June 1999.
17. K. Yang, G. David, S. Robertson, J.F. Whitaker, and L.P.B. Katehi, "High-resolution electro-optic mapping of near-field distributions in integrated microwave circuits," *IEEE MTT-S International Microwave Symposium Digest 1998*, New York: IEEE, pp. 949-952.
18. G. David, K. Yang, W. Wang, L.W. Pearson, J.F. Whitaker, and L.P.B. Katehi, "3-D near-field analysis of a 4 x 4 grid oscillator using an electro-optic field imaging system," 1998 European Microwave Conference, Amsterdam, Netherlands
19. S. Ortiz and A. Mortazawi, "A Perpendicular Aperture-Fed Patch Antenna for Quasi-Optical Amplifier Arrays," to be presented at 1999 IEEE International Symposium on Antennas and Propagation, Orlando, FL, July, 1999.
20. S. Ortiz and A. Mortazawi, "A Perpendicular Aperture-Fed Patch Antenna for Quasi-Optical Amplifier Arrays," to be presented at 1999 International Microwave Symposium, Anaheim, CA, June 1999.
21. M. Ozkar and A. Mortazawi, "An Inhomogeneous Waveguide Transformer with Hard Walls for the Excitation of Quasi-optical Amplifiers," to be presented at 1999 IEEE International Symposium on Antennas and Propagation, Orlando, FL, July, 1999.
22. L. W. Pearson, "Coupled-Oscillator Spatial Power Combining," to be presented at the XXVth General Assembly of the International Radio Science Union, Montreal, CA, August, 1999. (INVITED PAPER)
23. L. W. Pearson and R. J. Pogorzelski, A Fresh Look at Spatial Power Combining Oscillators, National Radio Science Meeting, Boulder, CO, January, 1999. (INVITED PAPER)
24. C. M. Snowden, "Electrothermal Transistor Models for Large-Signal Design," In *IEEE MTT-S Workshop Digest on 'New Developments in Time Domain Methods for Nonlinear Design,'* pp. 1-16, June 1998.

25. C. M. Snowden, "Electro-Thermal Microwave Transistor Models for Large-Signal CAD," Proc. Integrated Nonlinear Microwave and Millimeter-wave Circuits Conference, Duisburg, pp. 56-68, October 1998.
26. C. M. Snowden, "Non-Linear Microwave CAD using Physics-Based Active Device Models," Proc. Asia Pacific Microwave Conference, Yokohama, Japan pp. 1417-1424, 1998 (Invited Paper).
27. W. Wang and L. W. Pearson, "Phase-locking of Grid Oscillators," IEEE International Microwave Symposium, Baltimore, MD, June, 1998.
28. K. Yang, G. David, S. Robertson, J.F. Whitaker, and L.P.B. Katehi, "High-resolution electro-optic mapping of near-field distributions in integrated microwave circuits," *IEEE MTT-S International Microwave Symposium Digest* 1998, New York: IEEE, pp. 949-952.
29. K. Yang, G. David, W. Wang, T. Marshall, L.W. Pearson, Z. Popovic, L.P.B. Katehi, and J.F. Whitaker, Electro-Optic Field Mapping of Quasi-Optic Power-Combining Arrays, OSA Topical Conference on Ultrafast Electronics and Optoelectronics, Aspen, CO, April 12-16, 1999.

APPENDIX

Publications Stemming from MURI Activity

Original Report
Contained an Appendix Collecting Publications

This Appendix is Omitted
in
this Compilation

Spatial and Quasi-Optical Power Combining

A

Multidisciplinary University Research Initiative

ARO Grant No. DAAG 55-97-0132

Interim Progress Report

L. Wilson Pearson, Principal Investigator
Department of Electrical and Computer Engineering
Clemson University
Clemson, SC 29634-0915

January, 1998

Team Members

Linda P.B. Katehi
University of Michigan

Amir Mortazawi
University of Central Florida

Zoya B. Popovic
University of Colorado

Christopher M. Snowden
University of Leeds

Michael Steer
North Carolina State University

Approved for Public Release
Distribution Unlimited

TABLE OF CONTENTS

I. KEY TASKS.....	1
II. OVERVIEW OF ACCOMPLISHMENTS	3
III. SUMMARY OF ACCOMPLISHMENTS BY TOPIC.....	5
<u>1. Electro-Optical Near-Field Sampling</u>	5
<u>2. Phase Locking of Quasi-Optical Oscillators</u>	8
<u>3. Thermal Modeling of Active Semiconductor Systems</u>	9
<u>4. Quasi-Optical Amplifier Architecture</u>	11
<u>6. Electromagnetic Modeling of Quasi-Optical Systems</u>	15
APPENDIX Publications.	16

LIST OF FIGURES

Figure 1 Schematic representation of Michigan Electro-optic probe station.....	5
Figure 2 Electro-optic mapping of the normal field component of the T-junction at pos. A in Fig. 4; $f = 15$ GHz; (a) sketch of scanned area (b) relative amplitude in decibels, (c) relative phase in degrees.	6
Figure 3 Layout of 4x4 Voltage Controlled Grid Oscillator whose Near Fields were Scanned.....	7
Figure 4. Scan of vertical electric field 8 mm. Above a 4x4 Grid Oscillator ($f=4.6$ GHz) (a) Relative amplitude in decibels and (b)relative phase in degrees. The phase shift across the array is consistent with H-plane beam skewing observed in grid oscillators	8
Figure 5 Voltage Controlled Grid Oscillator output spectrum in (a) unlocked state and (b) locked state. Note the vestiges of sideband spurs in unlocked spectrum which disappear when the oscillator is locked.	9
Figure 6 Surface temperature distribution for an 8-finger power HEMT	10
Figure 7 Three-layer partitioning of a Quasi-Optical Amplifier.....	12
Figure 8 Configuration of UCF CPW-coupled QO Amplifier: (a) perspective view, (b) plan view.....	12
Figure 9 Measured gain of the active QO amplifier array.	12
Figure 10 Unit cell of lens amplifier array.....	13
Figure 11 Layout of a 14-element lens with 12 cm. focal length.....	13
Figure 12 Gain of the active lens. The distinction between the two curves involves details of the measurement configuration.....	14
Figure 13 Unit cell of NCSU 2-d spatial power combiner. The amplification elements reside in a stripline configuration between input and output waveguides.....	14

I. KEY TASKS

The MURI that is the subject of this report has maintained a near-term focus on several key areas of inquiry that are intended to lead to more fundamental understanding of spatial power combining systems.

1. What are the issues limiting performance of quasi-optical oscillators?
 - a. Temporal coherence among oscillating elements?
 - b. Spatial coherence among the radiation fields of individual elements?
 - c. Uniformity of current/field distribution across the face of the array? (quasi-plate distributions)
 - d. How can heat be extracted from devices without interfering with the intricate field coupling present in a grid structure?
2. What are the upper bounds on performance of quasi-optical amplifiers?
 - a. ... with regard to receiving aperture efficiency?
 - b. ... with regard to quality of field distribution illuminating the receiving array?
 - c. ... with respect to signal management in the feed-through process?
 - d. ... with respect to effective transmission schemes?
 - e. ... with regard to heat extraction?
3. Can quasi-optical oscillators be frequency stabilized and modulated?
4. A final overriding question is that of thermal management. The knowledge base is quite limited on heat generation, conduction and sinking for microwave devices and MMIC circuits. Any high-power system design hinges on the trade-off between RF power generation and thermal power dissipation. The tools are not currently available to approach this trade-off systematically.

The program, "Quasi-optical and Spatial Power Combining," seeks to deal with these questions and derivative questions. In order to deal with some of these questions, it is also necessary to develop key assay tools to allow observation of localized details of operating systems. It is also desirable to have CAD-worthy modeling tools for both electromagnetic and thermal performance.

There are clear interdependencies among the items listed above. For example, the development of assay tools depends on the ability to phase lock the (quasi-optical) device under test to the local oscillator(s) in the measurement system. The questions regarding thermal performance of both oscillators and amplifiers cannot be addressed readily without thermal modeling tools.

During 1997, efforts in the MURI program have concentrated on the following:

1. Optimum feeding of amplifier arrays (Mortazawi, Popovic)
2. Thermal modeling tools (Snowden)
3. Electromagnetic modeling tools (Steer)

4. Electro-optic imaging system development (Katehi)
5. Frequency/Phase control of QO Oscillators (Pearson)

A longer term agenda envisions enhanced performance of antenna arrays in QO systems through the use of so-called photonic bandgap materials (Mortazawi, Katehi, Pearson); integration of electromagnetic and thermal models into a self-consistent system (Steer, Snowden); the exploitation of MMIC technology in order to leverage upon this rapidly evolving technology; and generally, the control of factors limiting performance of QO and spatial combining systems.

Section II provides a detailed summary of accomplishments in bullet-point form. Section III provides an overview of the activities by topic. This organization inevitably obscures to some extent the collaborative interactions between institutions. These are pointed out in the respective narratives wherever possible. Publications that supply details of individual efforts are provided in the Appendix.

II. OVERVIEW OF ACCOMPLISHMENTS

ELECTRO-OPTICAL NEAR-FIELD SAMPLING (MICHIGAN)

- Phase/Amplitude Near-field Probing System Implemented (See Fig. 1)
 - Detector (BSO and LiTaO₃) Produces Optical Polarization Rotation proportional to electric field present
 - Laser Pulse Train Locked to Microwave Synthesizer
 - Scans (80x80) Grid in 45 min. (mechanical-system limited)
- System Validated for Coplanar Waveguide System (See Fig. 2)
- Initial Validation Undertaken for Radiating System (See Fig. 3)
 - Phase-Locked Grid Oscillator DUT(Clemson, see below)
 - Near-field Measured on a Radiating System
 - Phase Plots Derived Provide Basis for Investigation of Beam Shifting in Grid Systems

PHASE LOCKING OF QUASI-OPTICAL OSCILLATORS (CLEMSON)

- Grid Trimming Scheme to Maximize Tuning Range of Voltage-Controlled Grid Oscillator
- Phase-Locking of VCGO to Synthesized Source
 - Phase Noise Controlled to Level Present in Locking Source (-86 dBc/Hz 10 kHz off-carrier) (See Fig. 4)
 - Locking Scheme Permits Phase-modulation Loop External to Locking Loop

THERMAL MODELING OF ACTIVE MICROWAVE SYSTEMS (LEEDS)

- Existing HEMT Models Extended to Provide Electrothermal Descriptions of Wafer-scale Arrays
 - Leeds Physical Model in HP-Eesof Microwave Design System Extended to Arrays of Thermally Coupled Gate Fingers
 - Model will Provide Realistic Description of Thermal Breakdown
 - User Interface Needs to be Developed

- Non-Linear Thermal Equivalent Circuit Model for Wafer-Scale Arrays of HEMT Devices has been Constructed
 - Quasi-3D Thermal Matrix Description
 - User Interface Needs to be Developed
- Experimental Validation of Thermal Models Begun
 - Resistive Arrays of Heating Elements to Simulate an Active Array Constructed

QUASI-OPTICAL AMPLIFIER ARCHITECTURE (CENTRAL FLORIDA AND COLORADO)

- Coplanar-Waveguide-Based Feedthrough Architecture Developed (UCF)
 - Via Elimination Through Use of CPW Simplifies Assembly
 - Slot Feed-through in Common Ground Plane for Back-to-Back Patch Antennas (unit cell in Fig. 5)
 - Compatible with Egg-Carton Packaging of MMIC Devices
- Lens and Amplifying Array Integrated (See Fig. 6) (Colorado)
 - Meander Lines Delay Phase to Achieve Focusing
 - Two-stage Amplifier Included in Each Unit Cell
 - Permits Feeding of Amplifier Array in the Near Field of a Horn

TWO-DIMENSIONAL SPATIAL POWER COMBINING

- Unit Cell for Second-Generation 2-d Combiner Designed
- Hardware Tested for Passive Elements of the Unit Cell

ELECTROMAGNETIC MODELING OF QUASI-OPTICAL SYSTEMS (NCSU)

- Work Currently Underway under MAFET Thrust 3 Support
- Will Flow into MURI Activity and Couple with Leeds work in Late 1998

III. SUMMARY OF ACCOMPLISHMENTS BY TOPIC

Work in each major topic area in which significant progress has occurred is summarized below. Details are available in the publications in the Appendix.

1. Electro-Optical Near-Field Sampling

This program segment has been conducted at the University of Michigan under the direction of Prof. Linda Katehi. Dr. John Whitaker has supervised the day-to-day activity in this activity.

The objective of this program segment is the development of a minimally intrusive phase/amplitude near-field measurement system. This capability provides a means of assaying the field components in proximity of a radiating array, thereby revealing details of array interaction that are not observable in the radiation field. The Michigan activity has been highly productive during the first year of operation of the MURI. An earlier prototype of the Michigan EO system has demonstrated the ability to scan near fields of an operating microwave device and capture amplitude data (only). The activity under MURI funding has led to an amplitude/phase measuring capability through phase locking of the device under test (DUT) to the pulse train of the excitation laser.

A block diagram of the system appears in Fig. 1.

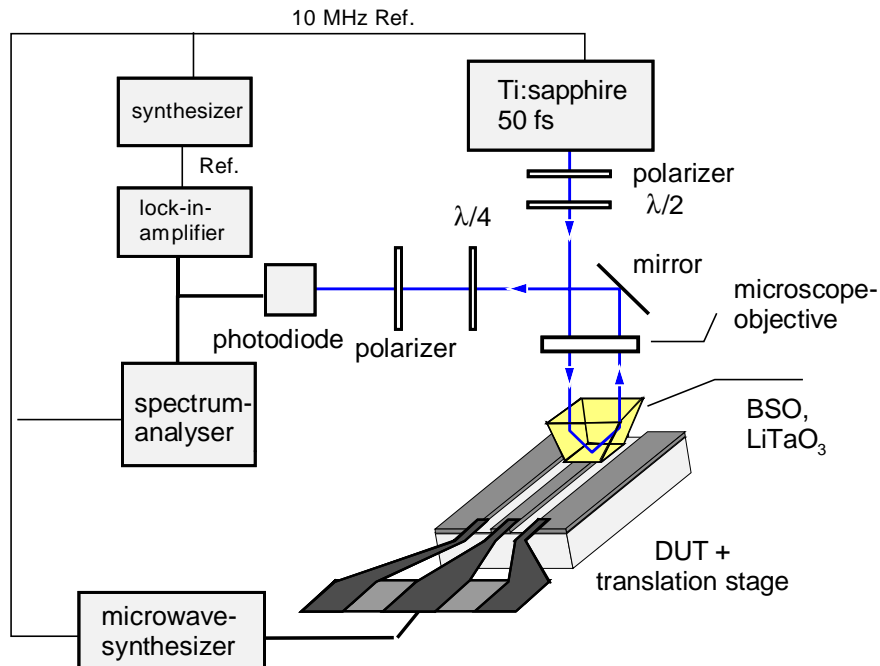


Figure 1 Schematic representation of Michigan Electro-optic probe station

The key element in the system is the electro-optical probe crystal. The crystal comprises lithium tantalate (LiTaO₃) for the measurement of tangential RF field components. A crystal of bismuth silicate (BSO) is used as the EO element for the measurement of

normal field components. The beam of a phase-stabilized Ti:Sapphire laser is passed through the crystal, which has been cleaved so that the beam is returned parallel to its entry path by way of total internal reflection. The polarization state of the beam is rotated in proportion to the electric field present at the focus point on the bottom surface of the crystal. Phase synchronization between the laser and the RF synthesizer exciting the circuit allow phase and amplitude to be recovered.

Figure 2 shows the layout of a tee-junction in coplanar waveguide, along with amplitude and phase plots of the normal component of electric field scanned in the vicinity of this junction. These measurements were carried out at 15 GHz.

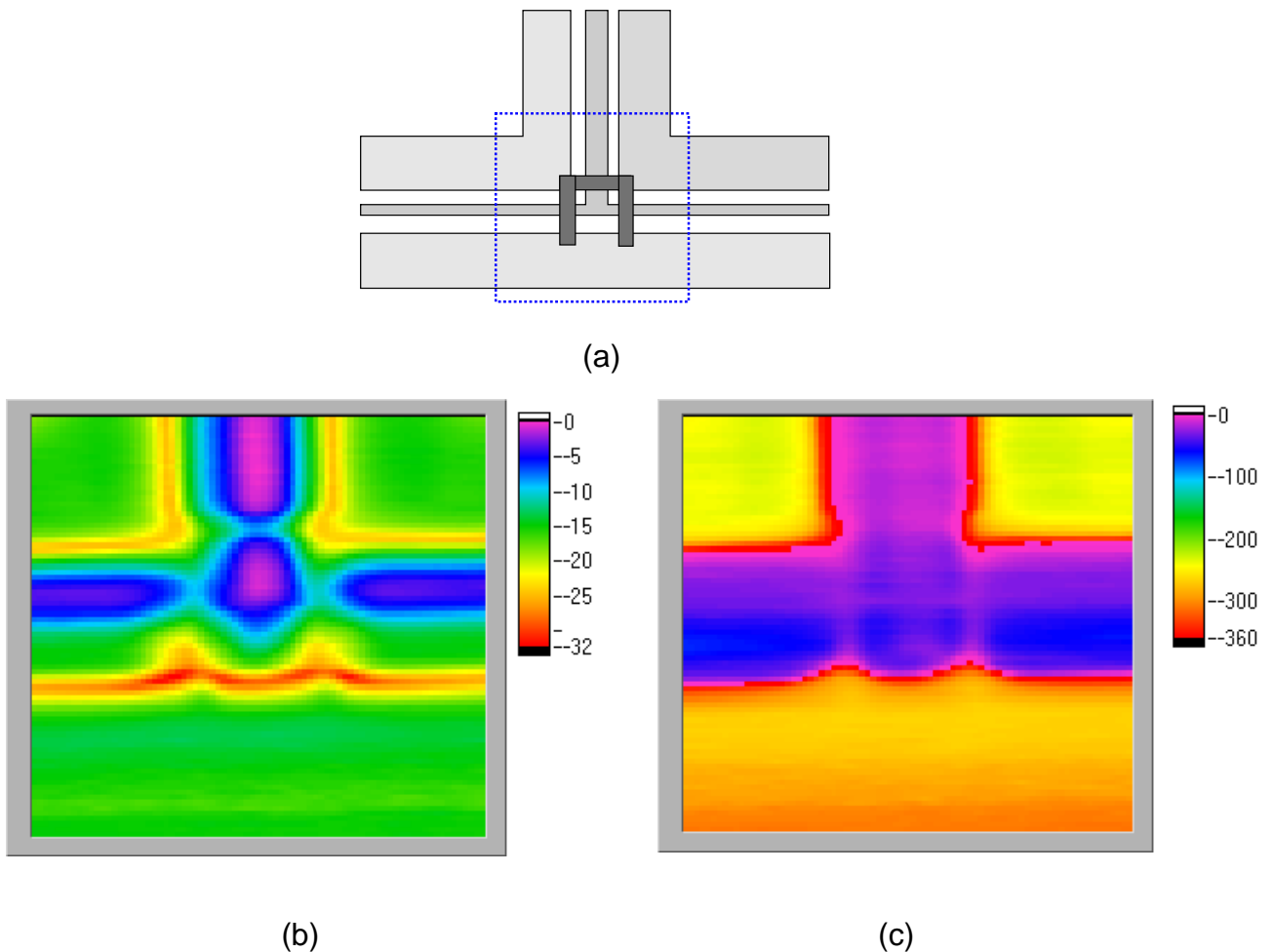


Figure 2 Electro-optic mapping of the normal field component of the T-junction at pos. A in Fig. 4; $f = 15$ GHz; (a) sketch of scanned area (b) relative amplitude in decibels, (c) relative phase in degrees.

The potential of this system as a diagnostic tool is quite evident. One now has the possibility to assay the electromagnetic performance at key points interior to a microwave/millimeter wave integrated circuit in with an non-invasive tool. In recent years, monolithic microwave technology has outstripped our ability to monitor performance at interior test points in the circuit. This measurement scheme allows one to view fields present at *any* interior point in the circuit.

Work in grid oscillators at Clemson University has recently led to the first phase-locked grid oscillator. The details of this work are provided in the next subsection. The ability to phase lock the grid oscillator, along with the availability of the Michigan EO system, has provided the first opportunity to assay the aperture fields of a radiating grid oscillator. (A free-running grid cannot not be measured because it cannot be synchronized to the laser pulse train.) The results of this study are not conclusive at this writing, but the achievement of the measurement is itself significant.

Figure 3 shows the layout of the grid, a sixteen element array operating at 4.6 GHz. Figure 4 shows scanned amplitude and phase plots of the fields across the aperture of the grid. The transistor sites are evident from the high-field areas (blue) in the amplitude plot. The third column of devices from the left is evidently operating at a lower level than the other three columns. The approximate 360 degree phase progression across the array is noteworthy, too. The phase progression is consistent with off-normal main beam directions often observed in the H-plane pattern of grid oscillators. Work is currently underway with a third member of the MURI team, North Carolina State University, to clarify the operating mode observed in this grid. NCSU has developed a self-consistent model of grid devices under Thrust 3 of the DARPA MAFET program. They are currently computing field results for the specific grid geometry shown in Figure 3, and we anticipate that the measured results can be interpreted definitively with the theoretical support of this model.

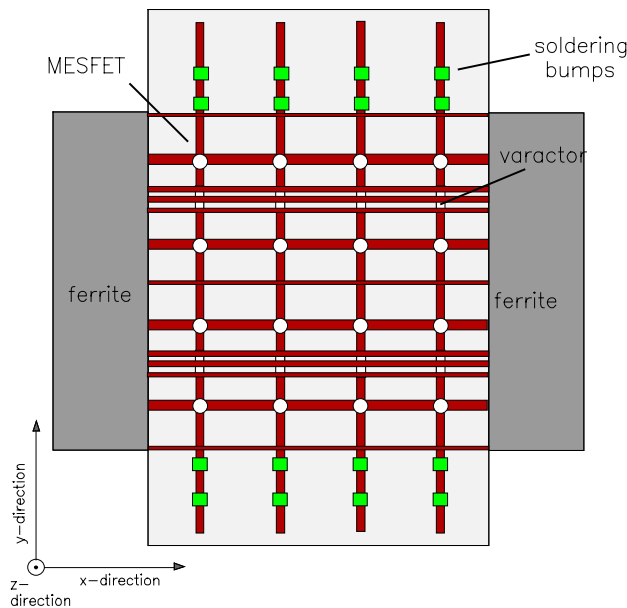


Figure 3 Layout of 4x4 Voltage Controlled Grid Oscillator whose Near Fields were Scanned

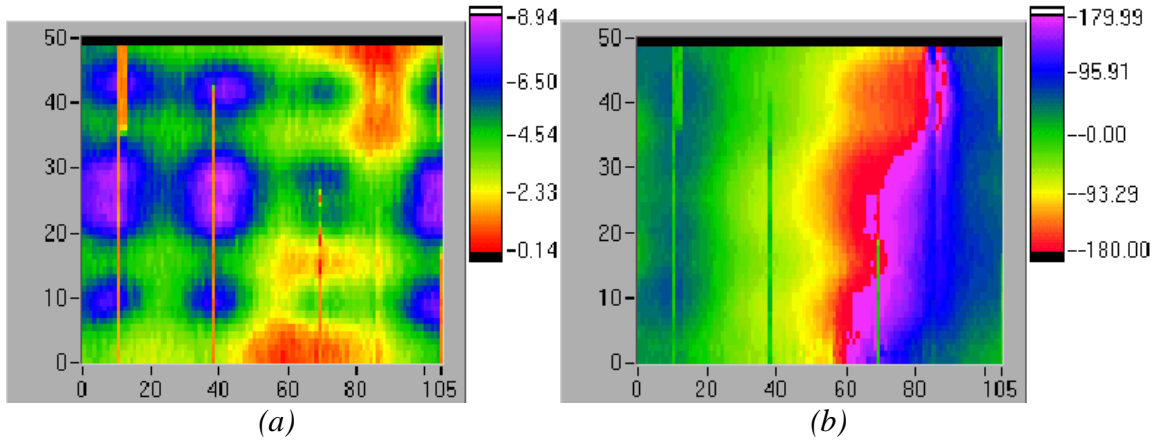


Figure 4. Scan of vertical electric field 8 mm. Above a 4x4 Grid Oscillator ($f=4.6$ GHz) (a) Relative amplitude in decibels and (b) relative phase in degrees. The phase shift across the array is consistent with H-plane beam skewing observed in grid oscillators

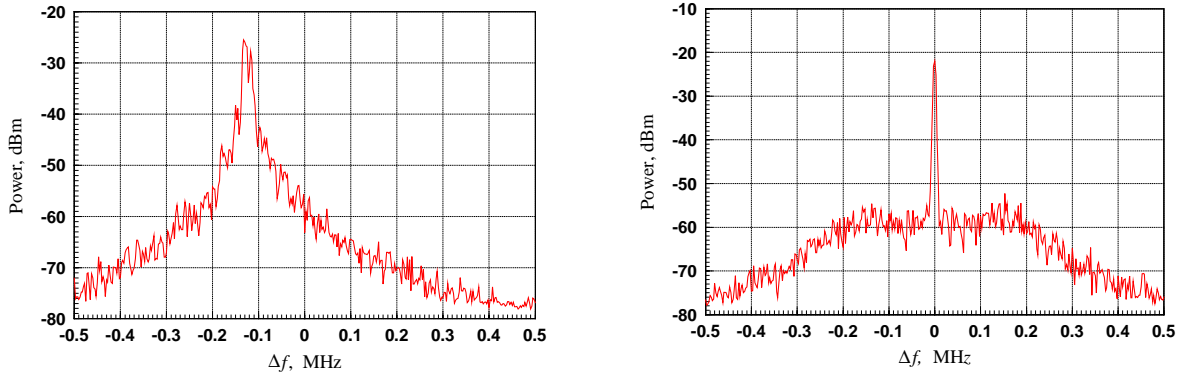
2. Phase Locking of Quasi-Optical Oscillators

Quasi-optical grid oscillators have been in existence for roughly ten years. During that time, they have been operated exclusively as free-running oscillators. As solid-state oscillators go, they are relatively unsophisticated devices, containing no element to define well the resonant frequency. Rather, the operating frequency is set by distributed effects—what some might call parasitics—and is weakly defined. This feature of grid oscillators limits both their utility in microwave systems and the ability to assay in detail the physics of their operation. (Practical assay methods generally require phase-coherent detection on measured microwave signals.)

Clemson University has been studying voltage controlled grid oscillators (VCGOs) in recent years. Wenzhang Wang, a Ph.D student at Clemson has achieved the widest published tuning range for a VCGO. Frequency/voltage sensitivity is concomitant with wide tuning range, thus making the Clemson devices highly controllable from an external voltage. During the course of the first-year MURI effort, the Clemson VCGO design has been refined so that grids may be designed and trimmed to provide a monotonic frequency-voltage relationship across the full tuning range. Without careful trimming, VCGOs exhibit a mode skipping, whereby frequency increases with increasing (negative) voltage bias for a time, then skips to a lower frequency from which it follows a locally monotonic tuning curve over another range.

The achievement of monotonicity and high sensitivity renders these grids appropriate for incorporation into a phase-locked loop. A PLL is formed by inserting a sampling loop in the brass mirror that backs the grid. The phase of this sample of the signal produced by the grid is compared with that of a reference source (microwave synthesizer) and produces a feedback control to the VCGO.

Figure 5 shows the spectrum of the 4x4 VCGO shown in Figure 3 in both free-running and phase-locked state. One observes that the spectrum delivered from the free-running device is quite ragged.



a. Free running grid oscillator

b. Phase-locked grid oscillator

Figure 5 Voltage Controlled Grid Oscillator output spectrum in (a) unlocked state and (b) locked state. Note the vestiges of sideband spurs in unlocked spectrum which disappear when the oscillator is locked.

In the phase-locked state, the signal has been pulled to the 4.6 GHz reference frequency of the synthesizer. The spectrum tightens to a single central spike, with concomitant reduction in phase noise. The measured phase noise is shown in Table 1 below. The locking source was an HP 8620B synthesizer. The phase noise readings in the table are all within 3 dB of the specified phase noise of the synthesizer, and there is a 3 dB uncertainty in the measurement used. Consequently, we believe that the phase locked grid’s noise performance is set by the phase noise performance of the synthesizer.

Table 1. Measured phase noise of the locked grid and the reference source.

f_{offset}	Locked Grid	Reference
100Hz	73dBc	70dBc
1kHz	78dBc	78dBc
10kHz	84dBc	86dBc
100kHz	88dBc	106dBc
1MHz	107dBc	N/A

3. Thermal Modeling of Active Semiconductor Systems

The University of Leeds has initiated its effort in thermal modeling within the framework of a cuboid die. The surface of the die is segmented into subareas over which dissipated power density is approximately constant. Thermal interactions among the subareas are expressed in terms of a *thermal interaction matrix*. Thermally active areas are defined in terms of prescribed *supplied* power densities. This matrix system allows the thermal diffusion equation to be reduced in approximation to an algebraic problem. The diffusion equation applied is nonlinear by virtue of a temperature-dependent thermal conductivity. This formulation is a central task enabling the achievement of most of the remaining

Leeds analysis effort. Refinement, embellishment and construction of appropriate user interfaces to the software are, of course, required and are significant in scope.

In the effort to date, this model has been applied to the Leeds Physical model of a HEMT device, which is contained in the Hewlett Packard EESoft Microwave Design System (MDS). Arbitrary arrays of thermally interacting gate fingers distributed over the top surface of a semiconductor die can be described through the resulting extension.

The uniform channel temperature version of the MDS software has been modified already. Adaptation of a version of the software with variable channel temperature is in progress, and will allow a more realistic description of thermal breakdown.

As an illustration, the surface temperature distribution calculated using the coupled electrothermal HEMT model is shown in Figure 6 for a power HEMT with eight $0.2 \times 30 \mu\text{m}$ fingers. Temperature is in $^{\circ}\text{C}$, $V_{\text{DS}} = 3 \text{ V}$, $V_{\text{G}} = 0 \text{ V}$, $T_{\text{S}} = 70 \text{ }^{\circ}\text{C}$.

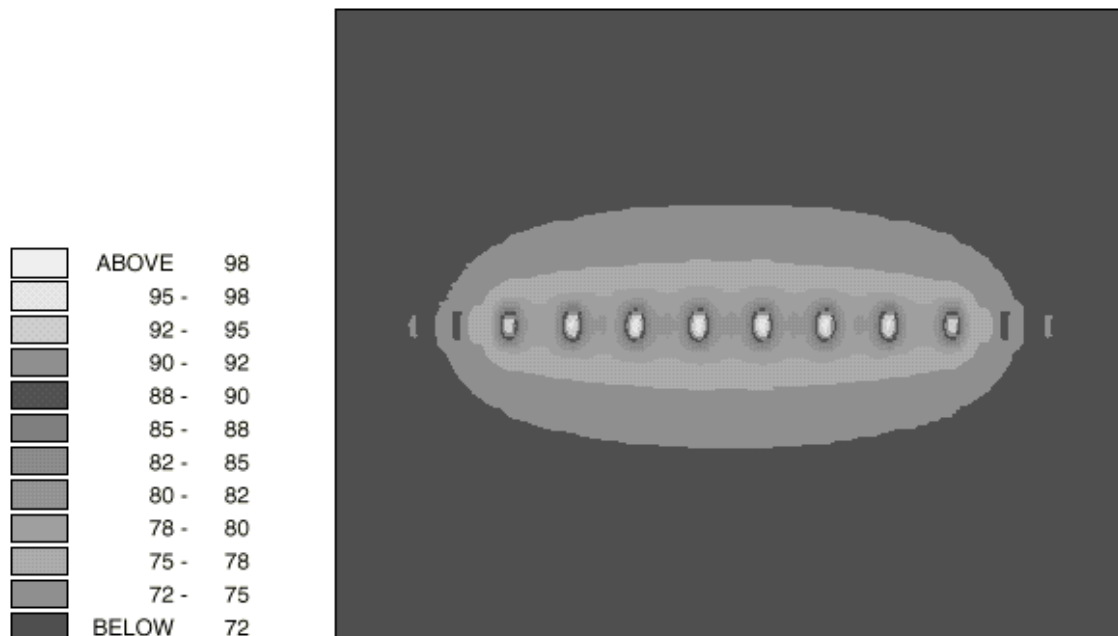


Figure 6 Surface temperature distribution for an 8-finger power HEMT

The University of Leeds has begun work on a test structure for validation of the computer simulations described above and their anticipated extensions. To date, a passive test grid has been fabricated in cooperation with the University of Colorado. This is a first step on a path leading to test models comprising arrays of active elements.

An infrared camera is under development to allow unobtrusive measurements of the localized temperature in a circuit that includes numbers of active devices. This camera provides the means of measuring a temperature map over the surface of the circuit. The camera is being designed to operate over a temperature range of -50 to $200 \text{ }^{\circ}\text{C}$. This dictates that the detectors in the camera be able to detect radiation in the 1.7 to $5.5 \mu\text{m}$ portion of the spectrum. The Leeds infrared camera will obviate the need for mechanical translation by focusing the image of the DUT onto a focal plane array (FPA) of PtSi.

Several challenging design problems are posed by such a camera configuration. First of all, the different materials on the surface of a device or MMIC die have different thermal emissivities. An emissivity calibration scheme has been developed so that the optical temperature detected on each pixel of the focal plane array can be corrected for the emissivity of the portion of the circuit surface of which it is the image.

The detectors of the FPA must be maintained at a temperature substantially lower than the lowest temperature to be measured. Else, the heat present in the array would present itself as noise in the data derived from the DUT. Conventional liquid nitrogen dewar arrangements are problematic in the proposed camera for several reasons. Consequently, a thermo-mechanical system, based on the Stirling cycle has been determined to be appropriate to the cooling needs for the FPA in the camera. A commercial cooler manufactured by Inframetrics has been chosen for this task.

A commercial source has also been identified for the objective lens. This lens must be fabricated from materials appropriate to the IR wavelengths involved in the measurement.

4. Quasi-Optical Amplifier Feeding

This task is directed toward understanding the requirements for and physical limitation to feeding amplifier arrays. Feeding an array from a source in close proximity leads to non-ideal distribution of field across the input aperture. Both phase and amplitude pose difficulty, though most believe that phase curvature poses the bigger performance limitation. Phase correction can be approached in two ways: either through external correction to the radiation field of the illuminating antenna, or through incorporating phase correction into the amplifying layer itself, thereby making it a lens.

It is useful to think of QO Amplifiers as three layer structures as shown in Figure 7: a receiving antenna layer, an amplifying layer, and a transmitting antenna layer. When the amplifier circuitry is implemented using microstrip transmission lines, then the ground plane of the microstrip structure is intrinsically asymmetric with respect to the respective input and output patch antenna layers. The University of Central Florida has developed an architecture that employs coplanar waveguide (CPW) in the device layer, thereby providing a symmetric location of the ground plane.

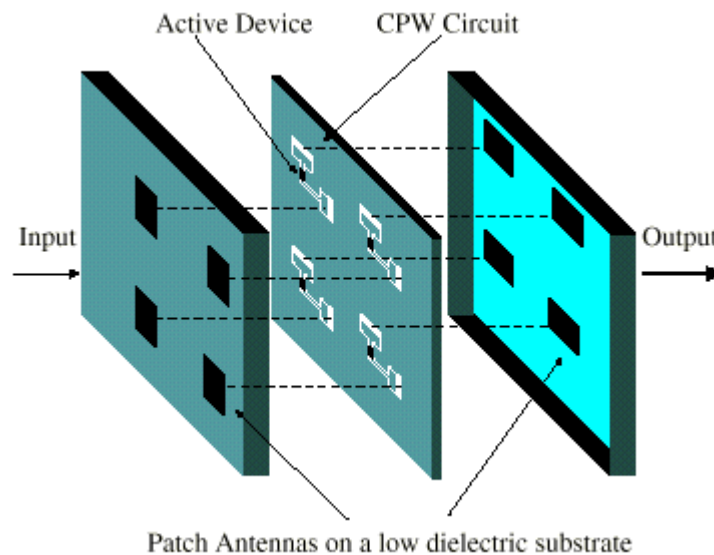


Figure 7 Three-layer partitioning of a Quasi-Optical Amplifier

The configuration of the patches and feed lines is pictured in Figure 6. Fifty ohm CPW lines connect the amplifier input and output to the patches by way of a slot folded dipole. The dimensions shown in the figure are for a 10 GHz design. The MMIC amplifier is embedded in the CPW layer.

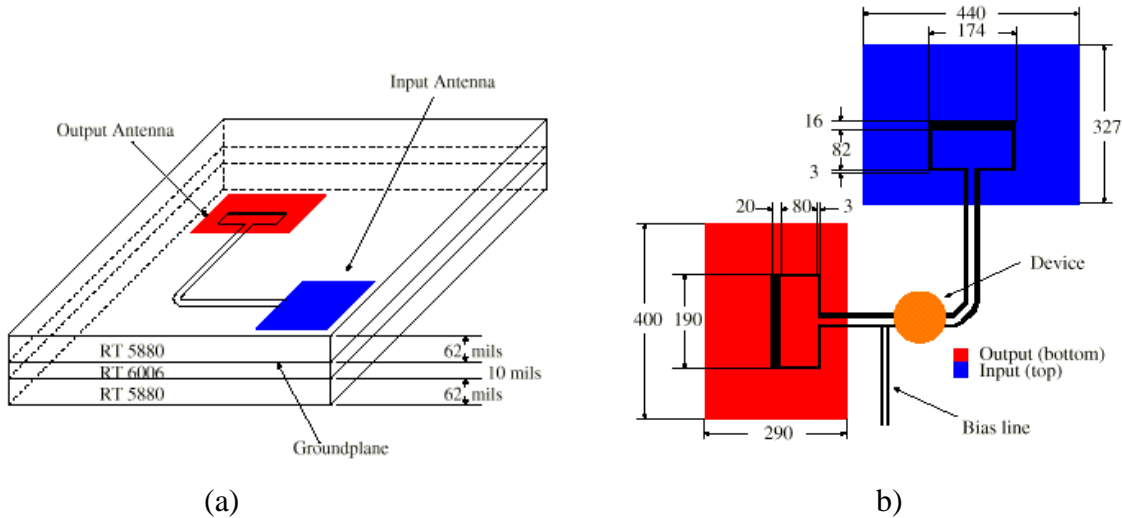


Figure 8 Configuration of UCF CPW-coupled QO Amplifier: (a) perspective view, (b) plan view.

The measured gain of the active configuration is shown in Figure 9.

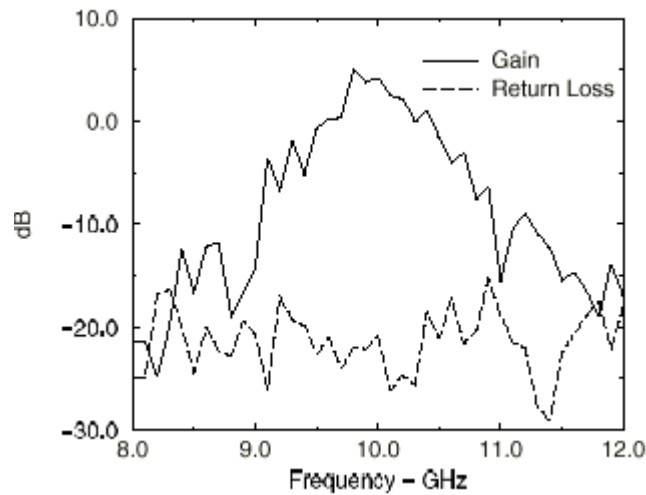


Figure 9 Measured gain of the active QO amplifier array.

The array described above is representative of one of two approaches under investigation for feeding amplifier arrays. The path from each receiving patch to each transmitting patch is identical for every patch in the array. This requires that the patches be excited

cophasally. A so-called hard horn is used to excite the receiving array and to receive the transmitted power, at least for measurement purposes.

The alternative feeding approach, whose properties are under investigation at the University of Colorado, is to correct for the phase front impinging on the array by designing a phase delay appropriate to each element in the array, forming what may be thought of as an active boot-lace lens. Figure 8 depicts the configuration of a single element of the lens array. The focusing element of the element is the delay line. Figure 10 shows the layout of an array of elements, and Figure 11 shows the layout of a 14-element lens for operation at X-band.

Figure 10 Unit cell of lens amplifier array

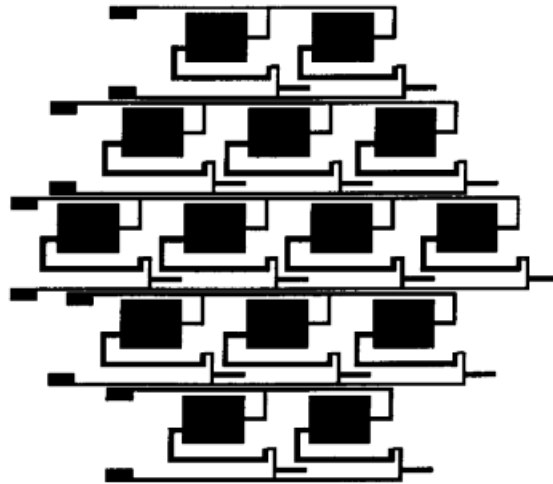
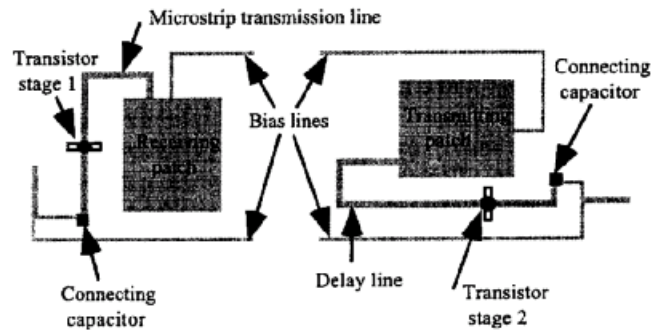


Figure 11 Layout of a 14-element lens with 12 cm. focal length.

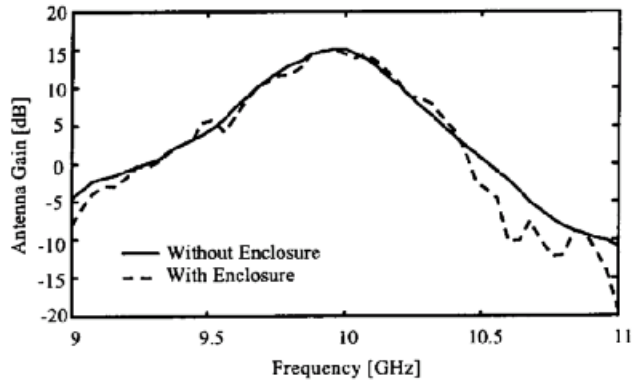


Figure 12 Gain of the active lens. The distinction between the two curves involves details of the measurement configuration.

The gain of the active lens shown in Figure 11 includes both the amplifier gain and the antenna gain of the array. A spatial combining efficiency estimated from measurements on this array yields a 75 % combining efficiency.

5. TWO-DIMENSIONAL SPATIAL POWER COMBINING

North Carolina State University has begun work on a second-generation 2-d spatial power combining system. A unit cell of the 2-D combiner is shown in Figure 13.

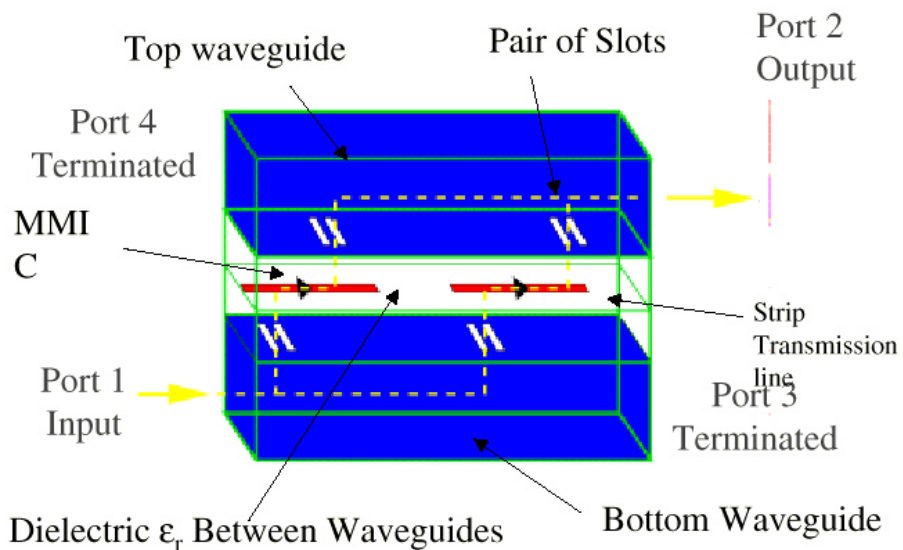


Figure 13 Unit cell of NCSU 2-d spatial power combiner. The amplification elements reside in a stripline configuration between input and output waveguides.

Development of this system is to begin in the first quarter of 1998. To date, the structure shown has been modeled using the HP EESoft HFFS simulator, and hardware models of the passive portions of the system have been fabricated.

6. Electromagnetic Modeling of Quasi-Optical Systems

North Carolina State University is currently prime contractor for the development of a quasi-optical CAD system under the MAFET Thrust 3 program. Upon completion of the MAFET-funded activities in late 1998, this CAD system will be developed further under this MURI activity. Particular emphasis is to be placed on incorporation of the Leeds thermal models to allow self-consistent electro-thermal modeling of QO systems.

APPENDIX

Publications Stemming from MURI Activity

Original Report
Contained an Appendix Collecting Publications

This Appendix is Omitted
in
this Compilation